

Information dynamics in controlled and uncontrolled quantum systems



Eoin Carolan

15352471

The thesis is submitted to University College Dublin in fulfilment of the requirements
for the degree of Doctor of Philosophy in Physics

UCD School of Physics

Head of School: Prof. Emma Sokell

Principal Supervisor: Assistant Prof. Steve Campbell

Research Studies Panel: Dr. Morgan Fraser

Dr. Alessandro Ferraro

August 31, 2024

Why though search for proof? ... Definitely the supreme action is to dispose of the mind, bring reality into something vital, felt seen, even smelt.

Ann Quin

Contents

1	Introduction	1
1.1	Closed Quantum Systems	1
1.2	Adiabaticity	3
1.3	Adiabatic Gauge Potential	4
1.4	Composite Quantum Systems	6
1.5	Open Quantum Systems	8
1.6	Overview	13
2	Control in the Impulse Regime	14
2.1	Background	14
2.2	Kibble-Zurek mechanism	15
2.3	Control in the impulse regime	17
2.4	Landau-Zener Model	19
2.5	Transverse-Field Ising Model	25
2.6	Conclusion	32
3	Robustness of Controlled Unitary Gates	33
3.1	Controlled Gate Techniques	34
3.1.1	Auxiliary Evolution	35
3.1.2	Inverse Engineering	43
3.2	Figures of merit	45
3.3	Hadamard Gate	48
3.4	Conclusions	53
4	Commutativity and the Emergence of Classical Objectivity	54
4.1	Introduction	55
4.2	Pointer States	56
4.3	Quantum Darwinism and Classical Objectivity	57
4.4	Collisional-model picture of the system-environment interaction	61
4.5	Role of commutativity	66
4.6	Conclusions	67

5 Operator Spread Complexity	69
5.1 Quantum Chaos	70
5.2 Krylov Subspaces	72
5.3 Spread Complexity	76
5.4 Minimisation of the spread complexity	77
5.5 Sachdev-Ye-Kitaev Model	79
5.6 Complexity vs decoherence	80
5.7 Conclusions	84
6 Conclusions and Outlook	85

Abstract

Harnessing quantum phenomena for technological applications relies heavily on preventing information loss through decoherence. To prevent this loss, it is crucial to develop strategies that enable the rapid and precise control of quantum systems, ensuring that desired processes are completed faster than decoherence times. From a control perspective, the environment is viewed as a disruptive force; however, this ignores the rich informational dynamics that interactions with an environment can induce. By relaxing the requirement for strict control and adopting a more active treatment of the environment, this thesis explores how these dynamics contribute to the emergence of classicality from quantum mechanics, and how it can change the internal information structure in quantum many-body systems.

The study begins by addressing the challenges of controlling quantum systems near critical points, where conventional adiabatic methods become inefficient due to closing energy gaps. We propose a novel control strategy that applies counterdiabatic driving selectively within the impulse regime, as recognised by the Kibble-Zurek mechanism. This reduces energetic costs while maintaining high fidelity. This approach is validated both numerically and analytically, demonstrating substantial energetic savings.

Next, we explore control strategies relevant to implementing unitary gates in two distinct physical settings. The first involves analytically determining a Hamiltonian that achieves gate operations with unit fidelity without external control, while the second leverages an auxiliary qubit that requires external driving. Despite the latter scheme being more resource intensive, we show that the additional complexity of driving and controlling an auxiliary qubit can be advantageous when we subject the systems to decoherence.

Moving beyond controlled systems, we examine the informational dynamics of quantum systems subject to the influence of their environment. Here, we investigate scenarios in which systems transition from pure quantum states to classically objective states as predicted by quantum Darwinism. By partitioning the environment into accessible and inaccessible parts, we reveal how the interplay between these partitions determines whether classical objectivity emerges or if the system equilibrates without the redundant encoding of the state of the system into the environment.

Finally, we explore the competition between two sinks for local quantum information - decoherence and information scrambling. Information scrambling refers to the flow of initially accessible quantum information into complex many-body correlations within the system itself. Typical measures of scrambling used in closed systems can fail to differentiate between the local information spreading throughout the degrees of freedom of the systems and the spreading of information due to decoherence. We introduce a method for probing information scrambling even in the presence of open system effects, demonstrating that the environment restructures remaining information, reducing the complexity of the system's dynamics.

Collectively, these findings provide a comprehensive framework for understanding information dynamics in open quantum systems, offering new strategies for preserving quantum coherence and diagnosing the impact of an environment on the structure of quantum information.

Statement of Original Authorship

I hereby certify that the submitted work is my own work, was completed while registered as a candidate for the degree stated on the Title Page, and I have not obtained a degree elsewhere on the basis of the research presented in this submitted work.

Publications and Collaborations

This thesis is based on the following publications:

- E. Carolan, A. Kiely, and S. Campbell, "Counterdiabatic Control in the Impulse Regime", *Phys. Rev. A* **105**(1), 012605 (2022) [1]
- E. Ryan, E. Carolan, S. Campbell, and M. Paternostro, "Commutativity and the emergence of classical objectivity", *Journal of Physics Communications* **6.9**, 095005 (2022) [2]
- E. Carolan, B. Cakmak, and S. Campbell, "Robustness of controlled Hamiltonian approaches to unitary quantum gates", *Phys. Rev. A* **108**(2), 022423 (2023) [3]
- E. Carolan, A. Kiely, S. Campbell, and S. Deffner "Operator growth and spread complexity in open quantum systems", *EPL* **147**, 38002 (2024) [4]

Acknowledgements

First and foremost, I wish to thank my supervisor, Steve Campbell. Taking me on as his student while restricted to working remotely brought its own unique challenges, but nonetheless he fostered an environment where I felt productive and excited by research. I am grateful to Steve for encouraging me to present our work at any opportunity, giving me opportunities to teach and to referee, pushing me to travel and engage with the broader physics community when possible, and most importantly for his trust in me to explore subjects that diverged from our original proposal.

I cannot thank Anthony Kiely enough for all of his guidance, patience, and confidence in me right from the very start of my time in UCD. I am also lucky to have been part of the CATS group alongside one of my oldest friends, Eoin O'Connor, as well as finding new friends in my fellow students who have made the quantum corner of UCD an exciting place to be part of these last few years. I am also grateful to the administrative staff of the School of Physics who have supported all of us through the period of remote work and the recent relocation of the department.

Discovery through collaboration is the most rewarding part of research, and I would like to thank those outside of UCD that I have had the privilege to work with - Mauro Paternostro and Eoghan Ryan of Queen's University Belfast, Barış Çakmak of SUNY Farmingdale, and Sebastian Deffner of the University of Maryland, Baltimore County. I am indebted to Sebastian for hosting me at UMBC, as well as for his continued support and mentorship.

When the lens of physics has made me view the world in a cold way, it has been my friends and family who have kept me in love with it. They all deserve better than to be called out for it in a piece of academic writing. I will make an exception for my parents Colette and Shane, and my grandmother Nuala. I hope that in me you see a part of each of you reflected back. Lastly I would like to remember my grandfather. I am proud to have followed in his footsteps in my own way.

Eoin Carolan, August 2024

List of Figures

- | | | |
|-----|---|----|
| 2.1 | Impulse regime for the Landau-Zener model: (a) Comparison between relaxation timescale τ (red solid line) and the relative rate of external parameter change $ g/\dot{g} $ (blue dashed line) for a quench duration of $\tau_Q\Delta = 2$. Intersection gives critical times t_{\mp} (green/black dots) (b) Impulse regime times t_{\mp} (green dotted and black dot-dashed lines respectively) for different quench times τ_Q . (c) Final state fidelity versus quench time τ_Q and duration of counterdiabatic driving 2η . Impulse regime $\eta = \mu$ (red points), $g_0 = -10\Delta$ and $m = 400\Delta^{-1}$ | 21 |
| 2.2 | Fidelity of the evolving state with the instantaneous ground state of the Landau-Zener model for no control (blue dashed line), impulse control (red solid line) and full control (green dotted line), for different quench times. Orange shaded area indicates the impulse regime $[t_-, t_+]$. (a) $\tau_Q\Delta=1$ (b) $\tau_Q\Delta=5$ (c) $\tau_Q\Delta=10$ (d) $\tau_Q\Delta=25$. Other parameters: $g_0 = -10\Delta$ and $m = 400\Delta^{-1}$ | 23 |
| 2.3 | Comparison between final state fidelity using impulse control and the resulting energetic savings. (a) Loss of fidelity at the end of the process using impulse control (red solid line). Also shown is the result after no control (blue dashed line). (b) Difference in energetic cost δE (green dotted line) and relative difference in energetic cost $\delta E/\mathcal{C}$ (black dot-dashed line). Other parameters: $g_0 = -10\Delta$ and $m = 400\Delta^{-1}$ | 24 |
| 2.4 | The instantaneous fidelity of TFIM for no control (blue dashed line), impulse control (red solid line) and full control (green dotted line), for different quench times. Orange shaded area indicates the impulse regime $[t_-, t_+]$ (a) $\omega\tau_Q = 10$ (b) $\omega\tau_Q = 25$ for $N = 16$. Panels (c) and (d) show the final state fidelity for TFIM versus quench time τ_Q and system size N for the (c) uncontrolled case and (d) impulse control. Red indicates high final state fidelity, with blue corresponding to low final state fidelity. Panels (e) and (f): Energetic savings versus quench time τ_Q . $N = 4, 8, 12, 18$ (blue dashed line, red solid line, green dotted line, black dot-dashed line) and thermodynamic limit (light gray thick solid line). (e) Savings δE (f) relative savings $\delta E/\mathcal{C}$. In all panels, $g_0 = 0$ and $m = 100\omega^{-1}$ | 29 |

2.5	The final state fidelity for the $N = 6$ TFIM versus quench time for uncontrolled evolution (dashed, blue), $M = 1$ (i.e. two-body control, solid red), $M = 2$ (three body control, dotted green) and $M = 3$ (i.e. full control, dot-dashed black). In panel (a) we show the performance when the control term is always on for the entire evolution, while panel (b) corresponds to impulse control. Panels (c) and (d) show the energetic savings versus quench time τ_Q for the same truncated-range impulse control protocol in (b), with the same colour scheme as before. (c) Savings δE relative to employing full range, full quench cost \mathcal{C} (d) relative savings $\delta E/\mathcal{C}$. Other parameters: $g_0 = 0.01$ and $m = 100\omega^{-1}$	31
3.1	(a) Shows the auxiliary control setting based on the protocol from Ref. [113]. Here an auxiliary qubit is coupled to the computational register, with control fields acting only on this auxiliary system. We assume the driven qubit can also experience environmental effects while the computational qubit is completely isolated. (b) Shows the setup for the Inverse Engineering setting. The Hamiltonian is designed without any additional resources, and therefore the computational qubit is driven directly and can be subject to environmental noise.	34
3.2	We show the trajectories of the qubits for both the CD and IE protocols of the Hadamard gate. We take the initial computational state to be $ +\rangle$. The yellow line corresponds to the path of the qubit in the IE case. The green and orange lines correspond to the computational and auxiliary qubits of the auxiliary evolution cases, respectively, which begins and ends with a separable global state of the two qubits while at intermediate times the reduced states of either qubit are mixed.	49
3.3	(a) Final gate infidelity, Eq (3.66) as a function of total protocol duration, for the Hadamard gate. The auxiliary evolution with counterdiabatic (CD) control is shown in the lowermost green, dotted curve. Inverse engineering (IE) performs similarly shown by the blue, dotted curve. The topmost, black, dot-dashed curve corresponds to an uncontrolled auxiliary evolution where the performance is several orders of magnitude worse. Floquet engineered (FE) auxiliary control is shown in the red, solid curve and is shown to be highly effective. (b) Dynamical gate infidelity for the Hadamard gate with $\tau = 1$ using the same styling as panel (a) to identify the different control protocols. The inset captures the oscillations present in the FE driving around the dynamics of the CD approach.	50
3.4	(a) We plot the cost, Eq. (3.67), of implementing the Hadamard gate vs. total protocol duration for IE, CD control, FE with $\omega/\omega_0 = 200$ in blue, green, and red, respectively. (b) Final gate infidelity for the Hadamard gate vs. timekeeping error, ϵ , for over- or under-shooting the intended ramp duration. The total (ideal) ramp time is $\tau = 1$. We show the performance for the linear (orange), the polynomial (cyan), the sinusoidal (purple) ramps. In all panels we fix $\omega_0 = 2\pi/\tau$, $\omega = 200\omega_0$ for the FE case.	51

3.5	(a) Qubit trajectories for the Hadamard gate under a dephasing channel, Eq. (4.20), where the channel acts on the driven qubit in each case with $\tau\gamma = 2$. Styling is same as in Fig. 3.2. As we dephase in the z -basis, both the state of the qubit in the IE case (yellow) and that of the auxiliary qubit in the CD case (orange) are pulled towards the z -axis. The computational qubit of the CD case (green) is not directly affected by the channel, and does not deviate from the ideal path, instead stopping along that trajectory once the auxiliary qubit driving the evolution has decohered. (b) We show the final gate infidelity, Eq. (3.66), for the dephasing channel for the Hadamard gate, with upper, dotted red and lower, dashed blue curves correspond to the IE and CD cases, respectively.	52
4.1	A heuristic diagram of how quantum Darwinism differs from the typical open system picture. (a) displays the decoherence paradigm, where the environment is treated as a monolithic bath into which the coherence of the system flows into. (b) displays the Darwinism paradigm. Here the environment is divided into <i>sub-environments</i> that are individually accessible to measurements. Treating the environment in a more active manner allows for us to study the type of correlations that emerge between the system and environment as the latter decoheres the former.	58
4.2	We plot the rescaled mutual information between a bath of seven qubits and a system qubit that interact with a dephasing-type interaction in the computational basis. Initially the system and environment begin in a pure product state with no correlations or mutual information between them. After some time ($Jt = 0.6$ in this case) correlations proliferate through the environment as prescribed by Quantum Darwinism, resulting in the above redundancy plateau.	60
4.3	(a) Schematic of the microscopic collision model employed. (b,c) Rescaled mutual information, \bar{I} , for (b) dephasing collisional environment and (c) thermalising collisional environment. We fix $J_{SAT_1} = 0.0075\pi/4$ and $J_{SET_2} = 0.015\pi/2$ and $\beta=0$. For both interactions the collisional environment drives the system towards a fully decohered state, however, in the case of a dephasing interaction the mutual information shared between system and accessible environment fragments shows the characteristic redundancy plateau transiently emerges with period dictated by the J_{SA} interaction strength. For a thermalising collisional bath there is an overall envelope where the redundancy plateaux are progressively damped. As elucidated in Sec. 4.5 this behaviour is explained by the commutativity, or lack thereof, between the system-environment interaction and system-accessible fragment interaction. In the dephasing case, the ability of the environmental fragments to create classical correlations with the system is unaffected by the presence of the collisional environment as the interactions commute, while this is not the case for a thermalising environment, which serves to fully decohere the fragments as well as the system in the long time limit.	63

4.4	Mutual information between the system and a single accessible environmental fragment (dashed grey), the system coherence (dot-dashed red), and the fragment coherence (solid blue). (a) Dephasing collisional bath and (b) thermalising collisional bath. The system's coherence (dot-dashed red) is identical in both cases, the collisional bath will fully decohere in the long-time limit. The primary difference between the two cases is that the coherence of the accessible environmental qubit is damped by the thermalising bath despite not coupling to it directly.	64
5.1	Dynamics for the open SYK model with $N = 8$ and 200 disorder realisations. Variance is shown as a shaded region (scaled to 20% of its value in panel (a) for clarity). (a) The average Krylov complexity (eq. (5.22)) with $\mu/J = 0.0, 0.025, 0.05, 0.075, 0.1$ corresponding to blue, orange, green, red, and black, respectively. (b) The average Krylov complexity at $Jt = 120$ vs decoherence strength μ/J . (c) The average dimension of the Krylov space for the dynamics vs μ/J	82
5.2	Dynamics for the open SYK model with $N = 8$ and 200 disorder realisations with $\mu/J = 0.0, 0.025, 0.05, 0.075, 0.1$ corresponding to blue, orange, green, red, and black, respectively. Variance is shown as a shaded region scaled to 20 % of its value for clarity. (a) Average spread complexity eq. (5.24) in the Krylov basis. (b) Average spread complexity in the string basis.	83

Chapter 1

Introduction

Fast and high-fidelity control of many-body quantum systems is key to outpacing decoherence and turning quantum science into technology [5]. This transition from theory to practice should also bring into focus practical problems associated with quantum technology to which quantum theorists can contribute. In particular, resource efficiency should be prioritised as the field matures. Already there have been calls for institutional initiatives to encourage this direction of research [6]. It is in this spirit that we will explore the energetic requirements of controlled dynamics of quantum systems in Chapter 2 and Chapter 3.

Throughout this thesis the degrees of freedom we will work with are two-level systems - qubits, or spins. Remarkable progress has been made in recent years to engineer qubits using trapped ions, spin states of nuclei, superconducting circuits, and NV centres in diamond. However, for these platforms it is impossible to completely isolate any quantum system from unwanted interactions that disrupt the desired quantum information dynamics. This manifests as spin relaxation and spin decoherence. The timescale for the latter is typically much shorter, and is the primary engineering issue with quantum computers. Decoherence is the unifying concept between each of the chapters of this thesis.

While in Chapter 2 and Chapter 3 we employ quantum control techniques to outpace the effect of the environment on the desired dynamics, in Chapter 4 and Chapter 5 we will embrace decoherence and explore what rich effects it can induce for the dynamics for a quantum system. Before discussing each of these topics in turn, we will first need to introduce a few key concepts and equations that will be used throughout the thesis, most notably closed system dynamics, adiabaticity in quantum systems, and open system dynamics.

1.1 Closed Quantum Systems

Quantum mechanics is typically first introduced by explaining the development of and transition from “old” quantum theory to the “new” quantum theory. “Old” quantum mechanics was born in 1900 when Max Planck communicated his modeling of the distribution of blackbody radiation [7]. The old quantum theory relied on putting in quantum numbers, integers that corresponded to

quanta of energy, by hand into the theory [8]. It was successful when applied to “simple” systems like the harmonic oscillator, hydrogen atom, rigid rotors, and oscillating rotors [9]. For more complex systems such as the the hydrogen halide molecules and diatomic molecules required half-integer quantum numbers in order for the theory to match observations, while energy levels of helium atom and hydrogen molecule ion could not be explained using the old theory. The “new” quantum mechanics was introduced with Schrödinger’s eponymous equation in a series of papers in the first half of 1926 [10], and is given by

$$i\hbar\partial_t |\psi(r,t)\rangle = H(r,t) |\psi(r,t)\rangle. \quad (1.1)$$

Schrödinger replaced the old rules of quantisation with his wave equation, which required “*no mention of whole numbers. Instead, the introduction of integers arises in the same natural way as, for example, in a vibrating string* [10].” He applied the wave equation (1.1) to a number of systems, including the diatomic molecule, and the hydrogen atom in the electric field, the latter of which required the development of perturbation theory. Wavefunction mechanics rapidly surpassed the old quantum theory, and has had immeasurable impact on both physics and chemistry. The Schrödinger equation was initially postulated for wavefunctions that were continuous functions of position and time (and momentum and time via a Fourier transform). The focus of this thesis restricts to matrix mechanics, where we consider state vectors that are elements of a finite-dimensional Hilbert space. The Schrödinger equation implies that the evolution of a quantum state is unitary. Let’s recast the equation with Dirac notation

$$i\hbar\partial_t |\psi\rangle = H |\psi\rangle. \quad (1.2)$$

Taking the Hamiltonian to be time-independent gives us the solution, for $t \geq t_0$

$$|\psi(t)\rangle = U(t, t_0) |\psi(t_0)\rangle, \quad (1.3)$$

where we have defined the time evolution operator

$$U(t, t_0) = \exp\left\{-\frac{iH(t-t_0)}{\hbar}\right\}. \quad (1.4)$$

We can immediately see that it is unitary, satisfying $U^\dagger U = \mathbb{1}$ as H is by definition a Hermitian operator. If the Hamiltonian is time-dependent then the formal solution becomes a time-ordered exponential [11]

$$U(t, t_0) = \mathcal{T} \exp\left\{-\frac{i}{\hbar} \int_{t_0}^t H(t') dt'\right\}, \quad (1.5)$$

where \mathcal{T} is the time-ordering operator. Even in this unitary, or *closed system* framework, quantum mechanics expands far beyond its original promise of explaining the spectra of atoms and molecules to have potential to revolutionise fields as diverse as chemistry [12, 13], agriculture [14], and neuroscience [15]. To leverage the inherent complexity of closed quantum dynamics, it is often

useful to remain in the ground state of the system, and change the Hamiltonian governing it. The adiabatic theorem for quantum systems is a powerful constraint for closed system dynamics to achieve this.

1.2 Adiabaticity

In classical thermodynamics, an adiabatic process is one that does not result in heat exchange between a system and the environment. In quantum mechanics, we define adiabaticity in a way that does not require a partitioning between system and environment. Adiabaticity in quantum mechanics demands that population changes do not occur in the instantaneous energy eigenbasis of the system when a parameter of the Hamiltonian is changed. What is common to both definitions is the concept of slow or “quasi-static” changes of the parameters of our system. From now on we take natural units, $\hbar = 1$, unless otherwise stated. Our quantum-mechanical system is described by the time-dependent Hamiltonian, $H(t)$, and therefore its dynamics are given by the time-dependent Schrödinger equation, restated here as

$$i\partial_t |\psi(t)\rangle = H(t) |\psi(t)\rangle. \quad (1.6)$$

At each moment in time, the Hamiltonian has corresponding eigenvectors $\{|n(t)\rangle\}$ and eigenvalues $\{E_n(t)\}$

$$H(t) |n(t)\rangle = E_n(t) |n(t)\rangle. \quad (1.7)$$

Let us consider the decomposition of an arbitrary state in the instantaneous eigenbasis of the system

$$|\psi(t)\rangle = \sum_n p_n(t) |n(t)\rangle,$$

We substitute this into the time-dependent Schrödinger equation

$$i \left[\partial_t \left(\sum_n p_n(t) |n(t)\rangle \right) \right] = H(t) \left[\sum_n p_n(t) |n(t)\rangle \right]. \quad (1.8)$$

Applying the product rule to the left-hand side gives

$$i \left[\sum_n \left(\dot{p}_n(t) |n(t)\rangle + p_n(t) |\dot{n}(t)\rangle \right) \right] = \sum_n p_n(t) E_n(t) |n(t)\rangle. \quad (1.9)$$

We act with the instantaneous eigenstate $\langle m(t)|$ to the left,

$$i \left[\sum_n \left(\dot{p}_n(t) \langle m(t) | n(t) \rangle + p_n(t) \langle m(t) | \dot{n}(t) \rangle \right) \right] = \sum_n p_n(t) E_n(t) \langle m(t) | n(t) \rangle. \quad (1.10)$$

By definition $\langle m(t) | n(t) \rangle = \delta_{mn}$, but derivatives of the state do not preserve orthonormality: $\langle m(t) | \dot{n}(t) \rangle \neq \delta_{mn}$. Application of this gives

$$i\dot{p}_m(t) = p_m(t)E_m(t) - ip_m(t)\langle m(t)|\dot{m}(t)\rangle - i \sum_{n \neq m} p_n(t)\langle m(t)|\dot{n}(t)\rangle. \quad (1.11)$$

Adiabaticity in quantum mechanics demands that no transitions between instantaneous eigenstates occur. In the previous line, the mixing of eigenstates arises from the $\langle m(t)|\dot{n}(t)\rangle$ term. Demanding it is zero gives rise to the following solution

$$p_n(t) = \exp \left[-\frac{i}{\hbar} \int_0^t (E_n - i\langle n(t')|\dot{n}(t')\rangle) dt' \right] p_n(0). \quad (1.12)$$

This implies that adiabaticity gives rise to an evolution where the instantaneous eigenstate populations remain unchanged, but pick up an additional phase along the way. The phase can be separated into two contributions, the usual dynamic phase $\phi_{d,n}(t) = \int_0^t E_n(dt') dt'$ and the geometric phase (or Berry phase) [16] $\phi_{g,n}(t) = -\int_0^t i\langle m(t')|\frac{d}{dt'}|m(t')\rangle dt'$. The only assumption we made so far is that there are no transitions between states in the instantaneous eigenspectrum. This adiabatic condition is quite strong, as can be seen by solving for the term in question that we set to zero. To do so, we take the time derivative of the instantaneous Schrödinger equation

$$\dot{H}(t)|n(t)\rangle + H(t)|\dot{n}\rangle = \dot{E}_n(t)|n(t)\rangle + E_n(t)|\dot{n}(t)\rangle.$$

Acting to the left with $\langle m(t)|$ gives

$$\langle m(t)|\dot{H}(t)|n(t)\rangle + E_m(t)\langle m(t)|\dot{n}(t)\rangle = \dot{E}_n(t)\langle m(t)|n(t)\rangle + E_n(t)\langle m(t)|\dot{n}(t)\rangle.$$

Rearranging to isolate the transition term gives

$$\langle m(t)|\dot{n}(t)\rangle = \frac{\langle m(t)|\dot{H}(t)|n(t)\rangle}{E_n(t) - E_m(t)}, \quad \forall m \neq n. \quad (1.13)$$

Adiabaticity is a strong requirement for the dynamics of the system, one which implies either large gaps in the system's spectrum (something we will take advantage of later) or slow changes in the time-dependent terms of the Hamiltonian.

1.3 Adiabatic Gauge Potential

We previously isolated the source of non-adiabatic transitions for the evolution of a system. We can recast this same term in such a way that it will allow for deeper understanding of deformations in instantaneous eigenstates as the control parameters are changed. We will recast the problem to have a control parameter, $\lambda = \lambda(t)$, giving us the eigenvalue equation for the “bare” Hamiltonian H_0

$$H_0(\lambda)|n(\lambda)\rangle = E_n(\lambda)|n(\lambda)\rangle. \quad (1.14)$$

Let us consider an arbitrary state $|\psi\rangle$. We transform it to the moving frame - i.e. the frame in which the instantaneous Hamiltonian is diagonal

$$|\tilde{\psi}\rangle = U^\dagger |\psi\rangle, \quad (1.15)$$

where U is the unitary transformation that diagonalises the Hamiltonian. The solution to the time-dependent Schrödinger equation in the moving frame is then

$$i\partial_t |\tilde{\psi}\rangle = \left(U^\dagger H_0 U - i\dot{\lambda} U^\dagger \partial_\lambda U \right) |\tilde{\psi}\rangle, \quad (1.16)$$

where we have dropped the implicit λ -dependence, and we recognise that

$$U^\dagger H_0 U = \text{diag}\{E_1(\lambda), E_2(\lambda), \dots, E_N(\lambda)\}. \quad (1.17)$$

The second term, $i\dot{\lambda} U^\dagger \partial_\lambda U$, contains the information about non-adiabatic transitions between the instantaneous eigenstates caused by the change in λ . Clearly if $\dot{\lambda} \rightarrow 0$ we achieve adiabatic transport. By transforming this term back into the lab frame we define an object denoted as the adiabatic gauge potential (AGP),

$$A_\lambda = U(iU^\dagger \partial_\lambda U)U^\dagger = i\partial_\lambda. \quad (1.18)$$

We can solve for the matrix elements of the AGP by using the fact that the Hamiltonian is diagonal in its eigenbasis,

$$\langle \langle m(\lambda) | H_0(\lambda) | n(\lambda) \rangle \rangle = 0. \quad (1.19)$$

Differentiating this with respect to λ gives

$$\langle \partial_\lambda m(\lambda) | H_0(\lambda) | n(\lambda) \rangle + \langle m(\lambda) | \partial_\lambda H_0(\lambda) | n(\lambda) \rangle + \langle \partial_\lambda m(\lambda) | H_0(\lambda) | \partial_\lambda n(\lambda) \rangle = 0. \quad (1.20)$$

Using the time-independent Schrödinger equation and the orthogonality condition, $\langle \partial_\lambda m(\lambda) | n(\lambda) \rangle = -\langle m(\lambda) | \partial_\lambda n(\lambda) \rangle$, we find that

$$i \langle \partial_\lambda m(\lambda) | \partial_\lambda n(\lambda) \rangle = \langle m(\lambda) | A_\lambda | n(\lambda) \rangle = \frac{i \langle m(\lambda) | \partial_\lambda H_0(\lambda) | n(\lambda) \rangle}{E_n(\lambda) - E_m(\lambda)}, \quad \forall m \neq n. \quad (1.21)$$

The AGP can also be interpreted as the generator of eigenstate deformations,

$$\partial_\lambda |n(\lambda)\rangle = A_\lambda |n(\lambda)\rangle. \quad (1.22)$$

Here we have taken a single parameter, but can be generalised to deformations in any direction of a n -dimensional parameter space for our system. We can use the AGP to design a control scheme for the system. Adding it to the lab frame Hamiltonian will cancel out the off-diagonal terms in the moving frame, and keep the evolution of the arbitrary state adiabatic. That is to say, we

evolve with the new Hamiltonian

$$H = H_0 + \dot{\lambda} A_\lambda = H_0 + H_{CD}, \quad (1.23)$$

which keeps us along the adiabatic manifold of H_0 for arbitrary driving rates $\dot{\lambda}$. Above we have rewritten the AGP as the counterdiabatic control Hamiltonian H_{CD} as this control scheme is equivalent to the well-known *counterdiabatic control* [17], which is typically stated as

$$H_{CD} = i \sum_n |\partial_\lambda n\rangle \langle n| - \langle n|\partial_\lambda n\rangle |n\rangle \langle n|. \quad (1.24)$$

In order to employ counterdiabatic control, we require full-knowledge of the spectrum of the system. This already highlights an issue with counterdiabatic control in many-body systems, as exact diagonalisation is computationally complex. However, as we shall discuss in Chapter 2 some models such as the 1-dimensional transverse-field Ising model admit analytical solutions for their counterdiabatic term for a finite number of spins. We will also leverage counterdiabatic control, and an approximation of it in Chapter 3 to ensure that we can theoretically implement quantum gates for arbitrarily fast times.

1.4 Composite Quantum Systems

We have previously made reference to the classical picture of thermodynamics when defining adiabaticity, where one must make a partition between what is considered the system, and what is considered the environment. Quantum systems may also be treated in a similar way. While not a requirement for the use of the Schrödinger equation, we will take care to introduce what is often referred to as the “zeroth” postulate of quantum mechanics [18]

The state of a composite system is the a vector in the Hilbert space that is a tensor product of the Hilbert spaces of the subsystems.

While seemingly innocuous, the idea that the quantum universe consists of *subsystems* gives rise to much of the rich phenomena associated to quantum mechanics. As we shall discuss later, even the idea of a measurement implies subsystems. Let us briefly introduce the framework of composite quantum systems. Consider two systems with Hilbert spaces \mathcal{H}_A and \mathcal{H}_B , respectively. States of the composite system are elements of the composite Hilbert space, $\mathcal{H}_{AB} = \mathcal{H}_A \otimes \mathcal{H}_B$. If \mathcal{H}_A is n -dimensional and spanned by the orthonormal states $\{|i\rangle_A, i = 1, 2, \dots, n\}$, and \mathcal{H}_B is m -dimensional and spanned by the orthonormal states $\{|j\rangle_B, j = 1, 2, \dots, m\}$, then \mathcal{H}_{AB} is an $(n \times m)$ -dimensional space spanned by states

$$\{|i\rangle_A \otimes |j\rangle_B, i = 1, 2, \dots, n, j = 1, 2, \dots, m\}. \quad (1.25)$$

A bosonic operator, O_A , acting on states in the Hilbert space of subsystem A is elevated to

$$O_A \rightarrow O_A \otimes \mathbb{1}_B. \quad (1.26)$$

Similarly, a bosonic operator O_B acting on states in the Hilbert space of subsystem B is elevated to

$$O_B \rightarrow \mathbb{1}_A \otimes O_B. \quad (1.27)$$

This structure can be expanded to an arbitrary number of subsystems

$$\mathcal{H}_{ABC\dots} = \mathcal{H}_A \otimes \mathcal{H}_B \otimes \mathcal{H}_C \otimes \dots . \quad (1.28)$$

For fermionic operators we must additionally take into account the parity of other subsystems in order to ensure global anticommutation. A *pure state* is that which can be represented by a single ket vector of the Hilbert space. A *mixed state* is statistical mixture of pure states, and cannot be represented by a single vector as a result. Instead, we represent mixed states with density matrices. A *density matrix* is a non-negative Hermitian operator with unit trace. It is the weighted sum of projectors of the mixed state onto a spanning orthonormal set of pure states $\{|\psi_i\rangle\}$ of the system's Hilbert space

$$\rho = \sum_i p_i |\psi_i\rangle \langle \psi_i|, \quad (1.29)$$

where $\sum_i p_i = 1$. In the case that the state represented is pure, the density matrix reduces to the outer product of that state

$$\rho = |\psi\rangle \langle \psi|. \quad (1.30)$$

For pure states, the density operator is idempotent, $\rho^2 = \rho$, and $\text{Tr}\rho=1$. For mixed states, this is not the case. Density matrices are particularly useful for calculating expectation values of operators

$$\begin{aligned} \langle O \rangle &= \sum_i p_i \langle \psi_i | O | \psi_i \rangle, \\ &= \sum_{i,j,k} p_i \langle \psi_i | j \rangle \langle j | O | k \rangle \langle k | \psi_i \rangle, \\ &= \sum_{i,j,k} p_i \langle j | O | k \rangle \langle k | \psi_i \rangle \langle \psi_i | j \rangle, \\ &= \sum_{j,k} O_{j,k} \rho_{kj}, \\ &= \text{Tr}(O\rho). \end{aligned}$$

Consider now a density matrix, ρ_{AB} representing a state in a bipartite Hilbert space \mathcal{H}_{AB} , and an operator, O_A , that only acts non-trivially on the subsystem \mathcal{H}_A . The expectation value of O_A is

$$\begin{aligned}
\langle O_A \rangle &= \text{Tr}_{AB}((O_A \otimes \mathbb{1})\rho_{AB}), \\
&= \sum_{i=1}^n \sum_{j=1}^m \langle i|_A \langle j|_B ((O_A \otimes \mathbb{1})\rho_{AB}) |i\rangle_A |j\rangle_B, \\
&= \sum_{i=1}^n \sum_{j=1}^m \langle i|_A O_A \langle j|_B \rho_{AB} |i\rangle_A |j\rangle_B, \\
&= \sum_{i=1}^n \langle i|_A \left(O_A \sum_{j=1}^m \langle j|_B \rho_{AB} |j\rangle_B \right) |i\rangle_A, \\
&= \text{Tr}_A(O_A \text{Tr}_B(\rho_{AB})), \\
&= \text{Tr}_A(O_A \rho_A),
\end{aligned}$$

where we have employed the *partial trace* of a density matrix

$$\rho_A = \text{Tr}_B(\rho_{AB}) = \sum_i \langle b_i | \rho_{AB} | b_i \rangle. \quad (1.31)$$

where $\{|b_i\rangle\}$ is an orthonormal basis for the Hilbert space of the subsystem B .

The dynamics of the total density matrix are governed by the Liouville-von Neumann equation of motion [19]

$$\frac{d}{dt} \rho(t) = -i[H, \rho(t)],$$

where we have introduced the commutator between operators, $[A, B] = AB - BA$. This has the solution

$$\rho(t) = U(t, t_0) \rho(t_0) U^\dagger(t, t_0),$$

where we have the same unitary operator as defined in (1.4).

1.5 Open Quantum Systems

While the global density matrix evolves unitarily, if we restrict ourselves to the reduced state of a subsystem, we may find that the evolution is no longer governed by a unitary operator. This is the case when subsystems interact with each other. Consider a partitioning of the global Hilbert space into a system, S , and environment, E , such that $\mathcal{H}_{SE} = \mathcal{H}_S \otimes \mathcal{H}_E$. A state in the total Hilbert space evolves unitarily with the Hamiltonian that generates the time evolution operator reading

$$H_{SE} = H_S \otimes \mathbb{1}_E + \mathbb{1}_S \otimes H_E + H_I, \quad (1.32)$$

where H_I is an interaction term between the subsystems. The object of interest is the reduced state ρ_S . We will make the assumption that the total state of system and environment begins in

a product of pure states (i.e. that there are no initial correlations) We obtain the reduced state of the system by employing the partial trace (where we suppress the time arguments apart from the initial states)

$$\rho_S = \text{Tr}_E(\rho_{SE}) = \text{Tr}_E\left(U_{SE}(\rho_S(0) \otimes \rho_E(0)) U_{SE}^\dagger\right). \quad (1.33)$$

We will write this equation using the Kraus representation [20]. We equip ourselves with an orthonormal basis for the Hilbert space of the environment, $\{|e_k\rangle\}$, such that the initial state of the environment is $\rho_E(0) = |e_0\rangle\langle e_0|$. We now can calculate the partial trace in (1.33)

$$\rho_S = \sum_k \langle e_k | U_{SE}(\rho_S(0) \otimes |e_0\rangle\langle e_0|) U_{SE}^\dagger | e_k \rangle. \quad (1.34)$$

We can rearrange the previous equation into a compact form

$$\rho_S = \sum_k K_k \rho_S(0) K_k^\dagger, \quad (1.35)$$

where we have introduced the Kraus operators

$$K_k \equiv (\mathbb{1}_S \otimes \langle e_k |) U_{SE} (\mathbb{1}_S \otimes |e_0\rangle). \quad (1.36)$$

The Kraus operators are not unique as they can be defined for any arbitrary choice of basis for the environment. They satisfy the trace-preserving relation

$$\sum_k K_k^\dagger K_k = \mathbb{1} \quad (1.37)$$

We can interpret the equation for the time-evolution of the reduced state as the action of a quantum channel \mathcal{E}

$$\rho_S = \sum_k K_k \rho_S(0) K_k^\dagger = \mathcal{E}(\rho_S(0)). \quad (1.38)$$

\mathcal{E} is a map acting on the state of the system, and as it maps a density matrix to a density matrix, it is a completely-positive trace-preserving map (CPTP). Treatment of E as an environment typically means that its Hilbert space dimension is far larger than that of the system, in which case it can become quickly intractable to find the Kraus operators that implement a quantum channel. However, we can calculate the reduced state of the system with a tractable equation that requires access only to information about the system itself using a few approximations. Firstly, we take the Born approximation

$$\rho_{SE} \approx \rho_S(t) \otimes \rho_E(0). \quad (1.39)$$

This implies that the for the purposes of time evolution that correlations between the system and the environment are not relevant, and global state is approximately separable at all times. The Markov approximation assumes that the environment has no memory of past interactions, that these correlations decay at a timescale much faster than the system's evolution. Finally we

take the rotating wave approximation to neglect fast-oscillations corresponding to counter-rotating terms in the time evolution of the density operator. This can be taken when the timescale of the system Hamiltonian is much shorter than the interaction Hamiltonian. These approximations hold remarkably well for many quantum systems of interest. As an example let us choose an atomic transition - say the hydrogen-alpha transition. Here the system is the hydrogen atom and the environment it is interacting with is the electromagnetic field. The timescale for the transition, or the inverse of the decay rate, is of order $t_{\text{emission}} \sim 10^{-9}\text{s}$, while both the period of the 656.28nm photon that is emitted and the correlation timescale of the electromagnetic field is of order 10^{-15}s . The large separation of timescales mean that all three approximations are quite natural in this setting. Correlations between the system and environment fall off rapidly compared to the timescale of the dynamics we care to model (the atomic transition). In reality the global state of the system and environment, (1.39), is not truly separable, the emitted photon causes correlations between the system and environment to grow. Physically we may think of the photon as travelling so far from the atom that the correlations it carries are no longer relevant for the future transitions of the system, meaning for all intents and purposes the global state is separable for the dynamics we are interested in. The sum of these approximations is to allow us to enforce the Markov semi-group property to the dynamical map \mathcal{E} [21]

$$\mathcal{E}_{t+s} = \mathcal{E}_t \mathcal{E}_s. \quad (1.40)$$

An exponential form, $\mathcal{E}_t = \exp\{\mathcal{L}t\}$ naturally satisfies the semigroup property

$$e^{\mathcal{L}(t+s)} = e^{\mathcal{L}t} e^{\mathcal{L}s}. \quad (1.41)$$

This implies that the equation of motion for the reduced state will have the following form

$$\frac{d}{dt} \rho_S(t) = \mathcal{L}(\rho_S(t)). \quad (1.42)$$

We can derive the most general form of this generator \mathcal{L} of the dynamical semigroup. We need a complete basis $\{O_i\}$ for our space of operators (which has dimension N^2 for a Hilbert space of dimension N). The elements are orthogonal with respect to the trace-norm

$$\text{Tr}\{O_i O_j\} = \delta_{ij}. \quad (1.43)$$

We take the last element of the basis to be the identity

$$O_{N^2} = \frac{1}{\sqrt{N}} \mathbb{1}, \quad (1.44)$$

which implies the other elements are traceless. We can write the quantum channel (1.5) in this basis as

$$\mathcal{E}_t(\rho_S) = \sum_{i,j=1}^{N^2} p_{ij} O_i \rho_S O_j^\dagger, \quad (1.45)$$

with

$$p_{ij} = \sum_k \text{Tr} [O_i K_k^\dagger] \text{Tr} [K_k O_j^\dagger]. \quad (1.46)$$

The matrix of coefficients, $p_{ij} = p_{ij}(t)$, is Hermitian and positive. We can expand \mathcal{L} for a small time-step (and leaving the time argument $\rho_S = \rho_S(0)$ as implicit)

$$\mathcal{L}\rho_S = \lim_{\epsilon \rightarrow 0} \frac{1}{\epsilon} \{ \mathcal{E}_\epsilon(\rho_S) - \rho_S \} \quad (1.47)$$

$$\begin{aligned} &= \lim_{\epsilon \rightarrow 0} \left\{ \frac{1}{N} \frac{p_{N^2 N^2}(\epsilon) - N}{\epsilon} \rho_S \right. \\ &\quad + \frac{1}{\sqrt{N}} \sum_{i=1}^{N^2-1} \left(\frac{p_{iN^2}(\epsilon)}{\epsilon} O_i \rho_S + \frac{p_{N^2 i}(\epsilon)}{\epsilon} \rho_S O_i^\dagger \right) \\ &\quad \left. + \sum_{i,j=1}^{N^2-1} \frac{p_{ij}(\epsilon)}{\epsilon} O_i \rho_S O_j^\dagger \right\}. \end{aligned} \quad (1.48)$$

We can redefine the coefficients for this small time-step as

$$a_{N^2 N^2} = \lim_{\epsilon \rightarrow 0} \frac{p_{N^2 N^2}(\epsilon) - N}{\epsilon}, \quad (1.49)$$

$$a_{iN^2} = \lim_{\epsilon \rightarrow 0} \frac{p_{iN^2}(\epsilon)}{\epsilon}, \quad i = 1, \dots, N^2 - 1, \quad (1.50)$$

$$a_{ij} = \lim_{\epsilon \rightarrow 0} \frac{p_{ij}(\epsilon)}{\epsilon}, \quad i, j = 1, \dots, N^2 - 1, \quad (1.51)$$

We group elements of our operator basis in terms of these redefined coefficients as

$$O = \frac{1}{\sqrt{N}} \sum_{i=1}^{N^2-1} a_{iN^2} O_i. \quad (1.52)$$

$$G = \frac{1}{2N} a_{N^2 N^2} \mathbb{1}_S + \frac{1}{2} (O^\dagger + O). \quad (1.53)$$

We can write a Hermitian operator from O

$$H = \frac{1}{2i} (O^\dagger - O), \quad (1.54)$$

which we recognise as the Hamiltonian of the system. This leaves us with

$$\mathcal{L}\rho_S = -i[H, \rho_S] + \{G, \rho_S\} + \sum_{i,j=1}^{N^2-1} a_{ij} O_i \rho_S O_j^\dagger. \quad (1.55)$$

As the map is CPTP, we have

$$\text{Tr}_S \mathcal{L}\rho_S = \frac{d}{dt}(\text{Tr}[\rho_S]) = 0. \quad (1.56)$$

Taking the trace of (1.55) and setting it to zero gives

$$\text{Tr}_S(-i[H, \rho_S] + \{G, \rho_S\} + \sum_{i,j=1}^{N^2-1} a_{ij} O_i \rho_S O_j^\dagger) = 0. \quad (1.57)$$

The trace of a commutator is zero, so we can eliminate the term that involves the Hamiltonian. After some manipulation, using the linearity of the trace and its cyclic property, we have

$$\text{Tr}_S(2G\rho_S + \sum_{i,j=1}^{N^2-1} a_{ij} O_j^\dagger O_i \rho_S) = 0. \quad (1.58)$$

As ρ_S has non-zero trace, we must have

$$G = -\frac{1}{2} \sum_{i,j=1}^{N^2-1} a_{ij} O_j^\dagger O_i. \quad (1.59)$$

This gives us the following form for the generator

$$\mathcal{L}\rho_S = -i[H, \rho_S] + \sum_{i,j=1}^{N^2-1} a_{ij} \left(O_i \rho_S O_j^\dagger - \frac{1}{2} \{O_j^\dagger O_i, \rho_S\} \right). \quad (1.60)$$

The coefficients are real and positive, and therefore the coefficient matrix a_{ij} can be diagonalised by some unitary transformation U_d to leave it with diagonal terms μ_i . The basis operators O_i also transform under this rotation to a set we denote as $\{L_i\}$. The result of this transformation is the Gorini-Kossakowski-Sudarshan-Lindblad master equation [21], henceforth the GKSL master equation

$$\mathcal{L}\rho_S = -i[H, \rho_S] + \sum_i^{N^2-1} \mu_i \left(L_i \rho_S L_i^\dagger - \frac{1}{2} \{L_i^\dagger L_i, \rho_S\} \right). \quad (1.61)$$

We refer to the operators L_i as jump operators, and μ_i as the coupling strength of the open system channel. We note that we recover the Liouville-von Neumann equation of motion in the limit that all coupling strengths are zero, resulting in a Hermitian generator for the dynamics. The terms proportional to μ_i are non-Hermitian, and have complex eigenvalues, resulting in phenomena such as decoherence. The GKSL equation is a powerful tool as it provides a theoretical framework for

quantum systems that are subject to noise and dissipation, as seen in experiment.

1.6 Overview

We will leverage all the above concepts throughout the remainder of the thesis. In Chapter 2 we will work in a closed system framework, exploring the energetic cost of using counterdiabatic control for quantum systems that exhibit a level crossing and continuous phase transition. We will leverage insights from non-equilibrium quantum physics to propose a novel counterdiabatic protocol that is highly effective while reducing the resource overheads for control compared to typical counterdiabatic methods. As we will also see, our protocol also allows for the natural relaxation of the system in question, which in certain cases means we outperform the more resource intensive “typical” schemes.

In Chapter 3 we will explore control in both a closed and open setting, this time with the aim of implementing quantum gates. We will again utilise the adiabatic gauge potential, but also introduce two more approaches to achieve transitionless dynamics. We compare and contrast the resource intensity, the robustness to timekeeping errors, and the susceptibility to environment-induced errors of each protocol when the dynamics are modelled by the GKSL master equation.

In Chapter 4 we leave the closed framework of quantum mechanics behind and embrace open system dynamics to explore how the environment can explain the transition from quantum to classical states. This transition is explained by the framework of Quantum Darwinism (QD). We will explore whether multiple open system channels acting on a system can support QD and leave the system in a classically objective state. Our novel insight is that it is the role of commutativity of the interaction Hamiltonians between the system and each of the modelled environments which allows us to discern whether competing channels allow for Darwinism or simply cause the state of the system to thermalise through a process known as information scrambling.

Finally, in Chapter 5 we will propose a measure of the *complexity* of dynamics that is governed by the GKSL master equation, which we denote as the operator spread complexity. We work in the Heisenberg picture, utilising the adjoint GKSL master equation to explore the evolution of a given test operator. We see that for chaotic systems, the operator rapidly grows in support in Hilbert space. This growth in support can be mitigated by open system effects, which tend to drive the operator towards more “simple” dynamics. We provide a proof that demonstrates that the operator spread complexity is minimised for a particular choice of basis for the operator spread complexity, namely the Krylov subspace.

Chapter 2

Control in the Impulse Regime

To fully exploit the promises of quantum devices [22, 23], efficient and effective techniques to achieve coherent control are crucial. Adiabatic methods are inherently stable but can require long timescales, particularly for many-body systems. These timescales are potentially longer than the decoherence time of the physical platform that realises the process of interest. Numerous approaches have been developed to control quantum systems quickly and to high precision. These additional controls imply an energetic cost for their implementation. A natural question arises - are we able to reduce the cost of control while still being able to implement processes quickly and with high precision? This chapter explores how we can answer this affirmatively, for a specific class of systems that are ubiquitous in quantum technology. Section 2.1 provides a background to the problem of control and energy efficiency, while section 3.1 outlines some of the technical framework that we leverage to minimise control time. The remainder of the chapter constitutes the original work found in [1], to which I contributed both theoretical work and each of the figures used below, with additional theoretical contributions and guidance from Steve Campbell and Anthony Kiely.

2.1 Background

In recent years, a number of techniques have been developed to control quantum systems. They can be broadly bisected into: (i) optimal control techniques [24], which efficiently find bespoke controls for a given task, often numerically, and (ii) shortcuts-to-adiabaticity [25, 26] which reproduce the same high fidelity as adiabatic passage but in significantly shorter times and are often analytic in nature. Recently, hybrid approaches have been shown to be highly effective [27–32].

Counterdiabatic driving [17, 33], as discussed in Chapter 1.2, is a particularly simple and effective shortcut-to-adiabaticity, achieving perfect control by adding auxiliary terms to a given system's Hamiltonian. Such an additional control term heuristically implies an overall increase in resources needed to evolve the system. Various cost measures have been developed [34–40] to characterise this. These measures have been shown to be closely related to quantum speed limits [39, 41, 42] and relevant for other control techniques [43–46]. In the case of critical systems with vanishing energy gaps, these cost measures indicate that the energetic resources needed to

implement high fidelity control diverge. Nevertheless, such systems offer significant promise in, for example, critical metrology [47], quantum annealers [48], and adiabatic quantum computing [49, 50]. Developing techniques which reduce the resource intensiveness while still achieving high fidelity control for critical systems is therefore timely for next-generation quantum technologies.

Topological defects were shown to be inevitable in field theories as a result of phase transitions in cosmological settings [51]. Remarkably, it was established that similar defect formation should occur in all phase transitions traversed withinin a finite time and it is precisely the critical slowing down in the vicinity of a phase transition that characterises the non-equilibrium dynamics of the system in terms of the equilibrium critical exponents [52]. Now, the celebrated Kibble-Zurek mechanism (KZM) has been applied in a great diversity of settings [53–59]. It predicts that the overall driven dynamics is split into two separate regimes. The evolution is “adiabatic” where the energy gap remains sufficiently large and the system can be driven without significant excitations being created; and “impulsive” when the system’s response freezes-out and defects rapidly form.

We exploit the insight provided by the KZM to devise an efficient strategy for achieving high fidelity control. We limit the application of the counterdiabatic control term to the duration of the system’s impulse regime, achieving significant energy savings without drastically sacrificing efficacy. While the system does generate some intermediate defects during the uncontrolled evolution in the adiabatic regimes [60], these regions are precisely those in which the KZM predicts that the system is able to relax. By restricting the application of counterdiabatic control to the impulse regime, we are still able to benefit from the good performance of adiabatic passage while simultaneously reducing the resource overheads compared with full evolution control.

2.2 Kibble-Zurek mechanism

As we have outlined, the KZM provides a framework to identify when a system crosses from the adiabatic to impulse regime and vice-versa. Let us formally introduce the mechanism. Consider a system $H(g)$ driven by an external field $g(t)$. We are interested in systems with a continuous second-order phase transition at $g=g_c$. Such a phase transition is typically described by equilibrium quantities [61, 62]

$$\xi(g) = \frac{\xi_0}{|g - g_c|^\nu}, \quad (2.1)$$

$$\tau(g) = \frac{\tau_0}{|g - g_c|^{z\nu}}. \quad (2.2)$$

Here, ξ and τ are the *correlation length* and *relaxation time* for our system, with the scaling for both as the driving parameter is changed given by the spatial exponent ν and the dynamical critical exponent z . These critical exponents define the universality class of the continuous phase transition. It is clear that both the relaxation timescale and correlation length in our system diverge as we approach the critical point, reducing the ability of the system to “heal”, or equilibrate out defects in its vicinity. More intuitively, we can understand this by recasting the relaxation timescale

of the system in terms of the gap, γ , between the two lowest energy levels of the system

$$\gamma(t) = E_1(t) - E_0(t), \quad (2.3)$$

where $E_1(t)$ and $E_0(t)$ are the ground and first-excited states, respectively. In natural units, the relaxation timescale, $\tau(t)$ is then

$$\tau(t) = \frac{1}{\gamma(t)}. \quad (2.4)$$

For critical systems, $\gamma(t) \propto g(t)$ [63]. The relaxation timescale reflects the ability for the system to react to changes in the driving parameter. As we get closer to the critical point during the ramp, the gap gets smaller and the relaxation timescale diverges. The system reacts slowly to perturbations, a phenomenon known as critical slowing down. As a result, defects arise in the state of the system. Far from the critical point, the gap is larger, allowing the system to easily react to changes in the ramp and evolve adiabatically. These two regimes are known as the impulse and adiabatic regimes respectively, and one of the key results of the Kibble-Zurek mechanism is the prediction of the crossover between the regimes. The transition times, t_{\mp} , are defined as when the relative rate of parameter change is comparable to the relaxation time. Formally, they are the solutions of

$$\left| \frac{g(t_{\mp}) - g_c}{\dot{g}(t_{\mp})} \right| = \tau(t_{\mp}). \quad (2.5)$$

We substitute (2.2) into (2.5) and rearrange to find

$$|g(t_{\mp}) - g_c| = \tau_0^{\frac{1}{z\nu+1}} |\dot{g}(t_{\mp})|^{\frac{1}{z\nu+1}}. \quad (2.6)$$

We consider a linear external field given by $g(t) = g_0 + g_d(t/\tau_Q)$. For convenience we assume a symmetric ramp, taking $g(\tau_Q/2) = g_c$. This fixes $g_d = 2(g_c - g_0)$. With this condition, we have

$$\left| 2(g_c - g_0) \frac{t_{\mp}}{\tau_Q} - (g_c - g_0) \right| = \tau_0^{\frac{1}{z\nu+1}} \left| 2(g_c - g_0) \frac{1}{\tau_Q} \right|^{\frac{1}{z\nu+1}}. \quad (2.7)$$

Multiplying through by $\tau_Q/2(g_c - g_0)$ and rearranging gives

$$t_{\mp} = \frac{\tau_Q}{2} \mp \tau_0^{\frac{1}{1+z\nu}} \left(\frac{\tau_Q}{2|g_0 - g_c|} \right)^{\frac{z\nu}{1+z\nu}}. \quad (2.8)$$

For the particular ramp we have defined, we can extract the adiabatic-impulse crossover times for a critical system given its universality class, and the dimensionful parameter τ_0 which is dependent on the exact system at hand. For $t \in [t_-, t_+]$, the system is in the impulse regime, where we expect the majority of diabatic transitions to occur. The correlation length at the crossover time

is

$$\xi = \xi_0 \left(\frac{2\tau_0 |g_0 - g_c|}{\tau_Q} \right)^{\frac{-\nu}{1+z\nu}}. \quad (2.9)$$

The density of defects for a system of dimension d then scales as $\xi^{-d} \sim \tau_Q^{-\frac{\nu d}{1+z\nu}}$. The dimensionful parameter τ_0 is dependent on the relevant energy gap of the specific model being employed. For some systems the gap is known explicitly, e.g. in the Landau-Zener model considered in Sec. 2.4, and therefore the exact expression for the relaxation time and resulting impulse regime can be employed. In the case of genuine many-body settings, such as the transverse field Ising model considered in Sec. 2.5, the gap can be approximated.

2.3 Control in the impulse regime

The KZM demonstrates that unwanted excitations or defects are mainly generated within the impulse regime, with the system evolving almost adiabatically otherwise. If our goal is to ramp this system quickly through its avoided crossing while remaining in its ground state, we will need to introduce some control. We will achieve this using the aforementioned counterdiabatic method, which we now briefly recap. Consider a Hamiltonian with spectral decomposition

$$H_0(t) = \sum_n \epsilon_n(t) |\phi_n(t)\rangle \langle \phi_n(t)|, \quad (2.10)$$

with $\epsilon_n(t)$ and $|\phi_n(t)\rangle$ the instantaneous energy eigenvalues and eigenstates, respectively. We will employ the counterdiabatic Hamiltonian [17],

$$H_{CD}(t) = i \sum_n [|\partial_t \phi_n(t)\rangle \langle \phi_n(t)| - \langle \phi_n(t)| \partial_t \phi_n(t)\rangle |\phi_n(t)\rangle \langle \phi_n(t)|]. \quad (2.11)$$

Evolving the system using the total Hamiltonian $H_0 + H_{CD}$ forbids any diabatic transitions. Adiabatic timescales diverge in critical systems due to vanishing energy gaps in the thermodynamic limit. Employing Eq. (2.11) for a given initial state allows one to adiabatically traverse a quantum phase transition (or avoided crossing in the case of the Landau-Zener model) in finite time [28, 64, 65]. However, the magnitude and complexity of the control fields near the critical point grow significantly with system size [34, 66] implying that control comes at a high energetic cost [39, 41, 43].

The intensity of this additional control field provides a meaningful of the energetic cost of the control [34, 66]¹

$$\mathcal{C} = \frac{1}{\tau_Q} \int_0^{\tau_Q} ds \|H_{CD}(s)\|, \quad (2.12)$$

¹In Ref. [34] the cost is defined as $\mathcal{C} = \frac{1}{\tau_Q} \int_0^{\tau_Q} ds \|H_{CD}(s)\|^n$, where the choice of n depends on the physical implementation. Here, we take $n=1$ for simplicity and remark that qualitatively similar behaviors are exhibited for other suitable choices of n .

where $\|\cdot\|$ is the Frobenius norm. The counterdiabatic Hamiltonian can physically be implemented by an external field coupled to the qubit, for example the magnetic field. We can then interpret this form of the cost as the time-averaged integrated power of the control field. It is clear that \mathcal{C} scales as $\sim 1/\tau_Q$ [34] from the form of H_{CD} . Note that the cost is lower bounded as

$$\mathcal{C} \geq \frac{\hbar}{\tau_Q} \int_{g_0}^{g(\tau_Q)} W[g] dg, \quad (2.13)$$

where $W[g] = \sqrt{\sum_{n,m \neq n} \left| \frac{\langle \phi_m | \partial_g H_0 | \phi_n \rangle}{\epsilon_n - \epsilon_m} \right|^2}$. The counterdiabatic Hamiltonian is inversely proportional to the level spacings in our system, as we demonstrated in (6.1). As a result we expect the cost to diverge as the gap closes and the matrix elements of the AGP correspondingly get large. In cases where the gap closes entirely, one may carefully regularise the AGP to remove degeneracies and keep it analytic. As the systems we will consider have a finite gap between the ground state and first excited state for finite system sizes we can neglect such a treatment of the AGP. In what follows, we consider a linear ramp for simplicity since any monotonic choice of g achieves the minimum of the cost measure employed.

In order to minimise energetic cost we propose limiting the use of a control strategy to only during the impulse regime, as opposed to employing control for the entire evolution. To test the effectiveness of this approach, we consider the Hamiltonian

$$H_\kappa(t) = H_0(t) + [\delta_{1\kappa} + \delta_{2\kappa} S(t)] H_{CD}(t), \quad (2.14)$$

where $\kappa \in \{0, 1, 2\}$ corresponds to uncontrolled, fully controlled, and control only in the impulse regime as recognised by the KZM, and δ_{ij} is the Kronecker delta. The crossover times for when the system crosses from the adiabatic to impulse regime and back are denoted as t_{\mp} , as given by Eq. (2.8). The control field H_{CD} is smoothly turned on during the impulse regime with a switching function $S(t) = f(t - t_-)f(t_+ - t)$, where $f(x) = 1/(1 + e^{-mx})$ is the logistic function and m a constant determining the abruptness of the switch. The relative energetic savings achieved by employing only impulse control ($\kappa = 2$) is $\delta E/\mathcal{C}$, where δE is the absolute energetic savings

$$\begin{aligned} \delta E &= \frac{1}{\tau_Q} \int_0^{\tau_Q} ds [1 - S(s)] \|H_{CD}(s)\|, \\ &\approx \frac{1}{\tau_Q} \left[\int_0^{t_-} ds \|H_{CD}(s)\| + \int_{t_+}^{\tau_Q} ds \|H_{CD}(s)\| \right]. \end{aligned} \quad (2.15)$$

As the quench time becomes shorter, $\tau_Q \rightarrow 0$, the impulse regime dominates $\{t_-, t_+\} \rightarrow \{0, \tau_Q\}$. Clearly then for impulse control, we should expect $\delta E \rightarrow 0$ and $\mathcal{F}(\tau_Q) \rightarrow 1$ in the short quench time limit. For long quench times, $\tau_Q \rightarrow \infty$, the impulse regime vanishes $t_{\mp} \rightarrow \tau_Q/2$. Therefore the relative savings $\delta E/\mathcal{C} \rightarrow 1$ and $\mathcal{F}(\tau_Q) \rightarrow 1$ due to the adiabatic theorem. As a rapid quench is dominated by the impulse regime and therefore would require control for the entire evolution, we do not expect much savings in this limit. Conversely, in the long time limit we will also expect

little in savings as adiabatic dynamics are achieved for most of the evolution without the need for control. We expect the protocol to be most advantageous in the intermediate regime, where we can establish a clear crossover between the adiabatic and impulse dynamics.

2.4 Landau-Zener Model

We begin our analysis with the Landau-Zener (LZ) model. It describes the transitions of a two-level quantum system interacting with an external field as it passes through resonance [67]. The Hamiltonian is

$$H_0(t) = \hbar\Delta\sigma_x + \hbar g(t)\sigma_z, \quad (2.16)$$

where $\Delta > 0$ determines the minimal energy gap at the avoided crossing. In what follows we take $\hbar = 1$. The Landau-Zener model is notable as, despite not exhibiting a bonafide quantum phase transition, it captures all basic features of the KZM [63, 68–70], including recovering the expected critical exponents: $\nu = 1$ and $z = 1$. Alongside this, it admits an analytical derivation of its transition amplitude. We shall outline the derivation of both features. Generally, we can write the state of the system as a complex combination of its eigenvectors

$$|\psi(t)\rangle = p_0(t)|g\rangle + p_1(t)|e\rangle, \quad (2.17)$$

where we have denoted the instantaneous ground and excited states as $|g\rangle$ and $|e\rangle$, respectively. The evolution of this state by Schrödinger equation results in a pair of coupled differential equations

$$i\dot{p}_0 = g(t)p_0(t) + \Delta p_1(t), \quad (2.18)$$

$$i\dot{p}_1 = \Delta p_0(t) - g(t)p_1(t). \quad (2.19)$$

We make the following change of variables

$$\tilde{p}_0(t) = e^{+i\int g(t)dt}p_0(t), \quad \tilde{p}_1 = e^{-i\int g(t)dt}p_1(t), \quad (2.20)$$

which leads to the coupled differential equations

$$i\dot{\tilde{p}}_0(t) = \Delta e^{+i\int g(t)dt}\tilde{p}_1(t) \quad (2.21)$$

$$i\dot{\tilde{p}}_1(t) = \Delta e^{-i\int g(t)dt}\tilde{p}_0(t) \quad (2.22)$$

Differentiation allows us to decouple the equations, giving

$$i\ddot{\tilde{p}}_0(t) - ig(t)\dot{\tilde{p}}_0(t) + \Delta^2\tilde{p}_0(t) = 0 \quad (2.23)$$

$$i\ddot{\tilde{p}}_1(t) + ig(t)\dot{\tilde{p}}_1(t) + \Delta^2\tilde{p}_1(t) = 0 \quad (2.24)$$

We consider a detuning function to be linear with a positive slope, $g(t) = \alpha t$, α having dimensions of frequency squared. In doing this we also set the crossing to be at $t = 0$. The amplitudes are constrained by $|p_0|^2 + |p_1|^2 = 1$ at all times, we need only solve for one of them. With the change of variables

$$\gamma(t) = e^{i\frac{\alpha t^2}{4}} \tilde{p}_1(t), \quad (2.25)$$

we can write (2.24) as

$$\ddot{\gamma} + \left(\frac{\alpha^2 t^2}{4} - i\frac{\alpha}{2} + \Delta^2 \right) \gamma = 0 \quad (2.26)$$

With one more change of variables [67], $z \equiv \sqrt{\alpha} e^{-i\pi/4} t$ and $x \equiv i\Delta^2/\alpha$, we can write (2.26) as

$$\partial_z^2 \gamma(t) + \left(x + \frac{1}{2} - \frac{z^2}{4} \right) \gamma(t) = 0. \quad (2.27)$$

This is the standard form of the Weber equation, which has two independent solutions, $\gamma(t) = \mathcal{D}_{-x-1}(-iz)$ and $\gamma(t) = \mathcal{D}_x(z)$ where $\mathcal{D}_x(z)$ is the parabolic cylinder function. This gives the solution for the amplitude as

$$p_0(t) = (a\mathcal{D}_{-x-1}(-i\sqrt{\alpha} e^{-i\pi/4} t) + b\mathcal{D}_x(\sqrt{\alpha} e^{-i\pi/4} t)) e^{i g_d t^2 / 4} \quad (2.28)$$

where a and b are fixed by initial conditions. By taking the initial and final times to $\mp\infty$ respectively, the asymptotic properties of the parabolic cylinder functions give rise to the Landau-Zener formula

$$|p_0(t \rightarrow \infty)|^2 \rightarrow 1 - e^{-2\frac{\pi\Delta^2}{\alpha}}. \quad (2.29)$$

This equation analytically predicts the probability of a diabatic transition from the initial state the system is in. For our purposes we will consider initialising the Landau-Zener model in its ground state. We will drive the system for some time, and a successful protocol is one that leaves the system in the ground state afterwards. We see from the Landau-Zener formula that for a finite driving rate, we will have some transitions away from our instantaneous ground state. Of course, one could drive with a slow (in our case, linear, but in principle arbitrary) ramp, taking $\alpha \ll 1$, which would lead to long times to implement any protocol in physical settings.

Next we need the control term for the LZM. We first write the exact energy eigenstates of the Landau-Zener model

$$|\phi_0(t)\rangle = \cos[\theta(t)]|0\rangle + \sin[\theta(t)]|1\rangle, \quad (2.30)$$

$$|\phi_1(t)\rangle = \sin[\theta(t)]|0\rangle - \cos[\theta(t)]|1\rangle, \quad (2.31)$$

where $\tan[\theta(t)] = -[g(t) + \sqrt{\Delta^2 + g(t)^2}] / \Delta$ and the energy gap between ground and excited states is $\gamma = \epsilon_1 - \epsilon_0 = 2\sqrt{g(t)^2 + \Delta^2}$. It is clear that its minimum is at $g(t_c) = 0$, which occurs

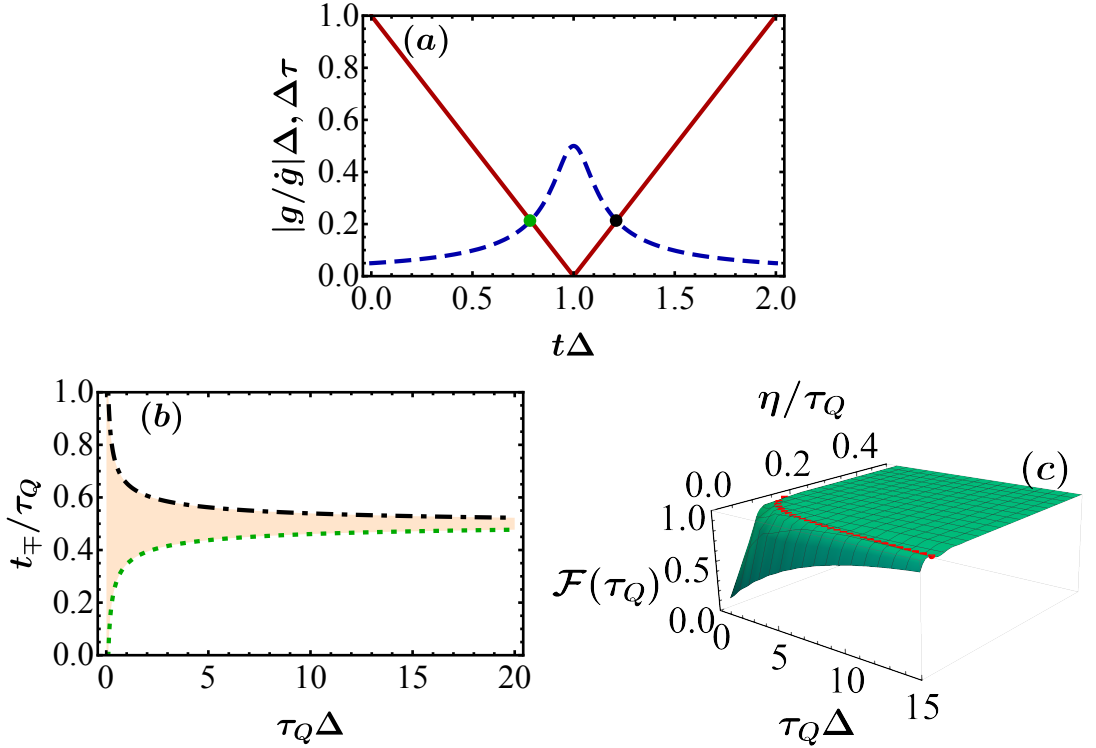


Figure 2.1: Impulse regime for the Landau-Zener model: (a) Comparison between relaxation timescale τ (red solid line) and the relative rate of external parameter change $|g/\dot{g}|$ (blue dashed line) for a quench duration of $\tau_Q\Delta = 2$. Intersection gives critical times t_{\mp} (green/black dots) (b) Impulse regime times t_{\mp} (green dotted and black dot-dashed lines respectively) for different quench times τ_Q . (c) Final state fidelity versus quench time τ_Q and duration of counterdiabatic driving 2η . Impulse regime $\eta = \mu$ (red points), $g_0 = -10\Delta$ and $m = 400\Delta^{-1}$.

halfway through our chosen ramping protocol. The counterdiabatic Hamiltonian is then [17]

$$H_{CD}(t) = \hbar\dot{\theta}\sigma_y = -\frac{\dot{g}(t)\Delta\hbar}{2[\Delta^2 + g(t)^2]}\sigma_y. \quad (2.32)$$

In Fig. 2.1(a) we show the adiabatic-impulse approximation of the KZM for a representative quench time of $\tau_Q\Delta=2$. The relaxation time of the LZM is shown in blue, while the rate of change of the driving field is shown in red. Where they intersect denotes the crossover time between the regimes, shown by the green and black dots. Note that the relaxation time of the system is the inverse of the gap, allowing us to recognise the avoided crossing of the Landau-Zener model where the gap is at its minimum. Solving for the real roots of Eq. (2.5) we find the exact adiabatic-impulse crossover time as given by the KZM to be $t_{\mp}=\tau_Q/2 \mp \mu$ where

$$\mu = \frac{1}{2}\sqrt{\frac{\sqrt{\tau_Q^4\Delta^4 + 4g_0^2\tau_Q^2} - \tau_Q^2\Delta^2}{2g_0^2}}. \quad (2.33)$$

Note that the impulse regime has a duration 2μ and $0 \leq \mu \leq \tau_Q/2$. For short operation times, the behaviour is $\mu \approx \sqrt{\tau_Q/|g_0|}/2$ which matches KZM scaling predictions for the $\nu=z=1$ universality class. Fig. 2.1(b) shows the impulse regime for a linear ramp of fixed magnitude as we vary the quench duration. The impulse regime is shown in the shaded region. It highlights that slow ramps recover effectively adiabatic dynamics with the width of the impulse regime closing as τ_Q grows, while for fast ramps the system is effectively always in the impulse regime. The performance of each protocol will firstly be quantified by focusing on the fidelity of the state of the system, $|\psi(t)\rangle$, evolving according to Hamiltonian Eq. (2.14) with the instantaneous ground state, i.e.

$$\mathcal{F}(t) = |\langle \psi(t) | \phi_0(t) \rangle|^2, \quad (2.34)$$

We assume $|\psi(0)\rangle = |\phi_0(0)\rangle$ as the initial condition in all cases i.e. the system starts in the ground state. In Fig. 2.1(c) we verify that control in the impulse regime is crucial for achieving a high fidelity final state. We implement a protocol in which the counterdiabatic control field is switched on for a duration of η before and after the system reaches the avoided crossing, i.e. H_{CD} is switched on/off at

$$\tilde{t}_{\mp} = \frac{\tau_Q}{2} \mp \eta, \quad (2.35)$$

where $\eta \in [0, \tau_Q/2]$. This smoothly interpolates between the three cases captured by Eq. (2.14) with $\eta = \{0, \tau_Q/2, \mu\}$ corresponding to $\kappa = \{0, 1, 2\}$ respectively. The red-dashed line delineates the adiabatic-impulse crossover and we see that there is a precipitous drop when the control is applied for a duration smaller than the impulse regime, i.e. $\eta < \mu$. For protocols with $\eta > \mu$ we see that there is little gain in target fidelity by continuing to employ the counterdiabatic term.

We now take a more systematic look at the three protocols, having established that high-fidelity final states are principally reliant on implementing control when the system is in the impulse regime. The instantaneous fidelity with the ground state for the three cases are shown in Fig. 2.2 for various quench durations. The evolution under full counterdiabatic control remains in the ground state at all times by construction and therefore results in a perfect fidelity. If no control is applied the system maintains a high instantaneous fidelity initially, but this rapidly decreases once it enters the impulse regime, delineated by the orange shaded area. For short quench times, once the fidelity drops off there is little revival. However, for sufficiently long times, where the impulse regime is short enough that significant defects are not generated (e.g. $\tau_Q = 25\Delta^{-1}$ in Fig. 2.2(d) [dashed, blue curve]), after an initial dip the fidelity increases again outside impulse regime. This dip and revival behaviour is a generic feature of adiabatic passage and is a result of the adiabatic error on the instantaneous fidelity scaling as $1/\tau_Q$, while the error on the final state fidelity scales as $1/\tau_Q^2$ [60].

For impulse control (solid, red curves) the instantaneous fidelity initially follows the uncontrolled case. However, when entering the impulse regime the counterdiabatic control is switched on which negates any non-adiabatic transitions between the energy eigenstates and therefore freezes the instantaneous fidelity in this region. By freezing the system only in the impulse regime we

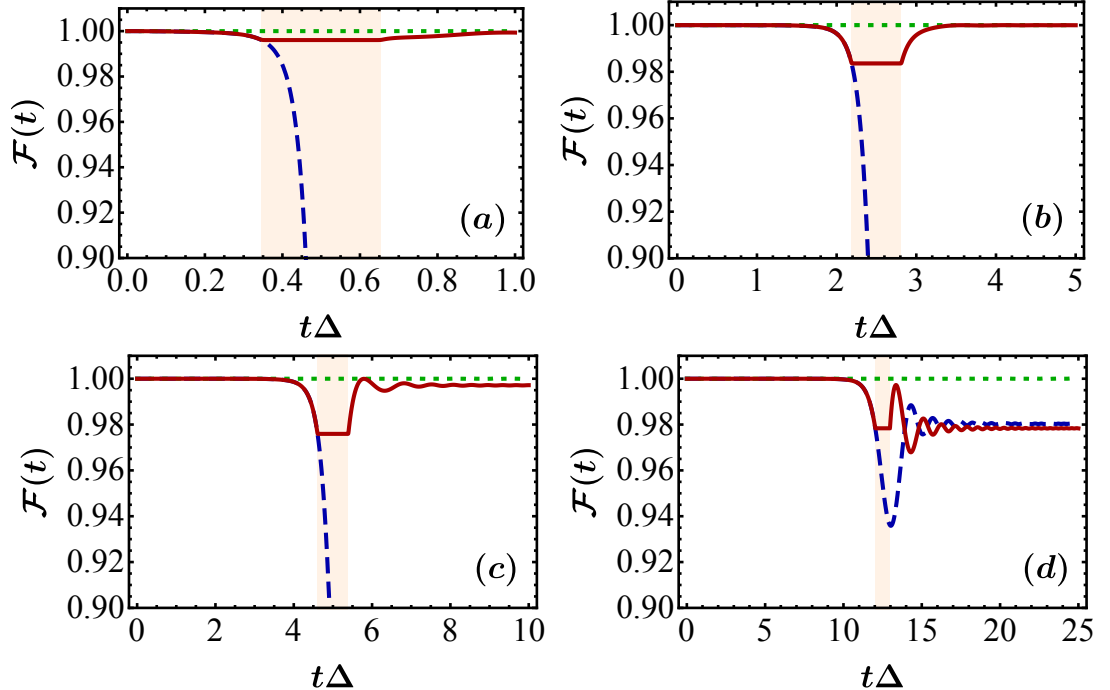


Figure 2.2: Fidelity of the evolving state with the instantaneous ground state of the Landau-Zener model for no control (blue dashed line), impulse control (red solid line) and full control (green dotted line), for different quench times. Orange shaded area indicates the impulse regime $[t_-, t_+]$. (a) $\tau_Q\Delta = 1$ (b) $\tau_Q\Delta = 5$ (c) $\tau_Q\Delta = 10$ (d) $\tau_Q\Delta = 25$. Other parameters: $g_0 = -10\Delta$ and $m = 400\Delta^{-1}$

are able to suppress most of the defects from forming such that the resulting final free evolution often leads to excellent state transfer. The resulting final fidelities are comparable to the case of full control despite the control field only being on for a fraction of the total quench time. As we increase τ_Q , resulting in a closing of the impulse regime, our impulse control scheme no longer provides an advantage over the uncontrolled evolution. Upon exiting the impulse regime the dynamics is adiabatic, leading to approximately constant fidelity, as seen in Fig. 2.2(d). Therefore any population lost in the first stage cannot be recovered. Note that we have focused on symmetric ramps for simplicity, but the strategy of impulse control can be easily generalised to asymmetric ramps.

Turning our attention to the energetic savings, Fig. 2.3 demonstrates that significantly better efficiency can be achieved with only a small loss in final state fidelity. In panel (a) we show the loss of final state fidelity, i.e. $1 - \mathcal{F}$, achieved for impulse control as a function of total quench duration and for reference we also show the no-control case which follows the well known Landau-Zener formula $\exp(-\pi\Delta^2/|\dot{g}|)$ [67, 71]. For large quench durations (corresponding to a small impulse regimes) $\tau_Q\Delta \sim 25$, implementing control turns out to be detrimental. For small quench times, where the impulse regime dominates most of the protocol, the loss in the final fidelities are vanishingly small since this case overlaps significantly with the full control case. As τ_Q is increased

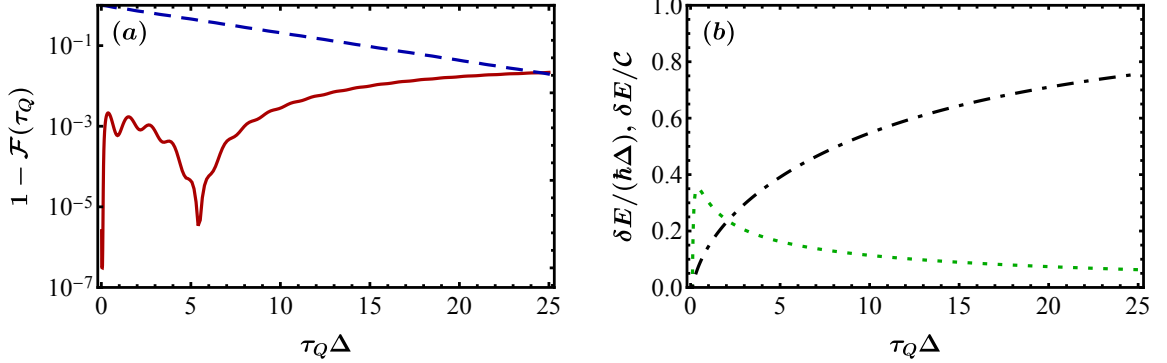


Figure 2.3: Comparison between final state fidelity using impulse control and the resulting energetic savings. (a) Loss of fidelity at the end of the process using impulse control (red solid line). Also shown is the result after no control (blue dashed line). (b) Difference in energetic cost δE (green dotted line) and relative difference in energetic cost $\delta E/\mathcal{C}$ (black dot-dashed line). Other parameters: $g_0 = -10\Delta$ and $m = 400\Delta^{-1}$.

we see a small increase in the loss of fidelity, which nevertheless remains $\lesssim 0.001$, indicating that the protocol is still highly effective. Impulse control is shown to be particularly effective around $\tau_Q \Delta = 5$ for the chosen final target state. Panel (b) demonstrates that while maintaining a high level of efficacy, impulse control allows for a significant reduction in the energetic cost, with fidelity losses of the order $\sim 10^{-5}$ while making a relative energetic saving of $\sim 40\%$. The absolute energetic saving clearly tends to zero in the short and long quench time limit and the relative energetic savings tends to 1 in the long quench time limit. We can analytically derive both the cost of control and the relative savings from truncating the control in time to the impulse regime. We assume for simplicity that $S(t)$ is exactly a step function and $g_0 < g_c$. Integrating the norm of the counterdiabatic term in the impulse regime gives

$$\int_{t_1}^{t_2} \|H_{CD}(s)\| ds = \sqrt{2} \left\{ \arctan \left[\frac{g(t_2)}{\Delta} \right] - \arctan \left[\frac{g(t_1)}{\Delta} \right] \right\}. \quad (2.36)$$

Substitution of this into our expression for the cost given by (2.12) gives

$$\mathcal{C} = -\frac{\sqrt{2}}{\tau_Q} \arctan \left(\frac{g_0}{\Delta} \right). \quad (2.37)$$

Similarly, the relative savings in this case are

$$\delta E = \frac{\sqrt{2}}{\tau_Q} \left\{ \arctan \left[\frac{g(t_-)}{\Delta} \right] - \arctan \left(\frac{g_0}{\Delta} \right) \right\}. \quad (2.38)$$

Using Eq. (2.15), we can then find the relative savings

$$\delta E/\mathcal{C} = 1 - \frac{\arctan [g(t_-)/\Delta]}{\arctan (g_0/\Delta)}. \quad (2.39)$$

The above analytic expressions align with the numerical results shown in Fig. 2.3 (b).

2.5 Transverse-Field Ising Model

We now turn our attention to the transverse field Ising model (TFIM). While the Landau-Zener model behaves according to the predictions of the Kibble-Zurek mechanism, it does not strictly have a second-order phase transition, and instead has an avoided crossing with a finite gap for finite Δ . The TFIM on the other hand is gapless at its critical point in the thermodynamic limit. We take the following Hamiltonian

$$H_0(t) = -\omega \sum_{i=1}^N [g(t) \sigma_i^x + \sigma_i^z \sigma_{i+1}^z]. \quad (2.40)$$

We impose periodic boundary conditions $\sigma_{N+1}^{x,y,z} = \sigma_1^{x,y,z}$ and take the number of spins, N , to be even. The TFIM is in the same universality class as the Landau-Zener model, exhibiting its second-order quantum phase transition at $g_c=1$ [70] between a ferromagnetic and a symmetric paramagnetic phase. It has a \mathcal{Z}_2 symmetry, generated by $\mathcal{S} = \prod_{i=1}^N \sigma_i^x$

$$\mathcal{S}\sigma_i^x = \sigma_i^x, \quad (2.41)$$

$$\mathcal{S}\sigma_i^z = -\sigma_i^z. \quad (2.42)$$

The model has two competing terms, we can first look at the interacting part

$$H_F = -\omega \sum_{i=1}^N \sigma_i^z \sigma_{i+1}^z. \quad (2.43)$$

This term has a degenerate groundstate, it can be a linear combination of the following two eigenvectors

$$|+\rangle = |\uparrow\uparrow \dots \uparrow\rangle, \quad (2.44)$$

$$|- \rangle = |\downarrow\downarrow \dots \downarrow\rangle. \quad (2.45)$$

For our purposes we will break the \mathcal{Z}_2 symmetry in this phase, to do so we will add a small biasing field, $-\epsilon\sigma^x$, with $\epsilon > 0$. This leaves us with a ferromagnetic ground state, i.e. one that favours spins aligning. The other term in the Hamiltonian is

$$H_P = -\omega g \sum_{i=1}^N \sigma_x. \quad (2.46)$$

Its groundstate is

$$|g\rangle = |\rightarrow\rightarrow\dots\rightarrow\rangle. \quad (2.47)$$

This unique paramagnetic ground state preserves the Z_2 symmetry. The interesting physics comes into play as the two terms compete as g is ramped. The system cannot smoothly interpolate from one groundstate to the other. We can make this a bit more precise with a small amount of perturbation theory. We prepare the system deep in the paramagnetic regime, i.e. $g \gg 1$. Here H_P dominates, and we note that an excitation above the ground state $|g\rangle$ involves flipping a single spin. There are N possible spins to flip, we denote each state with a single spin-flip at site n as $|n\rangle$,

$$|n=2\rangle = |\rightarrow\leftarrow\rightarrow\dots\rightarrow\rangle. \quad (2.48)$$

From (2.46) we can see that it takes $2\omega g$ units of energy for this single spin flip. We consider H_F as the perturbation. The action of σ_i^Z is $\sigma_i^Z |\rightarrow_i\rangle = |\leftarrow_i\rangle$, so the action of the ferromagnetic term is naturally

$$\sigma_i^Z \sigma_{i+1}^Z |\leftarrow_i\rightarrow_{i+1}\rangle = |\rightarrow_i\leftarrow_{i+1}\rangle, \quad (2.49)$$

i.e. it transfers the spin flip along one site. We can write an effective Hamiltonian for this first order perturbation as

$$H_{eff} |n\rangle = -\omega(|n+1\rangle + |n-1\rangle) + (E_0 + 2\omega g) |n\rangle, \quad (2.50)$$

where we denote the ground state energy of the TFIM as E_0 . We can solve this in momentum space, with the discrete Fourier transform

$$|k\rangle = \frac{1}{\sqrt{N}} \sum_{j=1}^N e^{-ikj}, \quad (2.51)$$

where we have taken the lattice spacing as unity and that the wavenumber is discretised as $k = 2\pi n/N$ for $n = 1, \dots, N$. This diagonalises (2.50), giving

$$H_{eff} |k\rangle = (2\omega g - 2\omega(g - \cos k) + E_0) |k\rangle. \quad (2.52)$$

The dispersion relation for the spinons, our excitations in momentum space of the effective theory, can read off as

$$\epsilon(k) = 2\omega(g - \cos k) \stackrel{\lim_{k \rightarrow 0}}{\approx} \Delta + Jk^2, \quad (2.53)$$

where $\Delta = 2\omega(g - 1)$. The gap in the spinon dispersion goes to zero at $g = 1$, the spin flip excitations condense. A similar calculation can be carried out from the other limit of the model, taking H_F as the Hamiltonian and H_P as the perturbation. Here the excitations are domain walls in the ground state, and similarly the perturbation at first-order is a kinetic term for these excitations. What is important is that in both cases we end up with a prediction of something interesting happening in the ground-state of the theory at $g = 1$. To find the exact spectrum of

the TFIM we employ the Jordan-Wigner transformation. First, we rotate Eq. (2.40) around the y axis to map $\sigma_i^z \rightarrow \sigma_i^x$ and $\sigma_i^x \rightarrow -\sigma_i^z$ and substituting

$$\sigma_j^x = 1 - 2c_j^\dagger c_j, \quad (2.54)$$

$$\sigma_j^z = -(c_j + c_j^\dagger) \prod_{m < n} (1 - 2c_m^\dagger c_m), \quad (2.55)$$

where c_j^\dagger and c_j are fermionic creation and annihilation operators respectively at site j . We again perform a discrete Fourier transformation $c_k = \frac{1}{\sqrt{N}} \sum_j e^{-ikj} c_j$. This decouples the Hamiltonian as $H_0 = \bigoplus_{k>0} \Psi_k^\dagger H_{0,k} \Psi_k$ where $\Psi_k^\dagger = (c_k^\dagger, c_{-k})$. Each momentum subspace is governed by a LZ type Hamiltonian

$$H_{0,k} = h_k^x \sigma_k^x - h_k^z(g) \sigma_k^z, \quad (2.56)$$

where $h_k^z(g) = 2\omega[g - \cos k]$ and $h_k^x = 2\hbar\omega \sin k$. Note that the momentum only takes on discrete values $k_n = \frac{\pi(2n-1)}{N}$ for $n = 1, \dots, N/2$. The eigenstates of $H_{0,k}$ are

$$|\phi_{0,k}(t)\rangle = \cos[\theta_k(t)] |0\rangle_k + \sin[\theta_k(t)] |1\rangle_k, \quad (2.57)$$

$$|\phi_{1,k}(t)\rangle = \sin[\theta_k(t)] |0\rangle_k - \cos[\theta_k(t)] |1\rangle_k, \quad (2.58)$$

where $\tan[\theta_k(t)] = [h_k^z - \sqrt{h_k^{x,2} + h_k^{z,2}}] / h_k^x$. The ground state of the system is then given by $|\phi_0(t)\rangle = \bigotimes_{k>0} |\phi_{0,k}(t)\rangle$. If the evolved state of the system is written as $|\psi(t)\rangle = \bigotimes_{k>0} |\psi_k(t)\rangle$, then the fidelity becomes

$$\mathcal{F}(t) = |\langle \psi(t) | \phi_0(t) \rangle|^2 = \left| \prod_{k>0} \langle \psi_k(t) | \phi_{0,k}(t) \rangle \right|^2. \quad (2.59)$$

To protocol we wish to implement is to start in the ground state of the ferromagnetic phase of the model, ramping it linearly from $g(0) \approx 0$ to $g(\tau_Q) = 2$, where we should end up in the ground state in the paramagnetic regime. The process hinges on arriving in the ground state. As we have shown with a simple calculation, the TFIM admits excitations quite easily at $g_c = 1$. Control is crucial to ensure we end up in the ground state after the ramping protocol. As the form of the Hamiltonian for each decoupled subspace after the Jordan-Wigner transformation has the form of the Landau-Zener model, we can map the form of its counterdiabatic term to it. This leads to [64] (for even N)

$$H_{CD,k} = \frac{\dot{g} \sin k}{2[g^2 - 2g \cos k + 1]} \sigma_k^y. \quad (2.60)$$

The Jordan-Wigner transformation is highly non-local, with higher subscript c_j operators requiring support over many-spins, and then each k subspace in the momentum picture having support over all c_j operators. The energy gap for each momentum subspace is given by

$\gamma_k = 4\hbar\omega\sqrt{g(t)^2 - 2g(t)\cos k + 1}$, which vanishes in the thermodynamic limit at the critical point. For a finite number of spins the gap between ground and first excited state remains finite, shrinking as $\sim 1/N$, and only the lowest subspace, k_0 , is critical. To determine adiabatic-impulse crossover times we approximate this gap as $\gamma_0 \approx 4\hbar\omega|g(t) - 1|$ [70, 72]. The resulting crossover times, assuming $g_0 < 1$, are again found by solving for the real roots of Eq. (2.5) giving

$$t_{\mp} = \frac{\tau_Q}{2} \mp \sqrt{\frac{\tau_Q}{8\omega(1-g_0)}}, \quad (2.61)$$

which agrees with the predicted KZM scaling, Eq. (2.8). Note that the impulse regime vanishes for long quench times $(t_+ - t_-)/\tau_Q \rightarrow 0$ but does not behave correctly for short quench times $\tau_Q < 1/(2\omega[1-g_0])$ due to the approximation of the energy gap.

In Fig. 2.4(a) and (b) we show the fidelity with the instantaneous ground state for the three cases of no control, full control, and impulse control for a system size of $N=16$, where qualitatively similar behaviors with the LZ model are exhibited. By employing control only during the impulse regime the most detrimental period of defect formation is suppressed and good target state fidelities are achieved. The effectiveness of impulse control is thoroughly demonstrated by comparing Fig. 2.4(c) and (d). Here we show the final target state fidelity as a function of system size and quench duration. When no control is applied, i.e. $\kappa = 0$ shown in panel (c), we see that defects rapidly form for larger systems due to the effect of the impulse regime, leading to small final fidelities (lighter, blue region). These results are well described by the Landau-Zener formula applied to the lowest momentum subspace $\mathcal{F}(\tau_Q) \approx 1 - \exp\left[-\frac{2\pi\omega}{|\dot{g}|}\sin^2\left(\frac{\pi}{N}\right)\right]$ [72]. Employing impulse control provides a significant increase in the final state fidelities, cfr. Fig. 2.4(b). For extremely short quench times, $\tau_Q\omega < 1$, the impulse regime dominates the dynamics and therefore the control term is effectively on for the entire protocol duration. There is then a region of low-fidelity (blue-coloured) for $1 < \tau_Q\omega < 6$ for sufficiently large system sizes. In this region the rapid losses in fidelity during the short adiabatic regimes are too severe to be recovered. Nevertheless, beyond this small pathological region in parameter space, impulse-only control is highly effective in comparison to uncontrolled evolution, consistently outperforming the uncontrolled case for a range of longer quench times. However, similar to the LZ case, once as approach adiabatic timescales the uncontrolled case can have a slightly higher fidelity than impulse control (upper left quadrant of Fig. 2.4(c) vs (d)). As previously noted in the LZ setting, this is due to eigenstate population being approximately constant leaving the impulse regime, removing any possibility to recover any lost fidelity from the initial period of free evolution.

We now focus on the energetic costs. In Fig. 2.4 we see that the absolute, panel (e), and relative, panel (f), energetic savings are consistent with the behavior exhibited in the LZ case. We see from Fig. 2.4(e) that the energetic savings are extensive with the size of the system, however the relative savings exhibits a clear converging, intensive behavior. Nevertheless, a significant saving in the energetic overheads can be achieved while still achieving effective control. Similar to the LZ model, exact expressions for the cost measures in this case can be determined. The

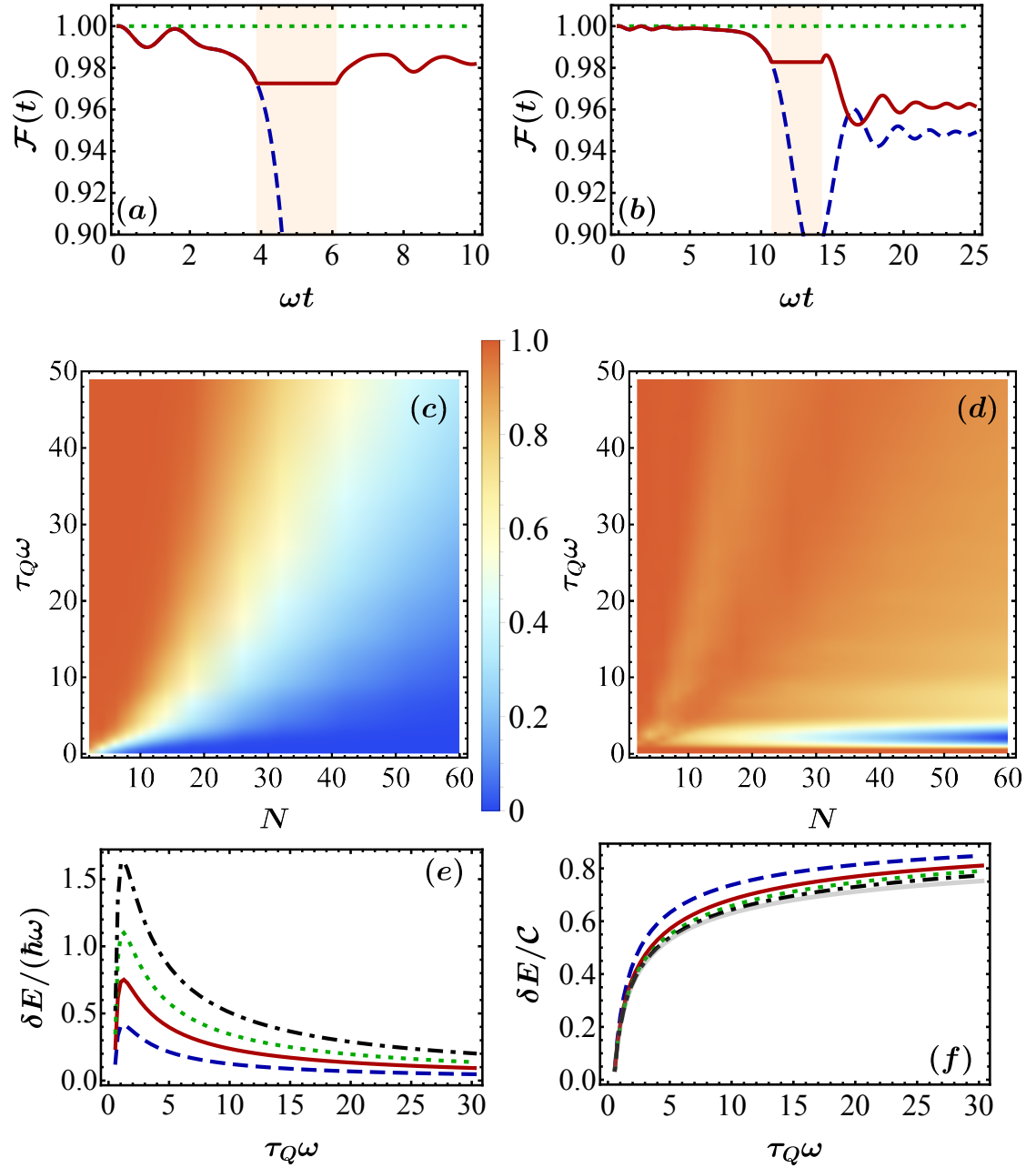


Figure 2.4: The instantaneous fidelity of TFIM for no control (blue dashed line), impulse control (red solid line) and full control (green dotted line), for different quench times. Orange shaded area indicates the impulse regime $[t_-, t_+]$ (a) $\omega\tau_Q = 10$ (b) $\omega\tau_Q = 25$ for $N = 16$. Panels (c) and (d) show the final state fidelity for TFIM versus quench time τ_Q and system size N for the (c) uncontrolled case and (d) impulse control. Red indicates high final state fidelity, with blue corresponding to low final state fidelity. Panels (e) and (f): Energetic savings versus quench time τ_Q . $N = 4, 8, 12, 18$ (blue dashed line, red solid line, green dotted line, black dot-dashed line) and thermodynamic limit (light gray thick solid line). (e) Savings δE (f) relative savings $\delta E/\mathcal{C}$. In all panels, $g_0 = 0$ and $m = 100\omega^{-1}$

norm can be written as $\|H_{CD}\| = \sum_{k>0} \|H_{CD,k}\|$. The associated energetic cost, Eq. (2.12), is then [42]

$$\mathcal{C} = \frac{\hbar}{\sqrt{2}\tau_Q} \sum_{k>0} \int_0^{\tau_Q} ds \left| \frac{\dot{g} \sin k}{g(s)^2 - 2g(s) \cos k + 1} \right|. \quad (2.62)$$

This can be rewritten as

$$\mathcal{C} = \frac{\hbar}{\sqrt{2}\tau_Q} \sum_{k>0} \left\{ \arctan \left[\frac{g(\tau_Q) - \cos k}{\sin k} \right] - \arctan \left[\frac{g_0 - \cos k}{\sin k} \right] \right\}. \quad (2.63)$$

The extensive nature of this and the absolute savings, Eq. (2.15) can be explicitly seen by noting that in the thermodynamic limit we can make the replacement $\sum_{k>0} \rightarrow \frac{N}{2\pi} \int_0^\pi dk$,

$$\delta E \approx \frac{\hbar N}{2\sqrt{2}\pi\tau_Q} \{ \Phi[g(\tau_Q)] - \Phi[g(t_+)] + \Phi[g(t_-)] - \Phi[g_0] \}, \quad (2.64)$$

where we have defined $\Phi[g] = \int_0^\pi dx \arctan \left[\frac{g - \cos(x)}{\sin(x)} \right]$. In this limit then, the relative cost becomes

$$\delta E/\mathcal{C} = 1 - \frac{\Phi[g(t_+)] - \Phi[g(t_-)]}{\Phi[g(\tau_Q)] - \Phi[g_0]}, \quad (2.65)$$

which is clearly intensive. These expressions agree with the numerical results shown in Fig. 2.4.

While the Jordan-Wigner transformation allows for a significant computational speedup over working with the Hamiltonian in the original spin basis, we do gain more insight into the importance of local and few body control terms for the system, which are typically more experimentally feasible. In the spin picture, the counterdiabatic control term has been exactly determined (again for even N) as [64, 65]

$$H_{CD} = -\dot{g} \left[\sum_{m=1}^{M-1} u_m(g) H_{CD}^{[m]} + \delta_{M,N/2} \frac{1}{2} u_{N/2}(g) H_{CD}^{[N/2]} \right], \quad (2.66)$$

$$H_{CD}^{[m]} = \sum_{n=1}^N \left[\sigma_n^x \left(\prod_{j=n+1}^{n+m-1} \sigma_j^z \right) \sigma_{n+m}^y + \sigma_n^y \left(\prod_{j=n+1}^{n+m-1} \sigma_j^z \right) \sigma_{n+m}^x \right], \quad (2.67)$$

$$u_m(g) = \frac{g^{2m} + g^N}{8g^{m+1}(1 + g^N)}. \quad (2.68)$$

Here M denotes the maximum range of the interactions, with the exact counterdiabatic term given by $M = N/2$. This Hamiltonian clearly highlights the necessity for non-local terms, which can incur high complexity and energetic costs [39].

We can truncate the control terms to restricted range(s) M . For clarity, we consider $N = 6$ although remark that we expect qualitatively similar behaviors to hold for larger systems. In Fig. 2.5(a) we plot the final state fidelity for a range of quench times, employing the control terms

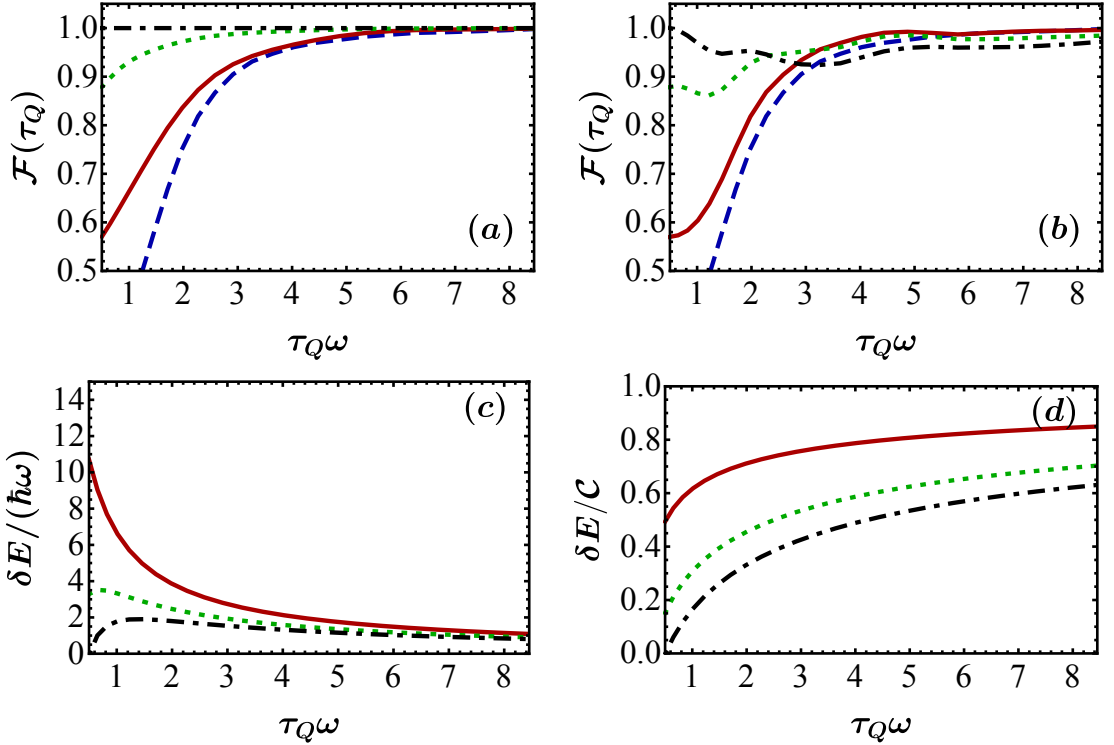


Figure 2.5: The final state fidelity for the $N = 6$ TFIM versus quench time for uncontrolled evolution (dashed, blue), $M = 1$ (i.e. two-body control, solid red), $M = 2$ (three body control, dotted green) and $M = 3$ (i.e. full control, dot-dashed black). In panel (a) we show the performance when the control term is always on for the entire evolution, while panel (b) corresponds to impulse control. Panels (c) and (d) show the energetic savings versus quench time τ_Q for the same truncated-range impulse control protocol in (b), with the same colour scheme as before. (c) Savings δE relative to employing full range, full quench cost C (d) relative savings $\delta E/C$. Other parameters: $g_0 = 0.01$ and $m = 100\omega^{-1}$

for the entire quench. In line with intuition, the fidelities arrange themselves into a hierarchy for short quench times. The uncontrolled case performs the worst, while longer range more complex control works increasingly well until it achieves perfect final fidelities for full control ($M=3$ in this case), with the relative difference in performance reducing as we approach the adiabatic limit. For the case of impulse control, Fig. 2.5(b), the same hierarchy holds for very fast protocols. However, as the quench time is increased we see several crossovers in relative performance, indicating that for such intermediate quench times, impulse control exhibits a “less is more” behavior whereby better (although not perfect) target state fidelities can be achieved by employing a simpler control term in the impulse regime and significant energetic savings can be achieved, cfr. Fig. 2.5(c) and (d).

2.6 Conclusion

We have demonstrated that high fidelity coherent control can be achieved at a lower resource overhead by restricting the application of control techniques to when they are strictly necessary. By exploiting the framework provided by the Kibble-Zurek mechanism, which divides the dynamical response of a system driven through a critical point into adiabatic and impulse regimes, we have shown that high target state fidelities can be achieved by only implementing control during the impulse regime. The intuition for this effect relies on the underlying physical principles of the KZM; the adiabatic regime is characterised by a dynamics which is varying sufficiently slow, compared to the energy gap, such that the system is still able to relax. Under these conditions, even though the system may transiently generate some excitations, the system recovers - a remarkably generic feature of adiabatic protocols [60]. In contrast, we have shown that control is essential in the impulse regime. Due to the typically high energetic cost associated with various control protocols [41, 43], we have shown that significant energetic savings can be achieved using impulse control without significantly sacrificing efficacy.

Chapter 3

Robustness of Controlled Unitary Gates

The idea of using quantum properties of matter and light to process information has given rise to an extensive research effort. Beyond the implications for basic science, quantum information technologies would entail a significant computational speed-up for particular applications [22, 23, 73] compared to classical algorithms. These quantum advantages have been theoretically predicted for a variety of information processing tasks, such as search and factoring algorithms, quantum cryptography, and Hamiltonian simulation. Experimentally it is now possible to implement them in systems such as superconducting qubits [74, 75], trapped ions [76], and photons [77]. Several approaches for universal quantum computation have been developed, chief among them being measurement-based [78–81], gate-based [82], and adiabatic models [83, 84]. The relative benefits and drawbacks of each approach notwithstanding [22, 73], gate-based quantum computation presents an attractive method. Any computation can be implemented by a relatively small set of gates on a qubit register [82, 85]. Indeed, small scale quantum devices provide remarkable platforms for simulation of quantum systems [86–88], insights from which can be greatly enhanced by improving the implementation of the basic building blocks for the gate-based approach for universal quantum computing, i.e. the quantum gates themselves.

Achieving this aim necessitates coherent control of quantum systems [1, 5, 25, 26, 89–91]. Beyond the basic requirement of enacting the desired gate operation, we must consider several additional factors to ensure the scalability and reliability of these operations. Among these are the resources necessary for their fast and accurate implementation [6, 92–104], understanding the spoiling impact of the environment [105–107], and the impact of operational errors [108, 109]. The assessment of the energetic efficiency of these devices is crucial in their design [6] and may enforce practical constraints for their implementation. The interplay between the performance of a quantum computing machine and its energetic efficiency determines a fundamental connection between quantum information processing and thermodynamics [110, 111].

Following this edict, in this chapter we consider three approaches to implement gate operations

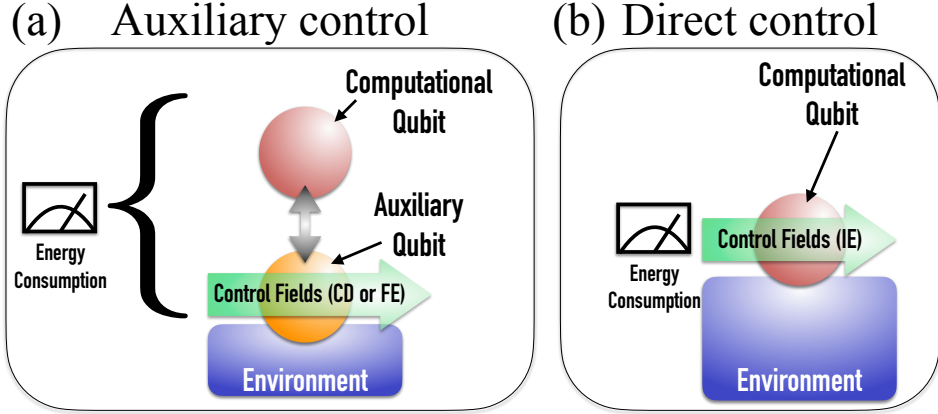


Figure 3.1: (a) Shows the auxiliary control setting based on the protocol from Ref. [113]. Here an auxiliary qubit is coupled to the computational register, with control fields acting only on this auxiliary system. We assume the driven qubit can also experience environmental effects while the computational qubit is completely isolated. (b) Shows the setup for the Inverse Engineering setting. The Hamiltonian is designed without any additional resources, and therefore the computational qubit is driven directly and can be subject to environmental noise.

on quantum systems through controlled Hamiltonian dynamics. In particular, we consider the auxiliary evolution approach introduced in Refs. [112, 113], where a driven *auxiliary* system is coupled to the computational register upon which the operation is faithfully induced provided the evolution is adiabatic. We augment this approach with techniques from shortcuts-to-adiabaticity [25, 26], specifically counterdiabatic driving (CD) [17, 33, 66, 114] and Floquet engineering (FE) [115], that allow to arbitrarily speed up the implementation, albeit with an increased energetic cost. In addition to these techniques, we consider an inverse engineering (IE) approach [116] where the computational register is *directly* driven by external control fields. We examine these approaches, both in terms of their resource overhead and their resilience to systematic errors stemming from imperfect timekeeping and environmental effects. Section 2.1 outlines the control techniques used in this work. Section 2.2 introduces the benchmarks for the robustness of a gate implementation. The remainder of the chapter constitutes the original work found in [3] which was done in collaboration with Barış Çakmak and Steve Campbell. The numerical and analytical results below were provided by myself.

3.1 Controlled Gate Techniques

Here we outline the three control techniques that are the focus of the present Chapter. As shown in Fig. 3.1 for the auxiliary evolution approach we consider two approaches to speed up the dynamics (*i*) counterdiabatic driving (CD) and (*ii*) Floquet Engineering (FE); we also consider a third controlled implementation where the computational register is directly driven via (*iii*) inverse engineering (IE).

3.1.1 Auxiliary Evolution

The first method we consider for implementing unitary gates is the adiabatic approach [112] where an auxiliary qubit is coupled to a computational register upon which we wish to perform the gate operation. By driving this auxiliary qubit adiabatically, the desired gate operation can be effected on the computational register. Let us first show the auxiliary evolution procedure for an arbitrary single-qubit gate. This unitary will generically have an eigenvalue $\lambda_+ = 1$, and we denote the corresponding eigenvector as $|n_+\rangle$. This is the vector that remains invariant under the action of the unitary - the rotation axis. We denote the other eigenvalue as λ_- and its corresponding eigenvector as $|n_-\rangle$. The action of a single-qubit gate on an arbitrary state in the eigenbasis of the unitary is then

$$\alpha|n_+\rangle + \beta|n_-\rangle \rightarrow \alpha|n_+\rangle + e^{i\phi}\beta|n_-\rangle, \quad (3.1)$$

where $e^{i\phi} = \lambda_-$. As an example, we consider the Hadamard gate. Its matrix representation in the computational basis is

$$\mathcal{H} = \frac{1}{\sqrt{2}} \begin{pmatrix} 1 & 1 \\ 1 & -1 \end{pmatrix}. \quad (3.2)$$

The “rotation axis,” or the unit vector that is left invariant by the action of the unitary, corresponds to the eigenvector with eigenvalue +1. For the Hadamard gate this is

$$|n_+\rangle = \frac{1}{\sqrt{1 + (1 + \sqrt{2})^2}} \begin{pmatrix} 1 + \sqrt{2} \\ 1 \end{pmatrix}. \quad (3.3)$$

The second eigenvalue is -1, with corresponding eigenvector

$$|n_-\rangle = \frac{1}{\sqrt{1 + (1 - \sqrt{2})^2}} \begin{pmatrix} 1 - \sqrt{2} \\ 1 \end{pmatrix}. \quad (3.4)$$

The action of the Hadamard gate on a general state is

$$\mathcal{H}(p_1|0\rangle + p_2|1\rangle) = \frac{p_1 + p_2}{2}|0\rangle + \frac{p_1 - p_2}{2}|1\rangle. \quad (3.5)$$

In the eigenbasis of the Hadamard gate (3.1), the amplitudes are

$$p_1 = \frac{\sqrt{2 + \sqrt{2}}}{2}\alpha - \frac{\sqrt{2 - \sqrt{2}}}{2}\beta, \quad (3.6)$$

$$p_2 = \frac{\sqrt{2 - \sqrt{2}}}{2}\alpha + \frac{\sqrt{2 + \sqrt{2}}}{2}\beta. \quad (3.7)$$

Recognising that the action of \mathcal{H} on the state in the eigenbasis is the transformation $\beta \rightarrow -\beta$, we denote the amplitudes after the unitary transformation as

$$p'_1 = \frac{\sqrt{2+\sqrt{2}}}{2}\alpha + \frac{\sqrt{2-\sqrt{2}}}{2}\beta, \quad (3.8)$$

$$p'_2 = \frac{\sqrt{2-\sqrt{2}}}{2}\alpha - \frac{\sqrt{2+\sqrt{2}}}{2}\beta. \quad (3.9)$$

A quick calculation then shows that $p'_1 = (p_1 + p_2)/2$ and $p'_2 = (p_1 - p_2)/2$, reinforcing the idea that we simply need to “tack-on” a local phase derived from λ_- onto $|n_-\rangle$ to perform our gate. To realise an arbitrary single-qubit gate in the auxiliary evolution framework, we first couple the computational qubit to an auxiliary qubit that is initialised in the $|0\rangle$ computational state. It is this qubit that is subject to the controlled drive. The combined initial state in the register-auxiliary Hilbert space is then

$$|\Psi_i\rangle = (\alpha|n_+\rangle + \beta|n_-\rangle) \otimes |0\rangle. \quad (3.10)$$

We consider the total Hamiltonian

$$H(t) = |n_+\rangle\langle n_+| \otimes H_0(t) + |n_-\rangle\langle n_-| \otimes H_\phi(t), \quad (3.11)$$

where the projectors are given by $|n_\pm\rangle\langle n_\pm| = (\mathbf{1} \pm \mathbf{n} \cdot \boldsymbol{\sigma})/2$, with \mathbf{n} being the Bloch vector representation of $|n_+\rangle$ and $H_\phi(t)$ given as

$$H_\phi(t) = -[\cos(\theta_f \lambda) \sigma_z + \sin(\theta_f \lambda) [\cos(\phi_k) \sigma_x + \sin(\phi_k) \sigma_y]]. \quad (3.12)$$

For the Hadamard gate we have $\phi = \pi$, derived from $e^{i\phi} = \lambda_-$. Adiabatically evolving under the Hamiltonian above yields time evolved state

$$|\Psi(t)\rangle = \alpha|n_+\rangle \otimes |\epsilon_0^g(t)\rangle + \beta|n_-\rangle \otimes |\epsilon_\phi^g(t)\rangle, \quad (3.13)$$

where $|\epsilon_\phi^g(t)\rangle$ is the ground state of Eq. (3.12), given by

$$|\epsilon_\phi^g(t)\rangle = \cos\left(\frac{\theta_f \lambda(t)}{2}\right)|0\rangle + e^{i\phi} \sin\left(\frac{\theta_f \lambda(t)}{2}\right)|1\rangle. \quad (3.14)$$

The overall state then reads

$$|\Psi(t)\rangle = \cos\left(\frac{\theta_f \lambda}{2}\right)(\alpha|n_+\rangle + \beta|n_-\rangle) \otimes |0\rangle + \sin\left(\frac{\theta_f \lambda}{2}\right)(\alpha|n_+\rangle + e^{i\phi}\beta|n_-\rangle) \otimes |1\rangle. \quad (3.15)$$

We see that the gate has been performed on the computational qubit with amplitude $\sin^2(\theta\lambda/2)$. If we measured the auxiliary qubit as $|1\rangle$ we would know the unitary has been performed successfully, while if we measured $|0\rangle$ we could infer that the computational qubit is in its original state. We can design a ramping protocol to deterministically perform the gate. Denoting the total drive time

as τ , we then choose $\theta\lambda(\tau)=\pi$ as the endpoint of the drive. The state at this time is

$$|\Psi(\tau)\rangle = (\alpha|n_+\rangle + e^{i\phi}\beta|n_-\rangle) \otimes |1\rangle. \quad (3.16)$$

Provided we drive the auxiliary qubit adiabatically with the parameters chosen above, we find that the desired unitary rotation has been performed on the computational qubit, and the auxiliary qubit is in the excited state of the computational eigenbasis. This framework was first introduced in [112], and we can expand upon it to show that one can also perform a desired rotation on the computational qubit with the auxiliary qubit starting in its excited state. That is to say, we initialise the overall system in the state

$$|\Psi_i\rangle = (\alpha|n_+\rangle + \beta|n_-\rangle) \otimes |1\rangle. \quad (3.17)$$

Evolving adiabatically with the same Hamiltonians as before gives the time-evolved state

$$|\Psi(t)\rangle = \alpha|n_+\rangle \otimes |\epsilon_0^e\rangle + \beta|n_-\rangle \otimes |\epsilon_{\phi-}^e\rangle, \quad (3.18)$$

where the excited state of the time dependent Hamiltonian is

$$|\epsilon_\phi^e\rangle = -e^{-i\phi} \sin\left(\frac{\theta_f\lambda}{2}\right)|0\rangle + \cos\left(\frac{\theta_f\lambda}{2}\right)|1\rangle. \quad (3.19)$$

The total time-evolved state then reads

$$|\Psi(t)\rangle = -\sin\left(\frac{\theta_f\lambda}{2}\right)(\alpha|n_+\rangle + e^{-i\phi}\beta|n_-\rangle) \otimes |0\rangle + \cos\left(\frac{\theta_f\lambda}{2}\right)(\alpha|n_+\rangle + \beta|n_-\rangle) \otimes |1\rangle, \quad (3.20)$$

which, for $\theta_f\lambda(\tau) = \pi$ deterministically performs the gate, with a global phase, provided that one chooses $-\phi$ instead of $+\phi$ for the driving parameter in (3.12). To that end, we consider the general total Hamiltonian (for the register and auxiliary qubit)

$$H(t) = \sum_k P_k \otimes H_{\phi_k}(t), \quad (3.21)$$

where P_k are projectors onto each of the eigenvectors of the desired unitary acting on the computational register, while $H_{\phi_k}(t)$ is the eigenvalue-dependent driving Hamiltonian given by (3.12) acting on the auxiliary qubit. We will briefly show how to utilise this for a two-qubit gate. One typical example is the controlled-phase gate. A phase shift operation for an angle ϕ applied to a qubit acts as $|0\rangle \rightarrow |0\rangle$ and $|1\rangle \rightarrow e^{i\phi}|1\rangle$. The controlled-phase gate implements this operation on the target qubit, provided the control qubit is in the $|1\rangle$ state. The matrix representation of

the unitary in the computational basis is

$$\mathcal{CP}(\phi) = \begin{pmatrix} 1 & 0 & 0 & 0 \\ 0 & 1 & 0 & 0 \\ 0 & 0 & 1 & 0 \\ 0 & 0 & 0 & e^{i\phi} \end{pmatrix}. \quad (3.22)$$

Explicitly, a two-qubit state in the computational basis is

$$|\psi\rangle = \alpha|0,0\rangle + \beta|0,1\rangle + \gamma|1,0\rangle + \delta|1,1\rangle. \quad (3.23)$$

Performing the controlled-phase gate yields the following output state

$$\mathcal{CP}(\phi) = \alpha|0,0\rangle + \beta|0,1\rangle + \gamma|1,0\rangle + e^{i\phi}\delta|1,1\rangle. \quad (3.24)$$

The unitary is already diagonal in the computational basis, meaning that the projectors onto its eigenvectors are simply the computational basis projectors. We simply need to generate a local phase of $e^{i\phi}$ to the $|1,1\rangle$ component of the state. Within the auxiliary evolution framework, the gate operation can again be implemented by performing a drive on the additional auxiliary qubit.

$$H_{\mathcal{CP}}^{AE}(t) = (|0,0\rangle\langle 0,0| + |0,1\rangle\langle 0,1| + |1,0\rangle\langle 1,0|) \otimes H_0(t) + |1,1\rangle\langle 1,1| \otimes H_\phi(t), \quad (3.25)$$

where the time-dependent driving Hamiltonians $H_0(t)$ and $H_\phi(t)$ applied on the auxiliary qubit are given as in Eq. (3.12). As before, we initialise the total state as

$$|\Psi(0)\rangle = (\alpha|0,0\rangle + \beta|0,1\rangle + \gamma|1,0\rangle + \delta|1,1\rangle) \otimes |0\rangle. \quad (3.26)$$

Evolving it adiabatically gives

$$|\Psi(t)\rangle = \cos \frac{\theta\lambda}{2}(\alpha|0,0\rangle + \beta|0,1\rangle + \gamma|1,0\rangle + \delta|1,1\rangle) \otimes |0\rangle \quad (3.27)$$

$$+ \sin \frac{\theta\lambda}{2}(\alpha|0,0\rangle + \beta|0,1\rangle + \gamma|1,0\rangle + e^{i\phi}\delta|1,1\rangle) \otimes |1\rangle. \quad (3.28)$$

Again, we can choose a ramping protocol such that $\theta\lambda(\tau) = \pi$, deterministically performing the gate by time τ . A similar argument as for the single-qubit case can be made for working in the excited state of the auxiliary qubit, again allowing one to recycle the auxiliary qubit for the next step in a circuit without resetting its state.

In order for the auxiliary evolution framework to implement high fidelity processes we need to minimise diabatic transitions. As discussed in Chapter 1, driving this system at finite timescales will result in these transitions. To reduce these transitions, we will employ two different control

methods for the auxiliary qubit. We again turn to counterdiabatic driving [17, 33], which allows us to arbitrarily speed up the evolution while still achieving perfect adiabatic dynamics by introducing additional term(s) to the system Hamiltonian. The CD term for Hamiltonian (3.12) can be found analytically, and is given by

$$H_{\phi}^{CD}(t) = \dot{\lambda} \frac{\pi}{2} [\sigma_y \cos(\phi) - \sigma_x \sin(\phi)], \quad (3.29)$$

where we have taken $\theta = \pi$. This form of counterdiabatic term looks natural for qubits that are manipulated by lasers such as trapped ions or neutral atoms. The above Hamiltonian could be implemented by adding a relative phase shift to the driving field of the laser. Note that the CD term is used in addition to the bare time dependent Hamiltonian in (3.11).

Our second control scheme, Floquet engineering, relies on an expansion of the adiabatic gauge potential (AGP), which we shall make clear below. We consider a general Hamiltonian $H_0(\lambda)$ where again $\lambda = \lambda(t)$ is the tuneable control term. The instantaneous eigenvalues and eigenstates are given by

$$H_0(\lambda) |n(\lambda)\rangle = E_n(\lambda) |n(\lambda)\rangle. \quad (3.30)$$

Consider the evolution of an arbitrary (potentially non-adiabatic) state $|\psi\rangle$ evolving with the unitary operator generated by $H_0(\lambda)$. We can transform to the co-moving basis of this evolution with the Hermitian conjugate of the same unitary, $|\tilde{\psi}\rangle = U^\dagger(\lambda) |\psi\rangle$. In the co-moving basis, the equation of motion reads

$$i\partial_t |\tilde{\psi}\rangle = (U^\dagger H_0(\lambda) U - i\dot{\lambda} U^\dagger \partial_\lambda U) |\tilde{\psi}\rangle. \quad (3.31)$$

The transformed Hamiltonian $\tilde{H}(\lambda) = U^\dagger H_0(\lambda) U = \sum_{n=1} E_n(\lambda) |n(\lambda)\rangle\langle n(\lambda)|$ is diagonal in the eigenbasis of H throughout the evolution, while the second term is responsible for transitions between the eigenstates. We can recast this last equation to look like a connection

$$i\partial_t |\tilde{\psi}\rangle = (\tilde{H}(\lambda) - \dot{\lambda} \tilde{\mathcal{A}}_\lambda) |\tilde{\psi}\rangle, \quad (3.32)$$

where $\tilde{\mathcal{A}}_\lambda$ is the adiabatic gauge potential in the co-moving frame. Transforming this term back to the lab frame and adding it to the original Hamiltonian will then leave us with a new Hamiltonian that will naturally be diagonal in the co-moving frame, giving us transitionless driving. This reads as

$$H(t) = H_0 + \dot{\lambda} \mathcal{A}_\lambda \quad (3.33)$$

where $\mathcal{A}_\lambda = U \tilde{\mathcal{A}}_\lambda U^\dagger = i(\partial_\lambda U) U^\dagger$. We can rewrite the adiabatic gauge potential by taking the derivative of $\tilde{H}(\lambda)$ [117]

$$i\partial_\lambda H_0(\lambda) - i \sum_{n=1} \partial_\lambda E_n(\lambda) |n(\lambda)\rangle\langle n(\lambda)| = [\mathcal{A}_\lambda, H_0(\lambda)]. \quad (3.34)$$

The second term on the left-hand-side still relies on us knowing the spectrum of the Hamiltonian,

so ideally we want to remove it. It naturally commutes with H_0 , allowing us to rewrite the equation as a gauge condition

$$[i\partial_\lambda H_0(\lambda) - [\mathcal{A}_\lambda, H_0(\lambda)], H_0(\lambda)] = 0. \quad (3.35)$$

This equation allows one to find the gauge potential through a minimisation scheme. It is equivalent to minimising the Hilbert-Schmidt norm of

$$G_\lambda = \partial_\lambda H_0 + i[\mathcal{A}_\lambda^g, H_0], \quad (3.36)$$

where \mathcal{A}_λ^g is a guess for the AGP [89]. Knowledge of the exact Lie algebra elements needed for this control term is difficult to obtain in many-body systems, and many of those terms which are needed for the full control term may be impractical in physical realisations. To resolve this, recent work has proposed an ansatz for \mathcal{A}_λ^g which can then be used to minimise (3.36) through a variational scheme [115]. They propose an approximation to the exact adiabatic gauge potential as a nested commutator expansion

$$\mathcal{A}_\lambda^{(l)} = i \sum_{k=1}^l \alpha_k \underbrace{[H_0[H_0, \dots [H_0, \partial_\lambda H_0]]]}_{2k-1}, \quad (3.37)$$

where l denotes the order of the expansion and, for an arbitrary system in the limit of $l \rightarrow \infty$, one obtains the exact expression for the adiabatic gauge potential, given by the Hellmann-Feynman theorem as

$$\langle m(\lambda) | \mathcal{A}_\lambda | n(\lambda) \rangle = -i \frac{\langle m(\lambda) | \partial_\lambda H_0 | n(\lambda) \rangle}{E_m(\lambda) - E_n(\lambda)}. \quad (3.38)$$

The coefficients for the expansion, α_k , are determined by minimising the action

$$S_l = \text{Tr}[G_l^2], \quad G_l = \partial_\lambda H_0 + i[\mathcal{A}_\lambda^{(l)}, H_0]. \quad (3.39)$$

This approach is particularly effective when dealing with many-body systems as it allows to truncate the complexity and spatial support of the control fields [115]. We can control up to order l of the approximation by evolving with the overall Hamiltonian

$$H = H_0 + i\dot{\lambda} \sum_{k=1}^l \alpha_k \underbrace{[H_0[H_0, \dots [H_0, \partial_\lambda H_0]]]}_{2k-1} \quad (3.40)$$

For a single two-level system, as will be the focus of the present work, we find that Eq. (3.37) is already identical to the full counterdiabatic term for $l = 1$, i.e. only the first term in the sum is required to achieve perfect control. However, our main interest in employing Eq. (3.37) is because it provides a means to engineer a Floquet Hamiltonian which approximately mimics the action of adiabatic gauge potential [115] and therefore opens up new possibilities in terms of feasible experimental implementations [118].

Floquet theory allows to design an effective Hamiltonian that stroboscopically mimics the

dynamics of another, potentially more complex or experimentally unfeasible Hamiltonian. In order to achieve this, we need only to oscillate the original driven Hamiltonian and its derivative with respect to the driving parameter. Such a Floquet Hamiltonian can stroboscopically recreate the dynamics of the full CD Hamiltonian $H = H_0 + \dot{\lambda} \mathcal{A}_\lambda$ with a comparatively reduced operator set. Formally, Floquet engineering recreates the evolution of a reference Floquet Hamiltonian, H^F , matching it at each end of a driving cycle

$$H^F(t) = \frac{1}{T} \int_t^{t+T} dt' H^{FE}(t'). \quad (3.41)$$

The periodically-driven Floquet-engineering Hamiltonian reads as

$$H^{FE} = \left[1 + \frac{\omega}{\omega_0} \cos(\omega t) \right] H_0(\lambda) + \dot{\lambda} \left[\sum_{k=1}^{\infty} \beta_k \sin((2k-1)\omega t) \right] \partial_\lambda H_0(\lambda), \quad (3.42)$$

where β_k are Fourier coefficients of the expansion of the reference Floquet Hamiltonian that we will fix shortly, $\omega_0 = 2\pi/\tau$ is a reference frequency derived from the total time of the drive, and $\omega = 2\pi/T$, where T is the period of a single drive period. The idea is to choose the correct Fourier coefficients for H^F such that H^{FE} stroboscopically implements the dynamics of (3.33). The advantage gained is that if this scheme is successful, we can implement the control term derived from the AGP (or an approximation of it) using only the Lie algebra elements that appear in its original Hamiltonian. By periodically driving the original Hamiltonian and its derivative, we will approximate the controlled dynamics, exactly recovering them in the $\omega \rightarrow 0$ limit. We demonstrate how to tailor $H^F(t)$ to match the controlled Hamiltonian given by (3.40). We first transform (3.42) by moving to the rotating frame of $(\omega/\omega_0) \cos(\omega t) H_0$.

$$\tilde{H}^{FE} = e^{i \int_0^t dt' \frac{\omega \cos(\omega t')}{\omega_0} H_0} H^{FE} e^{-i \int_0^t dt' \frac{\omega \cos(\omega t')}{\omega_0} H_0}. \quad (3.43)$$

We assume that the driving period is much faster than the rate of change of H_0 such that we can assume it is constant for the duration of the integral. This gives

$$\tilde{H}^{FE} = e^{i \frac{\sin(\omega t)}{\omega_0} H_0} H^{FE} e^{-i \frac{\sin(\omega t)}{\omega_0} H_0}. \quad (3.44)$$

From (3.44) it is clear that the rotating frame and the lab frame coincide at $t = 0$ and $t = T$, the start and end of each driving cycle. We will use this to fix the form of H^F . The dominant term in the Magnus series expansion [119] of (3.41) in the rotating frame is

$$\tilde{H}_{(0)}^F = \frac{1}{T} \int_0^T dt e^{i \frac{\sin(\omega t)}{\omega_0} H_0} H^{FE} e^{-i \frac{\sin(\omega t)}{\omega_0} H_0}. \quad (3.45)$$

We are interested in the off-diagonal elements, as the diagonal terms will just be those of H_0 as

they are assumed constant over a single cycle

$$\langle m | \tilde{H}_{(0)}^F | n \rangle = \frac{1}{T} \int_0^T dt e^{i \frac{(E_m - E_n) \sin(\omega t)}{\omega_0}} \dot{\lambda} \left[\sum_{k=1}^{\infty} \beta_k \sin((2k-1)\omega t) \right] \langle m | \partial_\lambda H_0 | n \rangle. \quad (3.46)$$

We can use the Jacobi-Anger expansion on the exponential

$$e^{iz \sin \theta} \equiv \sum_{j=-\infty}^{\infty} J_j(z) e^{ij\theta}, \quad (3.47)$$

where $J_j(z)$ are Bessel functions of the first kind. This lets us re-write (3.46) as

$$\langle m | \tilde{H}_{(0)}^F | n \rangle = \frac{\dot{\lambda}}{T} \sum_{j=-\infty}^{\infty} J_j\left(\frac{\omega_{mn}}{\omega_0}\right) \langle m | \partial_\lambda H_0 | n \rangle \int_0^T dt \left[\sum_{k=1}^{\infty} \beta_k \sin((2k-1)\omega t) \right] e^{i\omega jt}, \quad (3.48)$$

where $\omega_{mn} = E_m - E_n$, and we have again used the separation of timescales for H_0 and the period of a drive. The integral returns the Fourier coefficients β_k , giving us

$$\langle m | \tilde{H}_{(0)}^F | n \rangle = i \dot{\lambda} \sum_{j=1}^{\infty} \beta_j J_{2j-1}\left(\frac{\omega_{mn}}{\omega_0}\right) \langle m | \partial_\lambda H_0 | n \rangle. \quad (3.49)$$

As established before, the rotating frame and lab frames coincide at $t = 0$ and $t = \tau$, which lets us write (including the diagonal terms now)

$$H_{(0)}^F = H_0 + i \dot{\lambda} \sum_{j=1}^{\infty} \beta_j J_{2j-1}\left(\frac{\omega_{mn}}{\omega_0}\right) \langle m | \partial_\lambda H_0 | n \rangle. \quad (3.50)$$

We can Taylor expand the second term around $t = 0$

$$H_{(0)}^F = H_0 + i \dot{\lambda} \sum_{j=1}^{\infty} \beta_j \sum_{k=0}^{\infty} \frac{(-1)^k (2\omega_0)^{-2(j+k)+1}}{k!(k+2j-1)!} \underbrace{[H_0[H_0, \dots [H_0, \partial_\lambda H_0]]]}_{2j+2k-1}. \quad (3.51)$$

As we will see, we return the full counterdiabatic term for the single-qubit drive with a single commutation, this implies we need only the $j = 1, k = 0$ term in the expansion. In principle, one need only compare terms between (3.40) and (3.51) to fix the Fourier coefficients for the Floquet engineered Hamiltonian given by (3.42). For us, this implies $\beta_1 = 2\alpha_1\omega_0$. Let us apply this control scheme to the auxiliary drive Hamiltonian

$$H_\phi(\lambda) = - [\cos(\pi\lambda)\sigma_z + \sin(\pi\lambda) [\cos(\phi)\sigma_x + \sin(\phi)\sigma_y]]. \quad (3.52)$$

The first order, $l = 1$ term gives

$$\mathcal{A}_\lambda^{(1)} = i\alpha_1[H_\phi, \partial_\lambda H_\phi] = -2\pi\alpha_1(\cos\phi\sigma_y - \sin\phi\sigma_x). \quad (3.53)$$

From a term, we have already found the operator form of the counterdiabatic field, given by (3.29). Minimisation of the action given by (3.39) fixes $\alpha_1 = -1/4$, which gives us precisely the counterdiabataic term at $l = 1$ order. Even though this is for a single qubit, the control term has support on an operator that has no overlap with the operator set of the bare Hamiltonian. If we only had access to the operator set of the bare Hamiltonian, this is where the Floquet engineering control term has an advantage. It reads

$$\hat{H}_\phi^{FE} = \left[1 + \frac{\omega}{\omega_0} \cos(\omega t) \right] \hat{H}_\phi(\lambda) + \dot{\lambda} [\omega_0 \alpha_1 \sin(2\omega t)] \partial_\lambda \hat{H}_\phi(\lambda), \quad (3.54)$$

where $\omega_0 = 2\pi/\tau$ is the reference frequency tied to the total gate time and $\omega = N\omega_0$ with $N \in \mathbb{N} \gg 1$ is the frequency for a single periodic drive cycle. The Floquet Hamiltonian replaces the time dependent bare Hamiltonians in (3.11).

3.1.2 Inverse Engineering

As an alternative approach to auxiliary control, we consider a simpler approach by directly driving the computational register. The evolution of a closed quantum system obeys the time-dependent Schrödinger equation and an arbitrary initial state is connected to a designated final state by a unitary operator, $|\psi(t)\rangle = U(t)|\psi(0)\rangle$. The Hamiltonian that generates such a unitary time evolution is determined by

$$H(t) = i\dot{U}(t)U^\dagger(t). \quad (3.55)$$

It is possible to follow several approaches to inverse engineer the desired unitary [26, 116, 120, 121], and hence the corresponding Hamiltonian. In this work, we adopt the approach taken in Ref. [116] and express $U(t)$ in the following form

$$U(t) = \sum_n e^{i\pi\lambda_n(t)} |n(t)\rangle \langle n(t)|, \quad (3.56)$$

where the set $\{|n(t)\rangle\}$ forms a complete orthonormal basis, and $\lambda(t)$ has the initial condition $\lambda_n(0) = 2l$ where $l \in \mathbb{Z}$ to ensure $U(0) = \mathbb{I}$. By taking suitable choices for the free parameters that define the orthonormal basis and local phase information, we can construct a Hamiltonian that implements the desired unitary behaviour in such a way that is not dependent on a particular initial state. In what follows we construct the IE Hamiltonian such that $\lambda(t)$ is the driving parameter. The motivation for choosing IE is to showcase another control technique. However, as we noted in Chapter 1, the IE approach prescribed above and “typical” counterdiabatic control methods are intrinsically related [122, 123]. We inverse-engineer a protocol such that there are no diabatic transitions are allowed, it is diagonal in its co-moving frame. Therefore, the results reported for the IE case would be qualitatively similar if instead CD driving were applied to the computational qubit directly. What does differ is that with the IE approach we do not start with a reference Hamiltonian *a priori* for which the transitions need to be suppressed. Nevertheless, as depicted in Fig. 3.1, the key difference in our analysis is embodied by the two distinct settings where either

an auxiliary system is employed to achieve the gate or when the computational system is directly driven.

Let us first consider a single-qubit process. We consider the unitary operator

$$U_1(t) = |m_+(t)\rangle \langle m_+(t)| + e^{i\pi\lambda(t)} |m_-(t)\rangle \langle m_-(t)|, \quad (3.57)$$

where the basis states are defined as

$$\begin{aligned} |m_+(t)\rangle &= \cos[\vartheta(t)/2] |0\rangle + e^{i\varphi(t)} \sin[\vartheta(t)/2] |1\rangle, \\ |m_-(t)\rangle &= e^{i\varphi(t)} \cos[\vartheta(t)/2] |1\rangle - \sin[\vartheta(t)/2] |0\rangle. \end{aligned} \quad (3.58)$$

with parameters $\vartheta(t)$, $\varphi(t)$, and $\lambda(t)$ that can be tuned in order to define the desired gate operation. For a single qubit gate, the driving Hamiltonian found from Eq. (3.55) takes the form [116]

$$H(t) = \frac{1}{2} \boldsymbol{\omega}(t) \cdot \boldsymbol{\sigma}, \quad (3.59)$$

where the vector components are given as

$$\begin{aligned} \omega_x(t) &= (\cos \pi\lambda - 1) \dot{\varphi} \cos \varphi \cos \vartheta \sin \vartheta \\ &\quad + [\dot{\varphi} \sin \vartheta \sin \pi\lambda + (\cos \pi\lambda - 1) \dot{\vartheta}] \sin \varphi \\ &\quad + (\dot{\vartheta} \cos \vartheta \sin \pi\lambda + \pi \dot{\lambda} \sin \vartheta) \cos \varphi, \\ \omega_y(t) &= (\cos \pi\lambda - 1) \dot{\varphi} \sin \varphi \sin \vartheta \cos \vartheta \\ &\quad + [\dot{\varphi} \sin \vartheta \sin \pi\lambda - (\cos \pi\lambda - 1) \dot{\vartheta}] \cos \varphi \\ &\quad + (\dot{\vartheta} \cos \vartheta \sin \pi\lambda + \pi \dot{\lambda} \sin \vartheta) \sin \varphi, \\ \omega_z(t) &= -\dot{\vartheta} \sin \vartheta \sin \pi\lambda - (\cos \pi\lambda - 1) \dot{\varphi} \sin^2 \vartheta + \pi \dot{\lambda} \cos \vartheta. \end{aligned} \quad (3.60)$$

The action of this Hamiltonian is to transform the input state $|\mu(0)\rangle = a|0\rangle + b|1\rangle$ to the final state $|\mu(t)\rangle = \alpha(t)|0\rangle + \beta(t)|1\rangle$ where the populations are

$$\begin{aligned} \alpha(t) &= \frac{a(e^{i\pi\lambda(t)} + 1) - (e^{i\pi\lambda(t)} - 1)(a \cos \vartheta(t) + b e^{-i\varphi(t)} \sin \vartheta(t))}{2}, \\ \beta(t) &= \frac{b(e^{i\pi\lambda(t)} + 1) + (e^{i\pi\lambda(t)} - 1)(b \cos \vartheta(t) - a e^{-i\varphi(t)} \sin \vartheta(t))}{2}. \end{aligned}$$

One choice of parameters that gives the Hadamard gate are $\varphi(t) = 0$, $\vartheta(t) = \pi/4$, and ramping from $\lambda(0) = 0$ to $\lambda(\tau) = 1$, which in turn gives the populations of the final state as $\alpha(\tau) = (a + b)/\sqrt{2}$, and $\beta(\tau) = (a - b)/\sqrt{2}$. The corresponding Hamiltonian that drives our qubit is then given as

$$H_{Had}^{IE}(t) = \frac{\pi \dot{\lambda}(t)}{2\sqrt{2}} (\sigma_x + \sigma_z). \quad (3.61)$$

The same approach can be extended to a two-qubit process

$$U_2(t) = \sum_{k=1,2} |m_{k,+}(t)\rangle\langle m_{k,+}(t)| + e^{i\pi\lambda_k(t)} |m_{k,-}(t)\rangle\langle m_{k,-}(t)|. \quad (3.62)$$

The evolution basis is similarly defined

$$|m_{k,+}(t)\rangle = \cos[\vartheta(t)/2] |k-1,0\rangle + e^{i\varphi_k(t)} \sin[\vartheta(t)/2] |k-1,1\rangle, \quad (3.63)$$

$$|m_{k,-}(t)\rangle = e^{i\varphi_k(t)} \cos[\vartheta(t)/2] |k-1,1\rangle - \sin[\vartheta(t)/2] |k-1,0\rangle. \quad (3.64)$$

We now have six parameters, with the restriction that $\lambda_k(0) = 0$. All appear in the final state of the system under the action of the unitary. Through a suitable choice of the parameters we can design the Hamiltonian to implement the desired unitary dynamics. For example, adopting the general formalism above, we obtain the desired IE Hamiltonian that applies the controlled- Z operation as follows [116]

$$H_{C\pi}^{IE}(t) = \frac{\pi\dot{\lambda}(t)}{4} (\mathbf{1} \otimes \sigma_z + \sigma_z \otimes \mathbf{1} - \sigma_z \otimes \sigma_z). \quad (3.65)$$

Note that the implementation of the above Hamiltonian requires a pure-dephasing interaction between the target and control qubits.

In this section we have established two general ways of performing unitary processes on qubits - one that involves driving auxiliary qubits that are coupled to the register, and a second that requires us to drive the register directly. The latter is chosen such that it does not allow for diabatic transitions, and therefore can be performed arbitrarily fast. The former requires a more careful treatment - additional control terms must be included to drive it similarly quickly. We will explore both conventional counterdiabatic control and Floquet engineering for this task.

3.2 Figures of merit

To characterise how faithfully a gate has been implemented we need to adopt a fidelity measure that is agnostic to the initial state of the register. Typically one can use full-process tomography [124] to establish this, but this can be done with a more restricted set of states. Instead we adopt the average fidelity-loss measure [106]

$$J_T = 1 - \sum_{i=1}^3 \frac{w_i}{\text{tr}[\rho_i^2(0)]} \mathcal{R}e\{\text{tr}[U\rho_i(0)U^\dagger\rho_i(\tau)]\}, \quad (3.66)$$

and consider the average of the Hilbert-Schmidt norm of the ideal evolution of three specific initial states with the obtained state, weighted by w_i with $\sum_{i=1}^3 w_i = 1$. Three initial states satisfying particular conditions have been shown to be the minimum amount needed to address all the possible errors and characterise a general unitary operation for an open system evolution [106, 125]. For a

single qubit, the following set satisfies the necessary conditions [106]

$$\rho_1(0) = \begin{pmatrix} 2/3 & 0 \\ 0 & 1/3 \end{pmatrix}, \quad \rho_2(0) = \begin{pmatrix} 1/2 & 1/2 \\ 1/2 & 1/2 \end{pmatrix}, \quad \rho_3(0) = \begin{pmatrix} 1/2 & 0 \\ 0 & 1/2 \end{pmatrix}.$$

The first state, ρ_1 , checks errors in the fixed basis states, and therefore does not signal any possible errors that are diagonal in this basis. The second state, ρ_2 , addresses this and indicates the off-diagonal errors in the fixed basis. The first two states alone are enough to distinguish two unitaries in the closed case. The third state, ρ_3 , is chosen to ensure that populations are conserved, important for an open system setting. Depending on the choice of the weights in Eq. (3.66), it is possible to highlight the effect of a source of an error on the infidelity over the others, which could be numerically advantageous if one were tailoring parameters for an optimal control approach via machine learning [106]. For simplicity and without loss of generality, throughout this chapter we choose these weights to be equal, i.e. $w_i=1/3$.

As we discussed in 2, the addition of control terms to the Hamiltonian implies an overall increase in resources needed to evolve the system. We will again adopt the cost measure introduced in [34, 66, 126]

$$\mathcal{C} = \frac{1}{\tau} \int_0^\tau \|H\| dt, \tag{3.67}$$

where $\|\cdot\|$ denotes the norm of the Hamiltonian of interest, and again for simplicity we consider the trace norm. It is important to emphasise that, following the approach taken in [98], we take H to be the full Hamiltonian that generates the driven dynamics implementing the gate operation, not just the external control term. In fact, notice that it is only for the case of CD control where an explicit additional Hamiltonian term is added to the bare Hamiltonian. For both the FE and IE approaches, control is embedded into the same operators that appear in the bare Hamiltonian. Therefore, it is necessary to consider the cost of the full Hamiltonian generating the time evolution. This measure is well motivated by the functional form of the physical driving fields [34, 127] and it has been shown to have connections to a Landauer-type limit for the change in information encoded computational states [94].

The controlled dynamics require that the drives are implemented for a specific length of time, which we denote by τ . Since the control protocols are designed to be effective regardless of the specific functional form of the drive, this provides a useful additional degree of freedom for control protocols [53, 98]. We consider the following ramp profiles that satisfy the boundary conditions $\lambda(0)=0$ and $\lambda(\tau)=1$,

$$\begin{aligned} \lambda(t) &= \frac{t}{\tau}, && \text{linear} \\ \lambda(t) &= \frac{10t^3}{\tau^3} - \frac{15t^4}{\tau^4} + \frac{6t^5}{\tau^5}, && \text{polynomial} \\ \lambda(t) &= \sin\left(\frac{\pi t}{2\tau}\right). && \text{sinusoidal} \end{aligned} \tag{3.68}$$

We look to characterise the impact of timing errors in the drive, i.e. where the duration of the driving field over- or under-shoots the intended target time, τ , by assessing the resulting impact on the gate fidelity, Eq. (3.66). We note that these pulses are chosen to capture and compare certain pulse characteristics. Indeed much work has been done in designing more complex ramp profiles via optimal control and machine learning methods [128–130] seeking to optimise to a variety of relevant cost functionals. Our analysis can therefore provide useful information for the seed pulses to ensure robustness to, e.g. time keeping errors, while exploiting more advanced techniques to explore a greater optimization landscape.

We will be interested in considering how faithfully the gate operation is implemented when the controlled system is not completely isolated and therefore prone to environmental effects. To that end, we model the time evolution of the driven system with the GKSL master equation, which was introduced in Chapter 1, restated here as

$$\frac{d\rho}{dt} = \mathcal{L}\rho = -i[H, \rho] + \sum_i^{N^2-1} \gamma_i \left(L_i \rho L_i^\dagger - \frac{1}{2} \{ L_i^\dagger L_i, \rho \} \right). \quad (3.69)$$

We will consider just a single jump operator that acts on the driven qubit, σ_z^λ , with a single interaction strength, γ . The superscript λ implies our assumption that the environment only affects the driven part of the system, i.e. for the CD and FE cases we assume the environment acts only on the auxiliary qubit, while for IE it is applied directly to the computational qubit(s). This gives

$$\mathcal{L}\rho = -i[H, \rho] + \gamma \left(\sigma_z^\lambda \rho \sigma_z^\lambda - \rho \right), \quad (3.70)$$

The effect of the jump operator on the computational basis states is

$$\sigma_z |0\rangle = |0\rangle, \quad \sigma_z |1\rangle = -|1\rangle. \quad (3.71)$$

This implies that it flips the sign of the off-diagonal terms in the density matrix, ρ , of the system

$$\sigma_z \rho \sigma_z = \begin{pmatrix} 1 & 0 \\ 0 & -1 \end{pmatrix} \begin{pmatrix} \rho_{00} & \rho_{01} \\ \rho_{01}^* & \rho_{11} \end{pmatrix} \begin{pmatrix} 1 & 0 \\ 0 & -1 \end{pmatrix} = \begin{pmatrix} \rho_{00} & -\rho_{01} \\ -\rho_{01}^* & \rho_{11} \end{pmatrix}. \quad (3.72)$$

This then gives

$$\mathcal{L}\rho = -i[H, \rho] + \gamma \begin{pmatrix} 0 & -2\rho_{01} \\ -2\rho_{01}^* & 0 \end{pmatrix}. \quad (3.73)$$

We can solve the first-order differential equations that governs the off-diagonal terms, i.e. the coherence of the qubit.

$$\rho_{01}(t) = \rho_{01}(0)e^{-2\gamma t}. \quad (3.74)$$

The populations are unaffected by the environment, which will evolve according to the unitary part of the GKSL equation, while the coherence terms decay exponentially. This form of decoherence

is typically called pure dephasing. For our purposes it is a simple but accurate description of what occurs in many physical qubits, where energy relaxation is slow compared to the rate of dephasing. The self-Hamiltonian of computational qubits are typically proportional to σ_z . Fluctuations in this term, or noise that manifests as an operator that commutes with the system Hamiltonian will therefore manifest as pure dephasing. We will explore how decoherence effects the performance of the gates for the two physically distinct approaches to their implementation.

3.3 Hadamard Gate

We compare the approaches using the Hadamard gate as a benchmark. In the IE case the Hamiltonian is

$$H_{Had}^{IE}(t) = \frac{\pi\dot{\lambda}(t)}{2\sqrt{2}}(\sigma_x + \sigma_z). \quad (3.75)$$

while in the auxiliary evolution framework it reads

$$H_{Had}^{AE}(t) = |n_+\rangle\langle n_+| \otimes H_0(t) + |n_-\rangle\langle n_-| \otimes H_\pi(t), \quad (3.76)$$

where the projectors are given by $|n_\pm\rangle\langle n_\pm| = (\mathbf{1} \pm \mathbf{n} \cdot \boldsymbol{\sigma})/2$, with $\mathbf{n} = 1/\sqrt{2}\{1, 0, 1\}$ and $H_\phi(t)$ given as

$$H_\phi(t) = -[\cos(\pi\lambda)\sigma_z + \sin(\pi\lambda)[\cos(\phi)\sigma_x + \sin(\phi)\sigma_y]]. \quad (3.77)$$

This last equation will use both counterdiabatic control as given in (3.29) and Floquet engineering as given by (3.54).

Fig. 3.2 shows the trajectories for the various control approaches on the Bloch sphere in the absence of any errors. While the IE qubit (rightmost, yellow) follows a path on the Bloch sphere and therefore remains pure during the gate operation, the auxiliary evolutions' computational qubit cuts through the Bloch sphere (straight, green line) connecting the initial state ($|+\rangle$) to the final one ($|0\rangle$). The latter observation shows that, although the initial and final states of both the control and register qubits are pure in the auxiliary evolution approach, during the dynamics they are mixed, which indicates that they become entangled during the process. By having a detailed look at the Bloch vectors of the driven qubits for the auxiliary evolution and IE, it is possible to see that their x and z -components are equal to each other at all times, and only y -components differ (in fact, this component remains identically zero for the auxiliary evolution's qubit for this particular gate operation). Therefore, the path that this computational qubit takes is restricted to the $x - z$ plane and the projection of the path of the IE qubit to the same plane is identical and therefore, as we demonstrate explicitly below, the performance in terms of the implementation (in)fidelity, Eq. (3.66) are identical for the different processes despite their dynamics being distinct.

Fig. 3.3(a) shows the final target state infidelity for a Hadamard gate operation implemented using the three control strategies and for comparison we also show the uncontrolled auxiliary evolution (black, dashed) for a linear ramp $\lambda(t) = t/\tau$. As expected, CD and IE both achieve perfect implementations regardless of the timescale of the drive (bottom-most dotted lines). The solid red

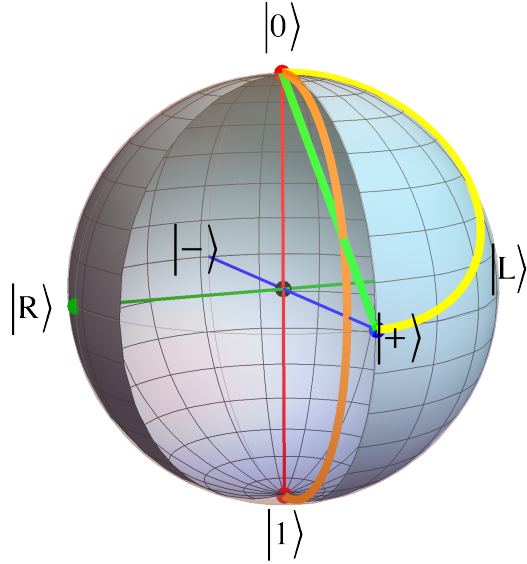


Figure 3.2: We show the trajectories of the qubits for both the CD and IE protocols of the Hadamard gate. We take the initial computational state to be $|+\rangle$. The yellow line corresponds to the path of the qubit in the IE case. The green and orange lines correspond to the computational and auxiliary qubits of the auxiliary evolution cases, respectively, which begins and ends with a separable global state of the two qubits while at intermediate times the reduced states of either qubit are mixed.

curve corresponds to the FE Hamiltonian, Eq. (3.42). We note that the FE evolution approach is exactly equivalent to the CD term only when the frequency of the Floquet driving is taken to infinity, and is otherwise approximate for finite values. Despite the approximate nature of the FE approach, provided that the chosen parameters are within the relevant regime of applicability [115], this approach is still highly effective in implementing the controlled evolution, tracking the same dynamics as the CD approach and maintaining an improvement of several orders of magnitude over the uncontrolled implementation. In Fig. 3.3(b) we fix $\tau=1$ and examine the computational qubit's approach to the target state during the evolution. This serves to demonstrate that despite the actual dynamics giving rise to distinct paths, the effectiveness of all control protocols in terms of gate infidelity is the same. The inset demonstrates that the FE drive is a remarkably accurate approximation to the exact drive, showing small oscillations around the desired trajectory. While Fig. 3.3(a) and (b) demonstrate that, at the level of implementation, all control protocols are largely equivalent insofar as they can faithfully achieve the desired unitary, we will see in the following some qualitative differences emerge when we consider alternative performance metrics.

We show the total cost of implementing the controlled gate operation, quantified using Eq. (3.67), in Fig 3.4(a) and for simplicity we consider a linear ramp for all protocols. To begin with, for very fast driving times, $\tau \rightarrow 0$, we are in the opposite limit of adiabatic evolution and the energetic costs of all control techniques diverge. This observation is in accordance with previous works [41, 126] which establish that the energetic resources necessary to drive a system arbitrarily

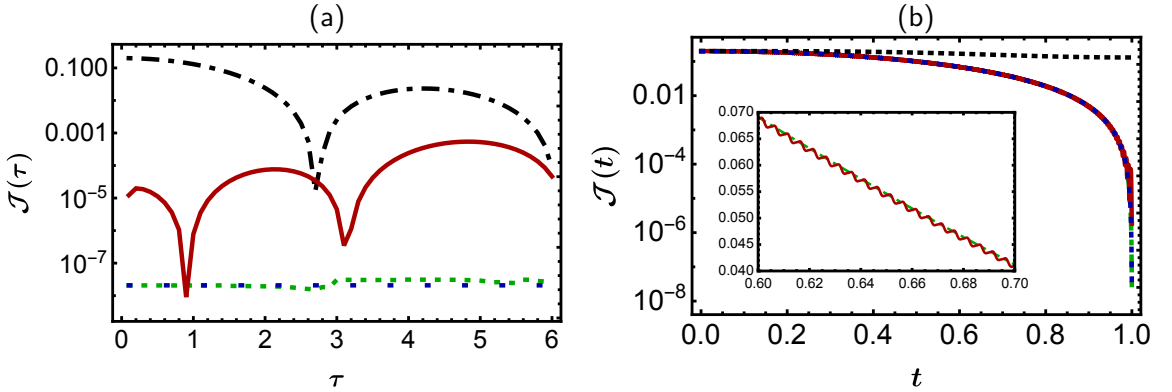


Figure 3.3: (a) Final gate infidelity, Eq (3.66) as a function of total protocol duration, for the Hadamard gate. The auxiliary evolution with counterdiabatic (CD) control is shown in the lower-most green, dotted curve. Inverse engineering (IE) performs similarly shown by the blue, dotted curve. The topmost, black, dot-dashed curve corresponds to an uncontrolled auxiliary evolution where the performance is several orders of magnitude worse. Floquet engineered (FE) auxiliary control is shown in the red, solid curve and is shown to be highly effective. (b) Dynamical gate infidelity for the Hadamard gate with $\tau = 1$ using the same styling as panel (a) to identify the different control protocols. The inset captures the oscillations present in the FE driving around the dynamics of the CD approach.

fast while keeping it in the adiabatic manifold requires to have access to arbitrarily large energetic resources. Naturally, for longer quench durations we asymptotically reach the adiabatic limit of the time evolution and the cost decays proportionally to $1/\tau$. Specifically, in the long time limit the CD cost asymptotically approaches to $2\sqrt{2}$, which corresponds to an unavoidable energy cost given by the energy change of bare Hamiltonian of the driven auxiliary qubit, while for IE the cost vanishes in the asymptotic limit. On the other hand, for the FE case, the leading term for the cost in the long time limit is $2\omega/\omega_0$ and proportional to the frequency of the Floquet driving, i.e. how many times the FE dynamics intersects with the true adiabatic dynamics. This requirement for high frequency driving manifests in a higher energetic cost for achieving the control.

We now turn our attention to timekeeping errors, or equivalently perturbations to the control field strength. For simplicity we focus on the case of IE, but remark the conclusions are qualitatively similar for both the auxiliary evolution cases as the dynamical overlap with the target states for the protocols coincide. In Fig. 3.4(b) we (arbitrarily) fix $\tau=1$ and consider the performance of the different ramp profiles given by Eqs (3.68) where we allow for the ramp to over- or under-shoot the target time by a factor proportional to $1 \pm \epsilon$. A simple linear ramp is the most susceptible to this type of error, with the infidelity rapidly growing as ϵ increases. Therefore, while the linear ramp has some notable advantages, e.g. resulting in a time-independent control term for IE [cfr. Eq. (3.75)], this comes at the expense of requiring potentially costly accurate timekeeping [131]. In contrast, due to their smooth start and end points the polynomial and sinusoidal protocols allow for more severe timekeeping errors while still faithfully implementing the gate, with timing errors of up to 20% still achieving infidelities $\lesssim 10^{-4}$. This can be understood from the behaviour of

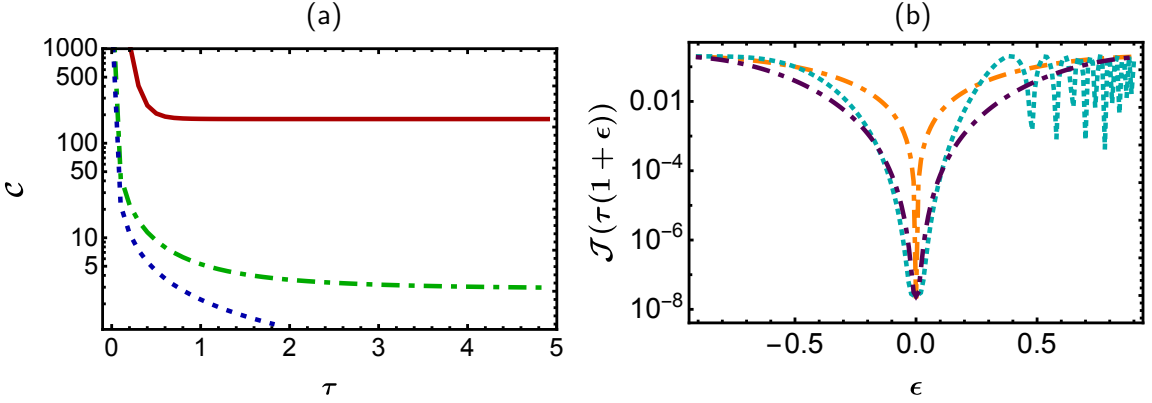


Figure 3.4: (a) We plot the cost, Eq. (3.67), of implementing the Hadamard gate vs. total protocol duration for IE, CD control, FE with $\omega/\omega_0 = 200$ in blue, green, and red, respectively. (b) Final gate infidelity for the Hadamard gate vs. timekeeping error, ϵ , for over- or under-shooting the intended ramp duration. The total (ideal) ramp time is $\tau = 1$. We show the performance for the linear (orange), the polynomial (cyan), the sinusoidal (purple) ramps. In all panels we fix $\omega_0 = 2\pi/\tau$, $\omega = 200\omega_0$ for the FE case.

these functions at their endpoints where the rate of change of the associated driving field remains sufficiently small for $\epsilon < 0.2$. As a result, the amplitude of obtaining the desired final state, which is given by $\sin^2(\theta_f \lambda/2)$ [see Eq. (3.13) and (3.14)] does not significantly deviate from unity. These results are consistent with complementary studies of different control problems [132] and demonstrates that the flatness of the applied ramp around the target is an important feature to have in terms of the robustness of the protocol.

The physical differences implied by the approaches become most apparent when considering open system effects on state evolution. Fig. 3.5 presents our results on the infidelity between the final state and the target state as a function of the total gate implementation time, scaled with the decoherence rate for a dephasing environment and the explicit trajectories of the qubits. In Fig. 3.5(a), we plot the trajectories of each qubit for the CD and IE Hadamard gate when the driven qubits are exposed to a dephasing channel. For the CD case, not driving the computational register directly can allay much of the spoiling effects of the environment. The auxiliary evolution approach requires the driven qubit to end in state $|1\rangle$. While the dephasing will leave the system in a mixed state, it nevertheless can have a large overlap with the intended target state of the auxiliary qubit which therefore still exhibits a good performance. Since we assume the computational qubit in the CD case does not directly feel the spoiling effects of the dephasing channel, it simply stops along its ideal trajectory when the auxiliary qubit falls short of its target state. In contrast, since we drive the computational qubit directly in the IE case while also exposing it to the dephasing channel, we see that IE qubit (yellow) starts in the $|+\rangle$ state and is drawn towards the z -axis, away from its ideal unitary dynamics by the environment. Fig 3.5(b) shows the final state infidelity for Hadamard gate as a function of the dephasing strength. The CD case (blue) displays better final state infidelity than the IE case (red) for all values of $\tau\gamma$. For larger gates, we expect that

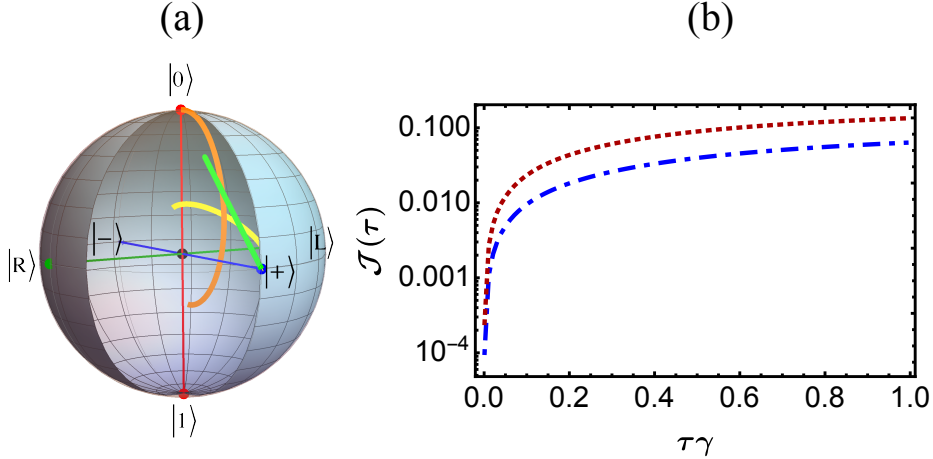


Figure 3.5: (a) Qubit trajectories for the Hadamard gate under a dephasing channel, Eq. (4.20), where the channel acts on the driven qubit in each case with $\tau\gamma=2$. Styling is same as in Fig. 3.2. As we dephase in the z -basis, both the state of the qubit in the IE case (yellow) and that of the auxiliary qubit in the CD case (orange) are pulled towards the z -axis. The computational qubit of the CD case (green) is not directly affected by the channel, and does not deviate from the ideal path, instead stopping along that trajectory once the auxiliary qubit driving the evolution has decohered. (b) We show the final gate infidelity, Eq. (3.66), for the dephasing channel for the Hadamard gate, with upper, dotted red and lower, dashed blue curves correspond to the IE and CD cases, respectively.

this difference will further widen in favour of the CD case. Despite the unfavourable cost scaling and relative complexity of the CD Hamiltonian compared to IE methods, it represents a potential attractive approach for robust gate implementation.

It is natural to consider extending the above framework to the implementation of N -qubit gates. The preceding analysis can readily be performed for two-qubit entangling gates, such as the controlled-phase gate [112, 116]. A qualitatively similar behaviour is observed: once again the overall performance in terms of process infidelity is consistent across all control approaches. Similarly, the effect of time-keeping errors is most significant for ramps that do not have smooth end points. A notable difference emerges when considering the energetic cost. While the auxiliary evolution approaches involve driving only a single qubit, and therefore the cost is essentially bounded, they can nevertheless facilitate a gate operation on an arbitrary sized register. However, this comes at the price of a difficult to implement Hamiltonian, Eq. (3.21), that requires many-body interactions. This is in contrast to the IE approach where the register is controlled directly and, as might be expected, the complexity and energy required to implement IE control on multiple qubits scales poorly with the register size.

3.4 Conclusions

We have systematically analysed the effectiveness CD, IE, and FE methods in the Hamiltonian implementation of unitary quantum gates. As the figures of merit for all considered methods, we have put the gate infidelity, the energetic cost, susceptibility to imperfect timekeeping, and robustness against the effects of environmental noise at the centre of our discussion. We have focused on the single qubit Hadamard gate and observed that all methods can faithfully achieve the desired gate, however, show some notable qualitative differences when examining performance metrics beyond target fidelities. For example, the energetic overhead of FE is the highest among the considered methods, due to the high-frequency driving necessary to achieve a gate operation closer to the ideal case. As for the imperfect timekeeping errors of the desired driving time, we have observed a subtle dependence on how the Hamiltonian is driven. Smoother ramping of the Hamiltonian results in a more successful gate implementation, in case the desired driving time is over- or under-shot. Finally, we have assumed that the driven qubit in CD and IE methods is in contact with a dephasing environment, and seen that the latter control technique is more adversely affected by such environmental spoiling effects than the former due to the fact that in this case computational degrees of freedom are affected by the noise. A qualitatively similar behaviour can also be observed for a finite temperature dissipative environment. We considered several commonly employed ramp profiles in order to highlight the natural robustness that each approach has under the same conditions and to provide insight into the properties that robust pulses should contain, e.g. smooth end points. This information can then be used to further enhance performance through the tailoring of ramp profiles by, e.g. optimal control techniques. However, the cost functional can be optimised over multiple metrics, such as energetic cost, pulse bandwidth, and robustness to noise to name a few, and therefore this rapidly becomes a complex problem.

We finally offer some comments on the applicability of these general Hamiltonians in light of recent experimental work has been done to implement transitionless (or superadiabatic) gates on promising candidate architectures, such as NV centres [133], superconducting qubits [134,135], and rare-earth ions [136]. Indeed the possible universal gate sets generated by the inverse engineering case discussed in this work presents an attractive prospect for applicability, owing to the relatively simple forms and interactions present and the potential to drive them with time-independent control fields. The counterdiabatic driving case represents a departure from the typical approach to implementing a gate as it makes use of an additional auxiliary resource to mediate the driving. One may view gates in this setting as controlled gates, the Hadamard gate is perfectly implemented on the register qubit if the auxiliary qubit is driven to $|1\rangle$ and the identity is performed on it if the auxiliary is found in $|0\rangle$. This implementation therefore requires a platform that can readily achieve controlled-gates, e.g. trapped-ion systems [76].

Chapter 4

Commutativity and the Emergence of Classical Objectivity

In the previous chapter, we saw how decoherence - modelled by a Lindblad master equation - prevented us from implementing high fidelity processes on qubits due to loss of coherence. The channel used had a steady-state that left the system in a classically mixed state in the computational basis. Decoherence theory provides the framework to understand the emergence of mixed states from quantum dynamics [137]. It posits that the nature of the system-environment interaction singles out a set of system states—the pointer states—which form a basis for the system’s description and are robust to the deleterious effects of the interaction. It is the commutativity between the system-environment interaction and the pointer basis that determines the classical mixture which the system is driven to by the dynamics [137].

While decoherence accounts for how the classical mixed state is achieved, it must be augmented to address the more general question of how we perceive classically objective states [138]. Decoherence simply accounts for the irretrievable loss of coherence due to environmental interactions. For a state to be objective, we require that multiple observers can access the same information about the system in question without perturbing it and come to a consensus over its state. Quantum Darwinism [138,139], and the more stringent strong quantum Darwinism [140–142], and spectrum broadcast structures [143–145], attempt to address this issue in a mathematically rigorous manner by treating the environment in a more active manner. The core tenet of quantum Darwinism is that for a classically objective state to emerge, the system must proliferate information about its configuration in the pointer basis to the environment. The standard framework that allows for quantum Darwinism to emerge is that of pure decoherence – that is to say the populations in the decoherence basis are untouched. The pointer states are the states of the decoherence basis, and objectivity of the classical state that emerges is observed. An interesting modification of this setup would be to allow for competition of two different environments on the system of interest. This could be due to the presence of not just an external environment, but loss of local coherence of a qubit to the rest of the computational register. The irretrievable loss of initially

local information about the qubit into the rest of the system is a phenomenon known as quantum information scrambling. Information scrambling within a system can be exactly described using the framework of decoherence [146]. The question we wish to answer is under what conditions do competing decohering channels allow for the emergence of quantum Darwinism. What follows constitutes the original work found in Ref. [2], which was carried out in collaboration with Eoghan Ryan and Mauro Paternostro of Queen's University Belfast, as well as my supervisor Steve Campbell. I contributed the numerical results that are included in this chapter, as well as to the overall theoretical discussion of the work.

4.1 Introduction

Quantum Darwinism, introduced by Zurek [137, 147], builds from decoherence theory to provide a mechanism for which information about a state gets *redundantly* encoded into an environment. To outline the problem that Darwinism addresses, we first must introduce relative states. We imagine a setup where we have both a quantum state $|\psi_S\rangle$ of the system \mathcal{S} and the state $|\mathcal{M}_0\rangle$ of an apparatus \mathcal{M} . The two are initially uncorrelated. We can choose a basis for the Hilbert space of the system - say $\{|S_i\rangle\}$ and generalise its initial state as a linear combination over this basis. The overall system-apparatus state then reads

$$|\psi_{SM}\rangle = \left(\sum_i p_i |S_i\rangle \right) \otimes |\mathcal{M}_0\rangle. \quad (4.1)$$

We assume that for every possible state of the system, there will be a corresponding apparatus state that correlates to it, allowing for read-out of the state. If the joint system evolves unitarily, these correlations will form, resulting in the following state

$$|\psi_{SM}\rangle = \sum_i p_i |S_i\rangle \otimes |\mathcal{M}_i\rangle. \quad (4.2)$$

This superposition of measurement states leads to much of the uneasiness with the postulates of quantum mechanics - all we require here is unitary evolution for the total state and the superposition principle. It is easy to extend the above setup to that of an atom in a superposition with a decay-triggered poison and cat all together in a box. One approach - the Copenhagen Interpretation [148]- to the *measurement problem* is to simply draw a dividing line between the classical and quantum world, to declare the measurement device as a macroscopic object to be classical by decree. Classical objects do not abide by the superposition principle, and we shift the problem of collapse only onto the microscopic system itself. What Darwinism demonstrates is that a transition to a *classically objective state* of system and apparatus can emerge with the postulates of quantum mechanics intact, and without resorting to a Copenhagen-style ontology. If we move past the immediate concerns with (4.4) and continue with the postulates intact, we find that the superposition postulate gives rise to another problem - that of *basis ambiguity* [149]. Instead of using $\{|S_i\rangle\}$ as our basis for the Hilbert space of \mathcal{S} , we can choose $\{|S'_i\rangle\}$ or any of an

infinite choice of representations. All contain the state of the systems

$$|\psi_{\mathcal{S}}\rangle = \sum_i p_i |\mathcal{S}_i\rangle = \sum_i p'_i |\mathcal{S}'_i\rangle. \quad (4.3)$$

The same argument applies to the apparatus states, giving us

$$|\psi_{\mathcal{SM}}\rangle = \sum_i p_i |\mathcal{S}_i\rangle \otimes |\mathcal{M}_i\rangle = \sum_i p'_i |\mathcal{S}'_i\rangle \otimes |\mathcal{M}'_i\rangle. \quad (4.4)$$

With infinite choices of basis, we must find a mechanism that constrains the choice to those states that are physically observable. A solution to the basis ambiguity problem comes from decoherence theory [149, 150]. We have seen decoherence previously with respect to the Lindblad master equation, but here we will treat it in a microscopic way in order to illustrate its significance for the basis ambiguity problem.

4.2 Pointer States

Consider that the system and apparatus interact with an environment, which itself starts in a pure state $|\mathcal{E}_0\rangle$ in some basis $\{|\mathcal{E}_i\rangle\}$. The global pure state of system-apparatus-environment, once all are allowed to interact, is

$$|\psi_{\mathcal{SME}}\rangle = \sum_i p_i |\mathcal{S}_i\rangle \otimes |\mathcal{M}_i\rangle \otimes |\mathcal{E}_i\rangle. \quad (4.5)$$

Treating the newly introduced part of the global state as an environment implies that we should employ the partial trace to give us only the parts of the state we should have access to

$$\rho_{\mathcal{SM}} = \text{Tr}_{\mathcal{E}} |\psi_{\mathcal{SME}}\rangle \langle \psi_{\mathcal{SME}}| = \sum_i |p_i|^2 |\mathcal{S}_i\rangle \langle \mathcal{S}_i| \otimes |\mathcal{M}_i\rangle \langle \mathcal{M}_i|. \quad (4.6)$$

By not taking the system and apparatus in isolation, and instead considering the global Hilbert space that encompasses all interactions to be larger, we have made some progress towards the issue at hand - the measurement apparatus is no longer in a pure state, but instead we see that it has decohered into a mixture of states. This process is known as *environment induced superselection*, or *einselection* [147]. This treatment does not even require the presence of the apparatus - the mixture of states it decoheres to are reliant on those of the system we are interested in. We can narrow our focus onto what set of states of the system are resilient to the interaction with the external degrees of freedom. We denote these as the *pointer states* [149]. We can define them via the *non-demolition observable* [151]

$$\mathcal{O} = \prod_i p_i |p_i\rangle \langle p_i| \quad (4.7)$$

where $|p_i\rangle$ are the pointer states. The non-demolition observable by definition is the non-trivial observable which commutes with the system-environment interaction Hamiltonian [152]

$$[H_{S\mathcal{E}}, \mathcal{O} \otimes \mathbb{1}] = 0. \quad (4.8)$$

Superpositions of the eigenspaces of \mathcal{O} will be suppressed by interactions with the environment, in the manner we have seen in Eq. (4.6). The reduced density matrix of the system ρ_S will then be diagonal in the eigenbasis of \mathcal{O} (where we consider the evolution by its own Hamiltonian to be irrelevant for the dynamics compared to that of the interaction). We will refer to the time in which it takes for the system to become diagonal in this basis as the *decoherence time*, denoted as τ_D .

When the system has decohered it is described by a probability distribution of pointer states - which could for example be position states. This naturally implies that the system is now classical, it is in a definite classical state, although we will not know what state in particular it is in until a measurement is performed. Decoherence causes a quantum-to-classical transition for the system, and for macroscopic systems the decoherence time will be small compared to any other relevant timescale for the system. Perhaps subtly, it is not the end of the measurement problem - it only prescribes a way for the system to be described as a classical probability distribution of states, it cannot determine exactly what classically accessible state the system evolves to, and thus the result of the experiment. Zurek prescribes a method for determining which states should be considered part of the preferred "classical" set - the *predictability sieve* [152]. Instead of looking for states that are totally unaffected by the environment degrees of freedom, we can search merely for those that are perturbed the least. The predictability sieve algorithm begins by initialising the system in a pure test state $|t_i\rangle$ and allowing it to evolve. The von-Neumann entropy of the resulting reduced density matrix of the system ρ_{t_i} is then

$$h_{t_i} = -\rho_{t_i} \log \rho_{t_i}. \quad (4.9)$$

The entropy measures the lack of predictability of the state - or by proxy a lack of classicality. The algorithm is run for all possible pure states, which are then ranked by the change in entropy. Those which change the least are admitted into the set of preferred states while the rest are filtered out. Clearly pointer states as defined previously will exhibit no increase in entropy, but we can also uncover states that lie very close to them in terms of predictability. While this seems *ad-hoc* - it is now seemingly arbitrary where to place the cut-off in the sieve - it allows for a relatively simple way of uncovering what sorts of states that the decoherence process should select.

4.3 Quantum Darwinism and Classical Objectivity

We have seen how decoherence from the presence of an environment allows for a quantum-to-classical transition of a system, as well as how it induces a basis of measurable states for the

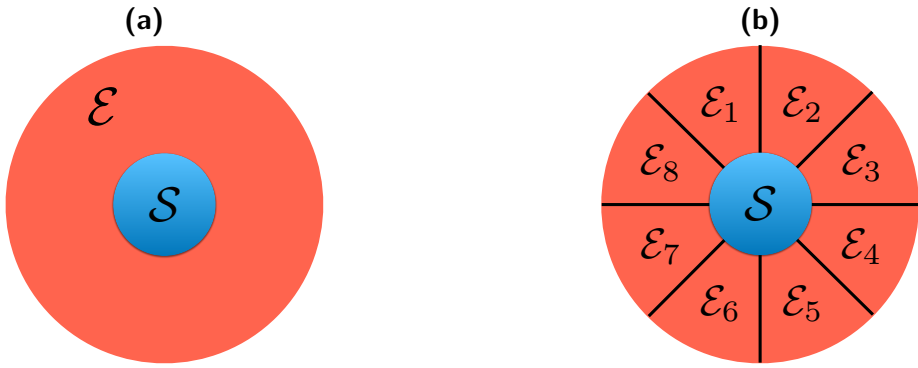


Figure 4.1: A heuristic diagram of how quantum Darwinism differs from the typical open system picture. **(a)** displays the decoherence paradigm, where the environment is treated as a monolithic bath into which the coherence of the system flows into. **(b)** displays the Darwinism paradigm. Here the environment is divided into *sub-environments* that are individually accessible to measurements. Treating the environment in a more active manner allows for us to study the type of correlations that emerge between the system and environment as the latter decoheres the former.

system. For Zurek, in order for a state to truly be classical it must also be *objective*. Objective in this sense means that multiple observers have access to and can reach a consensus on the state of the system. A system in a classically objective state should be unperturbed by these independent measurements. *Quantum Darwinism* [70, 137, 147] explains how such a state can be induced from interaction with an environment. Darwinism captures this in spirit by treating the environment microscopically. Information about the system must propagate into the environment in such a way that it is simultaneously available to all observers, who can learn about the system without perturbing it, and can reach a consensus about what the state of the system is. We do not directly probe a system we are interested in, instead information about the state is carried to us indirectly, say through photons carrying correlations with the system. In this spirit, Darwinism enforces structure on the environment. The total environment, \mathcal{E} , is considered as a collection of smaller fragments with which the system interacts and is able to share information

$$\mathcal{H}_{\mathcal{E}} = \mathcal{H}_{\mathcal{E}_1} \otimes \mathcal{H}_{\mathcal{E}_2} \otimes \dots \otimes \mathcal{H}_{\mathcal{E}_N}. \quad (4.10)$$

Figure 4.1 displays the difference between the typical open system paradigm and that of quantum Darwinism. What is formerly a monolithic environment, potentially modelled by a master equation, is treated in a more active manner by dividing it into *sub-environments*. Here sub-environments interact with the system and are accessible via measurements by an observer. What quantum Darwinism searches for is interactions that allow for multiple fragments of the environment to each have full information about the system. In this way the system will have encoded its state redundantly in the environment - i.e. having access to more fragments of the environment does not reveal more about the system.

Observers can each query one (or more) of the fragments of the environment. We note

that depending on the precise nature of the system-environment interaction or intra-environment interactions, we may need to consider several environmental degrees of freedom together as a single fragment in order to see a redundant encoding. As we outlined earlier, einselection occurs between the system and the environment, correlating the state of each environmental fragment with the pointer states of the system

$$|\psi_{S\mathcal{E}}\rangle = \sum_i p_i |p_i\rangle \otimes |\mathcal{E}_i^1\rangle \otimes \dots \otimes |\mathcal{E}_i^N\rangle. \quad (4.11)$$

This branching form of the state is essential a generalised GHZ state. It is clear that it is the distinguishability between the states of an environmental fragment that branch from the pointer state of the that allows for an observer to extract p_i from measurements on the fragment alone. In the case that the *conditional states* of each fragment $\{|\mathcal{E}_i^i\rangle\}$ are orthogonal, we call the global state in (4.3) a *spectrum broadcast structure* [153]. Einselection induces a structure that has proliferated information about the pointer states of the system throughout the environment, and measurements on each fragment or collection of fragments will not perturb the others. In order to satisfy the consensus requirement, we wish to see redundancy of information about the pointer states in the environment. The principle quantity of interest to see this is the quantum mutual information

$$\mathcal{I}(S : \mathcal{E}_f) = h(\rho_S) + h(\rho_{\mathcal{E}_f}) - h(\rho_S, \rho_{\mathcal{E}_f}), \quad (4.12)$$

where $h(\cdot)$ denotes the von Neumann entropy, and ρ_S is the density matrix of the system. While we divide the environment in to N sub-environments, we can in principle take several sub-environments together as a fragment \mathcal{F} . In this way, $\rho_{\mathcal{E}_f}$ is the density matrix of the fraction of the environment, $f = \mathcal{F}/\mathcal{E}$, which an observer has access to. When $\mathcal{I}(S : \mathcal{E}_f) = H(S)$, the information about the system is stored completely in the fragment \mathcal{E}_f . An observer who is able to interrogate this fragment will have access to all the available system information, and importantly, no additional information can be obtained even if a larger fraction of the environment is accessible [138]. Such a condition naturally implies a notion of objectivity, as two observers querying different fragments of the environment will nevertheless have access to the same system information. The system is therefore said to have redundantly encoded its state into the environment degrees of freedom and this redundancy is witnessed by a characteristic plateau in the mutual information, Eq. (4.12), for increasingly larger fractions of the environment. The upper bound on mutual information that an environmental fragment can hold about the system is simply the von Neumann entropy of the system. This limit is dependent on the initial state of the system, so we will use the rescaled mutual information between fragments of the accessible environment and the system

$$\bar{\mathcal{I}} = \frac{\mathcal{I}(S : \mathcal{E}_f)}{h(S)}, \quad (4.13)$$

which will show maximum correlation between the system and an environmental fragment when $\bar{\mathcal{I}} = 1$ regardless of the entropy of the system.

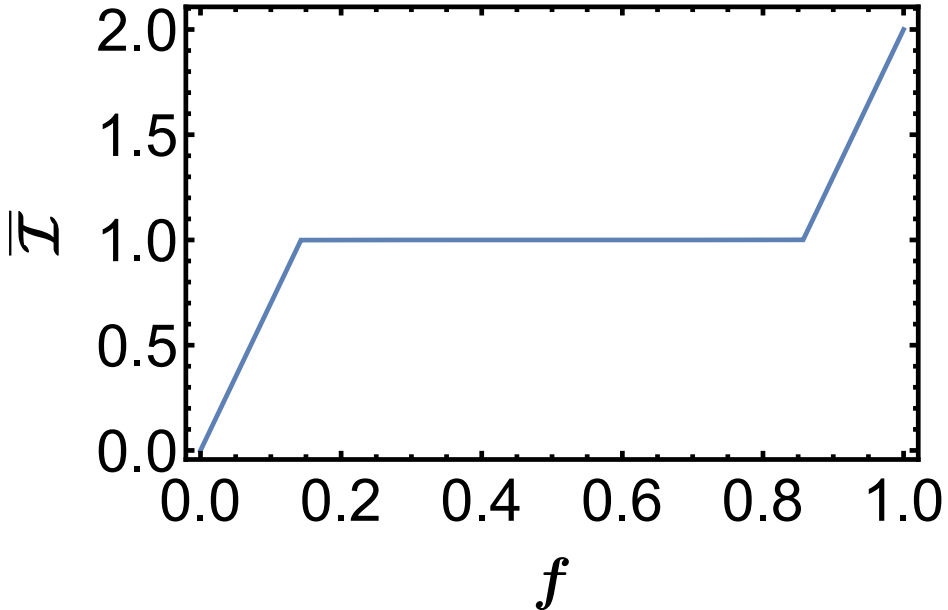


Figure 4.2: We plot the rescaled mutual information between a bath of seven qubits and a system qubit that interact with a dephasing-type interaction in the computational basis. Initially the system and environment begin in a pure product state with no correlations or mutual information between them. After some time ($Jt = 0.6$ in this case) correlations proliferate through the environment as prescribed by Quantum Darwinism, resulting in the above redundancy plateau.

As an illustrative example, let us consider a single qubit, initialised in the $|+\rangle$ state. It interacts simultaneously with 7 qubits, which we also initialise in the $|+\rangle$ state. We regard each of the 7 qubits as an environmental fragment. For interactions with the environment which give rise to a pure decoherence for the system, i.e. those interactions which only affect the coherences and leave the populations unchanged, it is known that such interactions lead to the type of global system-environment configurations that support classically objective states [154, 155]. This is precisely the phenomenological model of an open system that we discussed previously in Chapter 3. Therefore we take the interaction Hamiltonian between the system and the i^{th} environmental fragment to be

$$H_{int} = -J\sigma_z^S \sigma_z^{E_i}. \quad (4.14)$$

We let the global system evolve unitarily, and find the mutual information between the system and different sized collections of environmental fragments. The results are shown in Fig. 4.2. We see that after some time, the mutual information between the system and any one of the fragments maximises to $h(S)$. Interrogating larger fractions of the environment does not give us access to any more information about the state - it has been encoded redundantly. Only when we probe the entire environment do we find the mutual information of both system and environment. We refer to the shape of the figure we plot as the redundancy plateau.

This framework has been extensively explored for a system in contact with a single, possibly complex, bath [154–178] where the role of different bath characteristics can have a significant affect

on the system's ability to redundantly encode its information within the bath [179–183]. The key characteristic of the system-bath interaction is that it should be able to support a pointer basis - i.e. there are states of the system that are robust to decoherence, and that it generates few if any correlations between environmental fragments. A bath that has interactions between its degrees of freedom will wash out redundant encoding of the pointer states due to quantum information scrambling. Any correlations between environmental fragments will prevent the emergence of spectrum broadcast structures. As we shall see, direct interaction between the environmental fragments is not the only mechanism that causes information to mix in the environment.

We wish to consider a complementary setting where the system is in contact with two baths, one which we refer to as the “accessible” environment which consists of the fragments that hypothetical observers would be able to measure. The accessible environmental fragments do not interact directly with each other. As in our example above, we will assume that this accessible environment gives rise to a purely dephasing dynamics on the system which, in the absence of any other influences, provides the conditions necessary for quantum Darwinism and spectrum broadcast structures to be exhibited. In addition we assume that the system is also in contact with a second “inaccessible” bath. We aim to explore how the nature of this inaccessible bath effects the system’s ability to redundantly encode information about its pointer states into the accessible environment’s degrees of freedom.

We examine the microscopic model for the multiple bath setting, considering a minimal model for the accessible environment consisting of three qubits inducing a pure dephasing dynamics on the system, while we employ a collision model [184–186] to simulate the inaccessible environment.

4.4 Collisional-model picture of the system-environment interaction

We consider the situation as depicted in Fig. 4.3(a) where the system of interest, S with free Hamiltonian $H_S = \sigma_z^S$, is in contact with two distinct environments, one composed of a small number of constituents which we refer to as the accessible environment and represents the degrees of freedom which an observer would have access to. As in our example, we take the Hamiltonian governing the interaction between the system of interest and the fragments of the accessible environment, labelled A_i , to be

$$H_{SA} = J_{SA} \sum_i (\sigma_z^S \otimes \sigma_z^{A_i}). \quad (4.15)$$

Here σ_p^k is the $p = x, y, z$ Pauli operator of either the system (for $k = S$) or one of the fragments (when taking $k = A_i, \forall i$). We stress that redundancy is in terms of the size of an environment that the observer has access to - whether the observer has access to a single fragment, or the majority of the environment, they can only extract at most $h(\rho_S)$ bits of information, until they have access to the entire environment at which point they can extract $h(\rho_S) + h(\rho_E)$ bits of

information. For clarity, in what follows we will restrict the size of the accessible environment to three subsystems, which is the smallest size required for characteristic redundancy plateaux to be observed. With two accessible qubits, we would not find a plateau, as a measurement over both qubits would constitute the entire environment. Larger accessible environments than three qubits considered in the same way will simply result in faster times in which the redundancy plateau emerges. As we saw before, this setting will recover clear Darwinistic features.

In addition to the accessible environment, we allow the system of interest to be coupled to a second inaccessible bath, which could in principle be of a different nature. Such a setting is physically well motivated: nothing precludes augmenting the original paradigm of quantum Darwinism to allow for the system to be simultaneously coupled to a thermal bath for instance. Recently the delicate interplay between whether it is possible for states to be both thermal and classically objective has been explored [172]. Here, we address a complementary setting in order to gain qualitative insight into how the nature of the interactions between a system and an inaccessible environment affect the system's ability to redundantly proliferate information into accessible environmental degrees of freedom. To this end, we rely on a collision model description of the inaccessible environment.

Collision models provide a versatile tool for modelling open system dynamics and are particularly suited to our purposes [155, 184, 185]. Collision models simulate open systems by allowing the system to interact with a single incoming environmental unit for a short period of time, after which this unit is traced out and a "fresh" unit is introduced, therefore capturing the inaccessible nature of the environment we are modelling as any information regarding the state of the system which is imprinted on these units is irretrievably lost. A further advantage of exploiting the collisional model framework is that it allows to simulate different physically relevant environmental dynamics by simply tuning the microscopic details of the interaction. Care must be taken in this context: if the system-environment interaction does not commute with the system's Hamiltonian, the free-evolution of the system must be taken into account [187, 188]. However we will only consider two system-environment interactions that give rise to physically relevant dynamics, namely dephasing and thermalisation, and are unaffected by the inclusion of the free evolution term. The respective Hamiltonians are

$$\begin{aligned} H_{SE_j}^D &= J_{SE}(\sigma_z^S \otimes \sigma_z^{E_j}), \\ H_{SE_j}^T &= J_{SE}(\sigma_x^S \otimes \sigma_x^{E_j} + \sigma_y^S \otimes \sigma_y^{E_j}), \end{aligned} \tag{4.16}$$

where E_j is the label for the j^{th} unit of the inaccessible environment modelled through the collisional picture.

The system then interacts stroboscopically with the environments, first colliding for a time τ_1 with the all accessible fragments, then interacting with the collisional bath for a time τ_2 , i.e.

$$\rho(n+1) = U_{SE}U_{SA}\rho(n)U_{SA}^\dagger U_{SE}^\dagger, \tag{4.17}$$

where $U_{SA} = \exp\{-iH_{SA}\}\tau_1$ and $U_{SE} = \exp(-iH_{SE_j}\tau_2)$. The accessible fragments and system

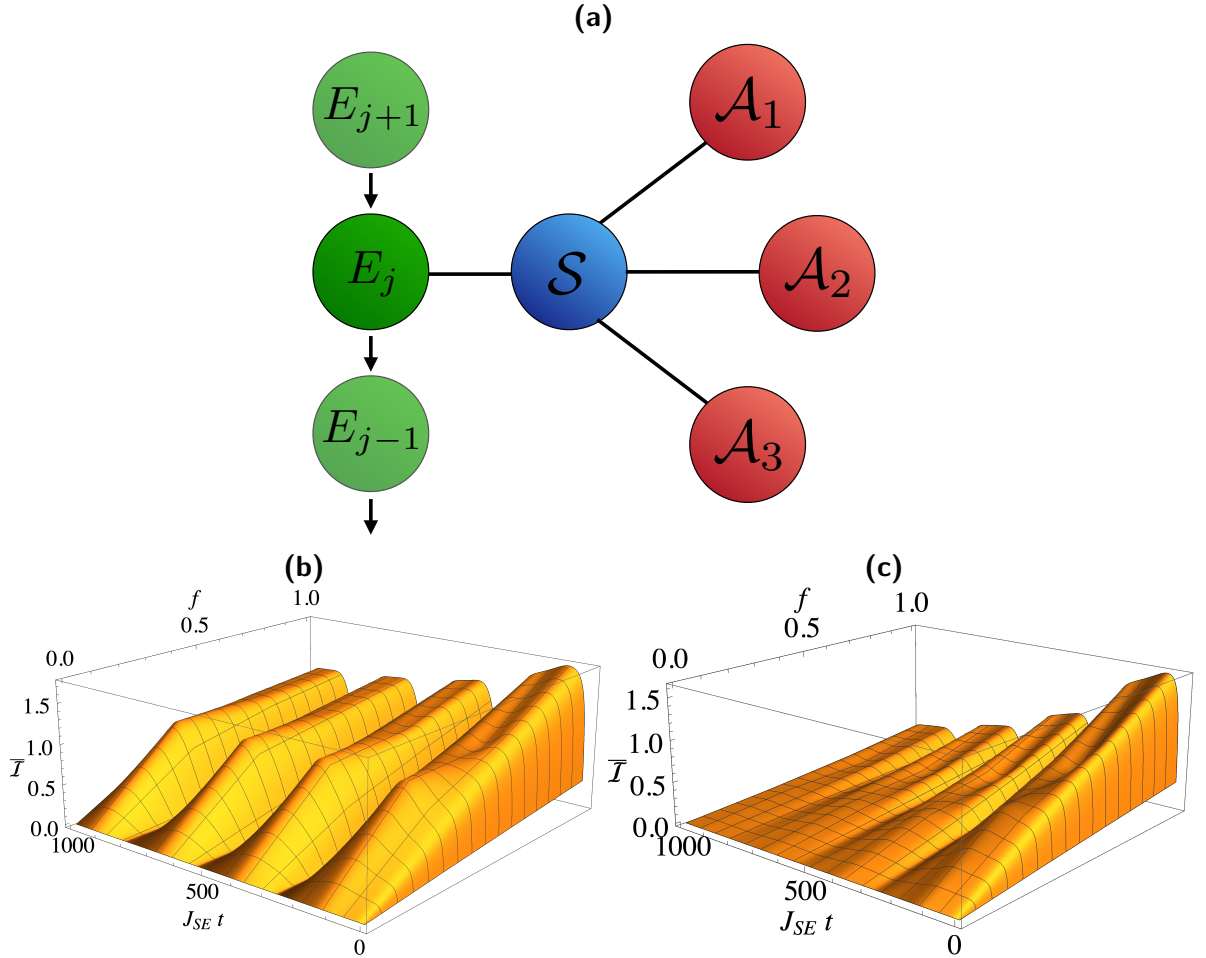


Figure 4.3: (a) Schematic of the microscopic collision model employed. (b,c) Rescaled mutual information, \bar{I} , for (b) dephasing collisional environment and (c) thermalising collisional environment. We fix $J_{SAT_1} = 0.0075\pi/4$ and $J_{SE}\tau_2 = 0.015\pi/2$ and $\beta = 0$. For both interactions the collisional environment drives the system towards a fully decohered state, however, in the case of a dephasing interaction the mutual information shared between system and accessible environment fragments shows the characteristic redundancy plateau transiently emerges with period dictated by the J_{SA} interaction strength. For a thermalising collisional bath there is an overall envelope where the redundancy plateaux are progressively damped. As elucidated in Sec. 4.5 this behaviour is explained by the commutativity, or lack thereof, between the system-environment interaction and system-accessible fragment interaction. In the dephasing case, the ability of the environmental fragments to create classical correlations with the system is unaffected by the presence of the collisional environment as the interactions commute, while this is not the case for a thermalising environment, which serves to fully decohere the fragments as well as the system in the long time limit.

are assumed to be initially prepared in state $|+\rangle = (|0\rangle + |1\rangle)/\sqrt{2}$ with $\sigma_z|0\rangle = |0\rangle$ and $\sigma_z|1\rangle = -|1\rangle$. Each incoming collisional unit is initialised in a Gibbs state with dimensionless inverse

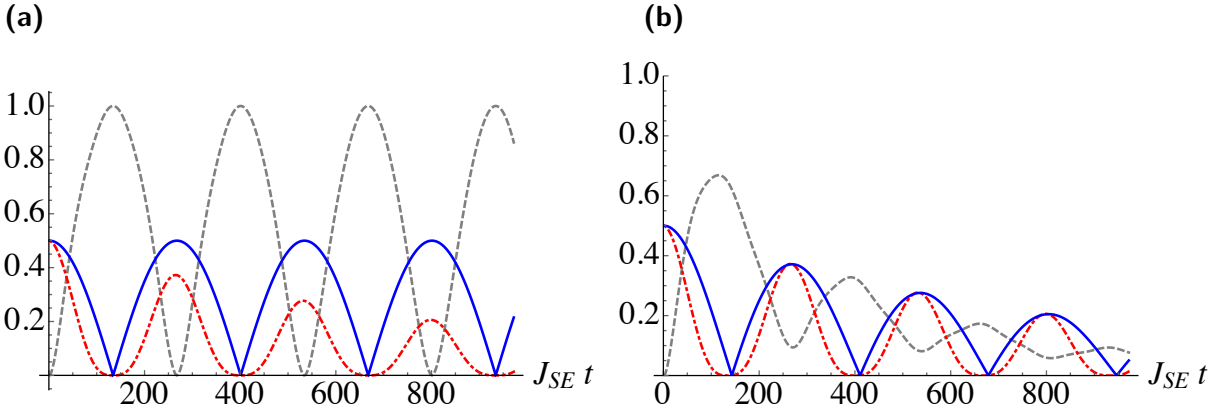


Figure 4.4: Mutual information between the system and a single accessible environmental fragment (dashed grey), the system coherence (dot-dashed red), and the fragment coherence (solid blue). **(a)** Dephasing collisional bath and **(b)** thermalising collisional bath. The system's coherence (dot-dashed red) is identical in both cases, the collisional bath will fully decohere in the long-time limit. The primary difference between the two cases is that the coherence of the accessible environmental qubit is damped by the thermalising bath despite not coupling to it directly.

temperature β , i.e.

$$\rho_{E_i} = \frac{1}{2} \begin{pmatrix} 1 + \tanh(\beta) & 0 \\ 0 & 1 - \tanh(\beta) \end{pmatrix}. \quad (4.18)$$

The system-accessible environment starts in a product state $\rho(0) = \rho_S(0) \otimes_{i=1}^3 \rho_{A_i}(0)$. For simplicity we take infinite temperature collisional units, however we remark, up to some minor qualitative differences, our results hold for finite temperatures. The infinite temperature assumption together with the considered initial states means that the resulting dynamics for the system is identical regardless of whether the interaction between system and collisional bath gives rise to dephasing or thermalisation.

We begin examining the mutual information shared between the accessible fragments and the system. For a dephasing interaction between the collisional bath and the system, Fig. 4.3(b) shows that the characteristic redundancy plateau emerges. For short time dynamics, where the effects of the collisional bath are small, the rise in mutual information when an observer has access to all constituents of the accessible environment, and therefore $f=1$, is evident. For longer times, where the collisional bath is able to decohere the system, we find that redundancy of the information shared between the system and accessible fragments is maintained, however, now there is no rise when an observer has access to all accessible fragments. In essence, while the system shares correlations with the collisional bath, it is still able to share the relevant classical information with fragments of the accessible environment. The emergence of the characteristic redundancy plateaux are periodic. This is due to the small size of the considered accessible fragments, with the period being fully determined by the strength of the system-fragment interaction, J_{SAT_1} . The interplay between the two environments becomes more interesting when we move away from pure dephasing, and instead allow for an interaction between system and collisional bath that gives rise

to thermalisation, as shown in Fig. 4.3(c). The short time dynamics is qualitatively similar, and this is again due to the fact that we have a separation of timescales between the two baths. At intermediate times, we see that the mutual information continues to plateau when an observer has access to larger fractions of the accessible environment. However, its value is no longer equal to the system entropy, therefore indicating that while information is being redundantly encoded, an observer cannot gain access to all the classical information about the state of the system due to the interaction with the thermalising environment. For very long interaction times we see that the information shared between system and accessible fragments $\bar{I} \rightarrow 0$, indicating the complete loss of all correlations - our global system has experienced “heat death.”

We reiterate that the system undergoes an identical evolution in both cases for the considered parameters. Given the choice of initial conditions, the populations remain fixed and the effect of the collisional bath is to simply dampen the coherences present in the system. We demonstrate this explicitly in Fig. 4.4 where the dashed red curve shows the behaviour of the coherence term of ρ_S [189]

$$C = \sum_{i,j} |(\rho_S)_{ij}|, \quad (4.19)$$

and is identical for both dephasing interactions (Fig. 4.4 (a)), and thermalising interactions (Fig. 4.4 (b)), with the collisional bath. If we focus on only a single accessible fragment, we can see a striking difference that the form of the system-inaccessible bath interaction has on the properties and correlations that the accessible fragment shares with the system. For a dephasing collisional bath, Fig. 4.4(a), we show the dynamics of the fragment coherence and the (rescaled) mutual information shared between this fragment and the system, solid blue and dashed grey curves, respectively. Periodic behaviour is exhibited, with perfect classical correlations established between the system and fragment when the accessible qubit’s coherence term vanishes, with this behaviour persisting regardless of the fact that the system coherence term is being damped by the collisional bath. In contrast, for the thermalising inaccessible bath we find that the accessible fragment loses coherence in line with the behaviour of the system. The accessible environmental qubits must “trade” their coherence for classical correlations with the system. Despite not coupling to the thermalising bath directly, their maximum coherence is dampened over time. This in turn reduces their ability to generate classical correlations with the system, with the overall effect being that all coherence and correlations are destroyed by the thermalising interaction in the long time limit [172]. A similar effect is seen for “structured” baths [170, 171], where interactions between accessible environmental qubits will cause Quantum Darwinistic characteristics to disappear over time.

Therefore, despite the dynamics of the system being identical in these two situations, the ability for the system to establish the requisite correlations is strongly dependent on the nature of the interaction with the inaccessible environment. While other choices of initial states and/or inaccessible bath temperatures will present minor quantitative differences, the overall picture remains the same: pure dephasing interactions between the inaccessible bath and the system always allows for

perfect redundancy of information to be encoded within the accessible environment, while thermalising interactions will eventually destroy all correlations leading to a loss of classical objectivity. As we will see, the reason for this difference in behaviour is rooted in the non-commutativity between the interactions of the system with the two separate baths.

4.5 Role of commutativity

In the previous section we demonstrated that the nature of the system-inaccessible environment can have a significant effect on whether the conditions for classical objectivity over time are fulfilled or not. We can gain insight into the reason for this dichotomy by examining the commutativity between the various interactions. As the accessible environment fragments are non-interacting with each other, and due to the considered form of the system-fragment Hamiltonians, we can restrict our attention to only a single qubit of the accessible environment since, given the symmetry of setting, the exhibited behaviour is identical for each individual accessible fragment. We can recast the problem using standard tools from open quantum systems, with the system simultaneously coupled to a GKSL bath and a single auxiliary qubit [190–193]. The dynamics of the system-accessible fragment is therefore governed by the Markovian master equation

$$\dot{\rho}_{SA} = -i[H_{SA}, \rho_{SA}] + \mathcal{L}(\rho_{SA}). \quad (4.20)$$

The superoperator, $\mathcal{L}(\cdot)$, determines the effect that the inaccessible environment has on the system. As previously, we consider both situations where \mathcal{L} gives rise to dephasing and thermalisation affecting the system only, i.e.

$$\begin{aligned} \mathcal{L}^D(\rho) &= \gamma(\sigma_z^S \rho \sigma_z^S - \rho), \\ \mathcal{L}^T(\rho) &= \gamma(\bar{n} + 1) \left(\sigma_-^S \rho \sigma_+^S - \frac{1}{2} [\rho, \sigma_+^S \sigma_-^S] \right) \\ &\quad + \gamma\bar{n} \left(\sigma_+^S \rho \sigma_-^S - \frac{1}{2} [\rho, \sigma_-^S \sigma_+^S] \right), \end{aligned} \quad (4.21)$$

where $\bar{n} = 1/(e^\beta - 1)$ is the mean number of thermal excitations in the environment. We can readily solve Eq. (4.20) for both types of bath and determine the reduced states for both system and accessible fragment. For clarity we fix both the accessible qubit and system to have the same initial state $\rho_S(0) = \rho_A(0) = |+\rangle\langle+|$, although remark that our results are qualitatively unaffected for other suitable choices. In the case of dephasing, the system's populations are unaffected, while for a thermalising bath the populations are driven to the relevant values as dictated by the canonical Gibbs state given by the choice of n . Regardless of the nature of the system-inaccessible environment interaction, the accessible fragment's populations are invariant. We find that it is the behaviour of the coherence terms in the various reduced density matrices that determine whether

classically objective states can be achieved. The coherences are given by

$$\begin{aligned} \text{dephasing: } & \begin{cases} \langle 0 | \rho_S^D | 1 \rangle = e^{-2\gamma t} \cos(J_z t), \\ \langle 0 | \rho_A^D | 1 \rangle = \cos(J_z t) / 2, \end{cases} \\ \text{thermalising: } & \begin{cases} \langle 0 | \rho_S^T | 1 \rangle = e^{-\gamma(\bar{n} + \frac{1}{2})t} \cos(J_z t), \\ \langle 0 | \rho_A^T | 1 \rangle = \frac{e^{-(\gamma + 2\bar{n}\gamma + \alpha)t/2}}{4\alpha} [(e^{\alpha t} + 1)\alpha + \gamma_{\bar{n}}(e^{\alpha t} - 1)], \end{cases} \end{aligned} \quad (4.22)$$

where $\gamma_{\bar{n}} = \gamma(2\bar{n} + 1)$ and $\alpha = \sqrt{-4J_z(J_z + i\gamma) + \gamma_{\bar{n}}^2}$. We see that for both types of environment, the system coherence undergoes two competing effects. The dephasing interaction with the accessible fragment gives rise to an oscillatory behaviour, while the interaction with the inaccessible environment leads to an exponential decay. Regardless of the nature of the inaccessible bath, the system coherence will vanish asymptotically. If we turn our attention to the behaviour of the fragment's coherence we see the markedly different effect that the nature of the inaccessible environment now has. For a dephasing Lindblad bath, due to the fact that the interactions of the system with the two baths commute, we find that the accessible fragment is blind to the presence of the inaccessible bath, with its coherence term oscillating with a period dictated by the strength of the system-fragment interaction [155], while the Lindblad bath has no effect on its dynamics. In contrast, for a thermalising bath, we see that despite the accessible fragment not interacting directly with the Lindblad bath, its coherence term is nevertheless exponentially suppressed. This, in conjunction with the behaviour of the system coherence term, means that no correlations can be maintained in the long time limit, leading to the loss of the conditions necessary to support classically objective states. It is worth stressing the difference between the system-inaccessible environment interactions, which is clearly seen when considering the microscopic description captured by Eq. (4.16). In the case of dephasing, purely informational exchange occurs, while the thermalising interaction supports both information and energy exchanges, with the latter destroying all correlations in the long time limit.

4.6 Conclusions

In this chapter we have examined the emergence and suppression of signatures of classical objectivity when a system is in contact with multiple environments. Assuming an observer can query an accessible environment, which interacts with the system via pure dephasing interactions, which are known to support the conditions necessary for the establishment of classically objective states, we have demonstrated that the nature of the interaction of the system with the remaining inaccessible environment(s) can drastically affect the establishment of classical objectivity, as captured by quantum Darwinism. We have shown that for system-inaccessible environment interactions that commute with the system-accessible environment interaction, the relevant system information can proliferate into the accessible fragments since these environmental degrees of freedom

are unaffected by the presence of the other bath. However, for other interaction terms which do not commute with the system-accessible Hamiltonian, while partial redundancy can be established transiently, the interaction of the system with the inaccessible environment leads to the loss of all correlations, and thus also of the conditions for classical objectivity. We established that the commutativity between the two Hamiltonians governing how the system interacts with the respective baths dictates whether conditions for classical objectivity can be maintained in the long-time limit. Our results indicate that commutativity plays a central role in a system's ability to redundantly encode its information and may be complementary to the subtle role that commutativity plays in, for instance, equilibration which has recently been established [194–196] or accurately modelling open system dynamics [197].

One may make the argument that this latter scenario, where the redundancy plateau emerges only transiently, but is washed out in the long-time limit is a more reasonable model of the emergence of classical objectivity. In our scenario we observe *heat-death* in our toy universe, with a small window in which classical objectivity is allowed. A similar scenario is observed in [198]. Here Riedel, Zwolak, and Zurek couple a central spin to only a single environment, but allow for Ising-type interactions between the spins that constitute that environment. Similarly, they see that quantum Darwinism emerges only for intermediate times, before environmental interactions eventually scramble all the information about the system, and the global state equilibrates. As we have seen in our work, information scrambling in the environment is not the only cause of this equilibration, simply having non-commuting interactions on the system is enough. One natural question would then be to ask how “natural” is quantum Darwinism? We have selected specific interactions on an object that we give special status to as a system. Relaxing these assumptions may look like a lattice of spins with random nearest-neighbour interactions with strengths drawn from the same distribution. The homogeneous and isotropic setup we have outlined above will not allow for Darwinism as even if there were interactions that distinguished a single site with a pointer basis, there is no separation of timescales between Darwinism and scrambling. In recent times much work has been done into classifying the types of interactions and partitions that would allow for quantum Darwinism [171, 199], typically with an aim at finding scenarios in which Darwinistic features are maintained for long times. It is the view of the author that it is enough to search for setups with minimal assumptions that allow for Darwinism transiently in the face of inevitable information scrambling and thermalisation of the global system. Such an outcome is a generic phenomenon for quantum systems with interactions, with few notable exceptions. In the next chapter we will delve into this phenomenon in more detail.

Chapter 5

Operator Spread Complexity

In classical computation, the complexity of a Boolean function refers to the number of elementary operations needed to evaluate it. Complexity allows one to classify problems based on how their evaluation scales with the size of the input. “Easy” problems are regarded as those that can be solved in a number of steps that is a polynomial of the number of inputs, while “hard” functions to evaluate are those whose evaluation involves a number of operations that scale exponentially with the number of inputs. The circuit-based model of quantum computing allows for a similar definition of complexity, namely the minimal-size circuit that evaluates the problem to a high-precision, albeit with some ambiguity over what particular universal set of gates are admitted.

There is much motivation for defining a complexity measure for specific quantum mechanical models [200]. For instance, we could similarly define a notion of state complexity by the depth of the circuit needed to engineer the state from an initial state [201]. States that are easy to prepare should involve circuits that have a depth that scales polynomially with the number of qubits, meaning that they physically can be prepared in polynomial time. The volume of these preparable states occupy a vanishingly (exponentially) small portion of Hilbert space for a many-body quantum system, meaning that the majority of quantum states for a many-body system are too *complex* to be physically realisable [202]. The set of available unitaries that govern the evolution form a continuum, allowing for a geometric interpretation of complexity, as a geodesic path on the manifold of operators [203]. Operator complexity has gained much interest for its role as an indicator of quantum chaos [204], probing topological phases of matter [205], and in the holographic conjecture [206].

The exact operational definition of complexity in this case remains open. The circuit based approach admits a geometric interpretation, but is difficult to compute [207]. Operator size, or the number of contributing components (be it fundamental fields or basis elements) to the expansion of the time evolved operator has been posited as a measure of complexity with motivation from quantum circuits [208], many-body physics [209], and high-energy theory [206]. The operator growth hypothesis (OGH) [204], which we shall introduce in more detail later, leverages the Lanczos algorithm [210] to provide a measure of complexity for a system’s dynamics. It has gained significant interest as a result of its close relationship to out-of-time-ordered correlators,

autocorrelation functions, spectral functions, and as a probe of quantum chaos. For the latter, it can provide false positives [211], and anti-correlations [212], perhaps indicating the need for a stronger statement for the OGH. It also is limited in its scope, being restricted to time-independent unitary evolution, and those governed by a Lindblad master equation.

We take motivation from both operator growth and Krylov complexity to define a probe of quantum complexity that is more flexible in scope - the *operator spread complexity*. The framework provided by operator spread complexity unifies both concepts of operator size and Krylov complexity and exhibits the phenomena required of a complexity measure [213]. Crucially, the spread complexity does not prescribe a particular basis, and therefore in principle any suitable basis can capture the same qualitative complexity behaviour, with universal statements made possible by a choice of basis that minimises the complexity measure. Remarkably, we show that such a minimisation is done by the Lanczos algorithm, with the Krylov space (and its complement) forming the minimal basis for the spread complexity. These results constitute the original work found in Ref. [4], which was a collaboration between several authors, with the analytical and numerical work performed by myself and Anthony Kiely.

5.1 Quantum Chaos

In classical mechanics, chaos is typically considered synonymous to an exponential sensitivity of the trajectories to initial conditions, characterised by the Lyapunov exponent. Specifically it quantifies how rapidly two infinitesimally close trajectories in phase space diverge over time. In a chaotic system, the separation between two points in phase space grows as $\delta(t) \approx \delta(0)e^{\lambda t}$, where $\delta(0)$ is the initial separation vector between the two points and λ is the Lyapunov exponent. We define the Lyapunov exponent λ as

$$\lambda = \lim_{t \rightarrow \infty} \lim_{\delta(0) \rightarrow 0} \frac{1}{t} \ln \frac{\|\delta(t)\|}{\|\delta(0)\|}, \quad (5.1)$$

where $\|\delta(t)\|$ denotes the Euclidean norm of the separation vector. Many quantum systems exhibit chaotic behavior in the classical limit, such as the quantum kicked rotor [214]. However, defining quantum chaos in a dynamical way is significantly more difficult owing to the linearity of the Schrödinger equation, and lack of defined trajectories [215]. A quick aside must be made about integrable systems: a system described by the Hamiltonian H_I (we treat the system as quantum, but the same definition holds true with the appropriate classical equations of motion) is classified as integrable if there are as many independent constants of motion, I_i as degrees of freedom

$$[H_I, I_i] = 0, \quad [I_i, I_j] = 0. \quad (5.2)$$

One may be tempted to describe quantum chaotic systems as all those which are non-integrable, but non-integrable systems can still exhibit quasi-integrable or periodic behaviour [216]. Systems with disorder are typically non-integrable, but can exhibit Anderson localisation [217], preventing thermalisation.

The major breakthrough for defining chaos in quantum systems originated in the development of random matrix theory (RMT), independently by Wigner [218] and Dyson [219]. It was initially developed in the context of nuclear physics to explain the spectra of atomic nuclei. In a small energy window, and with a generic basis, the Hamiltonian of the complicated system will look like a random matrix, where the entries are drawn from a Gaussian distribution. By taking ensembles of random matrices with the relevant symmetries for the highly-structured system of interest, we can gain insight into the statistical properties of their spectra instead of attempting to calculate the eigenvalues exactly. Specifically, we study the level-spacing statistics, the distribution of the difference between consecutive energy levels. The level-spacing statistics of RMT follow the Wigner-Dyson distribution. For a spacing s_i between consecutive energy levels E_i and E_{i+1} , the probability distribution $P(s)$ for an RMT ensemble of 2x2 real symmetric matrices with time-reversal symmetry is given by

$$P(s) = \frac{\pi s}{2} \exp\left(-\frac{\pi s^2}{4}\right), \quad (5.3)$$

where s is the spacing normalized to the mean level spacing. The above ensemble is known as also known as the Gaussian Orthogonal Ensemble (GOE). Remarkably, the above distribution is seen when plotting the level spacing histogram for various heavy nuclei [220].

Numerical studies of the level spacing statistics of quantum chaotic systems with classical analogues showed that they also could be modelled by the Wigner-Dyson distribution. The connection between quantum chaos and RMT was formalised in 1984 by a conjecture by Bohigas, Giannoni, and Schmidt [214]. The BGS conjecture states that for a quantum system whose classical analog is chaotic, the statistical properties of its energy levels are the same as those of the eigenvalues of a random matrix from one of the standard ensembles. This conjecture has been shown to hold true not only for the original class of systems that had a classical analogue, but also for quantum chaotic systems that do not [221]. In addition, level-spacing statistics are fundamentally linked with the ergodicity of a system, indicating whether or not the system obeys the eigenstate thermalisation hypothesis (ETH) [222]. Many non-integrable quantum systems can display complex dynamics and fast operator growth without displaying Wigner-Dyson level spacing statistics [223, 224], pointing to a need for a probe of chaotic dynamics that is separate from a probe of ergodicity. And while level spacing statistics can give much insight into the dynamics of the system, it still does not give a quantitative measure of the complexity of the system or particular initial conditions in the same way as the classical Lyapunov exponent.

Attempts to define a quantum analogue of the Lyapunov exponent lead to the development of out-of-time-order correlation functions (OTOCs) [225]. We will first introduce the double commutator

$$C(t) = \langle [W(t), V]^\dagger [W(t), V] \rangle. \quad (5.4)$$

where $W(t) = e^{iHt}We^{-iHt}$ and $W(0)$ and V have no mutual support in Hilbert space. This quantity therefore starts at zero and saturates at $C(t) = 2$ if $W(t)$ grows in support and no longer commutes with V . The motivation for this quantity can be seen when taking $W = x$ and $V = p$,

the position and momentum observables, and then taking the semi-classical limit [225]

$$C(t) = \langle [x(t), p]^\dagger [x(t), p] \rangle \rightarrow (i\hbar)^2 \left(\frac{\partial x(t)}{\partial x(0)} \right)^2 \sim e^{2\lambda_L t}. \quad (5.5)$$

The autocorrelation function of the commutator can be directly linked to the classical Lyapunov exponent, and the exponential growth of it at short times is seen for quantum chaotic systems, for generic choices of operators that initially commute. Eq. (5.1) can be rewritten as

$$C(t) = 2(1 - \text{Re}\langle W(t)^\dagger V^\dagger W(t), V \rangle), \quad (5.6)$$

where the object that we take the real part of is the out-of-time-ordered correlation function (OTOC). This object exponentially decays from 1 to 0 for systems with fast growing entanglement structures [225], however for systems with local interactions this decay will only be polynomial in time [226]. The decay of an OTOC is an indicator of *scrambling*—the spread of initially local information throughout a many-body system. While information scrambling intuitively resembles classical chaos - information about the initial configuration of the system is rapidly lost - it is a necessary but not sufficient condition for a system to be chaotic [227, 228]. Subsequently, interest in other dynamical signatures of chaos and information scrambling has grown, with much focus on the behaviour of autocorrelation functions [229], the Loschmidt echo [230], the hydrodynamical behaviour of many-body quantum systems [231–236], and the spread of support of both states and operators [237–240].

Recent work has explored the competition and similarities of scrambling and decoherence, as well as similarly finding a definition for quantum chaos for open systems [146, 240–247]. Decoherence is a channel for information from the system to leak into the environment, as opposed to being spread into entanglement structures in a many-body system. The OTOC has been shown to not distinguish between these two effects [241], meaning that other measures must be used in the open system setting. Complex spacing ratios [248] and dissipative form factors [240, 249] have been developed to characterise the level repulsion for chaotic systems in non-Hermitian settings, where the spectrum is no longer purely real. The operator growth hypothesis (OGH) [204] has gained significance as a tractable method of calculating the complexity of a system and has placed upper bounds on the Lyapunov exponent extracted from the OTOC. The OGH relies on being able to find the *Krylov subspace* of an operator, and tracks the support of the time evolved operator in this subspace. This subspace can be found for time-independent closed dynamics [204], dynamics described by the Markovian GKSL master equation [250]. We will outline the operator growth hypothesis as well as how these spaces are found for both cases.

5.2 Krylov Subspaces

The phenomena that the OGH leverages is the tendency for operators to grow support in Liouville space as they evolve. To determine the growth rate, consider a system described by a Hamiltonian

H , and an initially local Hermitian operator, denoted by $|X_0\rangle$. The operator evolves under the action of the superoperator \mathcal{L} . The Maclaurin series expansion of the operator follows as $|X_t\rangle = e^{i\mathcal{L}t}|X_0\rangle = \sum_n \frac{(it)^n}{n!} \mathcal{L}^n |X_0\rangle$. In the closed case the superoperator is simply $\mathcal{L}\bullet := [H, \bullet]$ and operators that do not correspond to a conserved quantity with respect to the Hamiltonian will spread in support with repeated applications of this commutator. All of the information about the evolution of the operator is therefore contained in the set $\{\mathcal{L}^n |X_0\rangle\}$. It is advantageous to transform this set into an orthonormal subspace of the overall Hilbert space. To do so, one must first define an inner product between operators. We choose the standard Bogoliubov inner products (also called the Kubo-Mori scalar product, or Duhamel two-point function) for inverse temperature β

$$(A|B)_\beta^g = \frac{1}{Z} \int_0^\beta g(\lambda) \text{Tr} \left(e^{-\beta H(1-\lambda)} A^\dagger e^{\beta H\lambda} B \right) d\lambda, \quad (5.7)$$

where Z is the partition function of the system, and $g(\lambda)$ is the metric to be defined. Different choices of metric will induce different inner products. For instance, we could choose the Fisher information metric,

$$g(\lambda) = \frac{\delta(\lambda) - \delta(\lambda - \beta)}{2}, \quad (5.8)$$

which gives the inner product

$$(A|B)_\beta^{FI} = \frac{1}{2Z} \text{Tr}(e^{-\beta H} A^\dagger B + A^\dagger e^{-\beta H} B). \quad (5.9)$$

Alternatively, we could pick the Wightmann inner product

$$g(\lambda) = \delta(\lambda - \beta/2), \quad (5.10)$$

which places operators $|A\rangle$ and $|B\rangle$ halfway along the thermal circle when taking the two point function

$$(A|B)_\beta^{FI} = \frac{1}{Z} \text{Tr}(e^{-\beta H/2} A^\dagger e^{-\beta H/2} B). \quad (5.11)$$

This inner product is notable as it is the one chosen to derive the “bound on chaos” [251], which places an upper bound on the Lyapunov exponent extracted from the OTOC

$$\lambda_L \leq \frac{2\pi}{\beta}. \quad (5.12)$$

It is noted that the above bound is tied to the choice of metric for the inner product, other choices can have inconsistent behaviour [204, 252]. We will work at infinite temperature, taking $\beta \rightarrow \infty$, removing the metric ambiguity.

Returning to the time evolved operator, we consider the case where its dynamics are generated by the superoperator $\mathcal{L} := [H, \cdot]$. With the specific choice of inner product, we can now employ the Lanczos algorithm to orthogonalise the set $\{\mathcal{L}^n |X_0\rangle\}$. This algorithm involves iteratively applying the superoperator to the initial operator, normalising at each step with a Gram-Schmidt-like process. Starting with $|O_0\rangle := |X_0\rangle$ we then define $|O_1\rangle := b_1^{-1} \mathcal{L} |O_0\rangle$ where $b_1 := (O_0 \mathcal{L} |O_0\rangle)^{1/2}$.

The rest of the basis is then found iteratively

$$\begin{aligned} |A_n) &:= \mathcal{L}|O_{n-1}) - b_{n-1}|O_{n-2}) , \\ b_n &:= (A_n|A_n)^{1/2} , \\ |O_n) &:= b_n^{-1}|A_n) . \end{aligned} \quad (5.13)$$

From this we obtain an orthonormal set of operators - the Krylov basis $\{|O_n)\}$, and set of constants - the Lanczos coefficients $\{b_n\}$. The algorithm terminates when $b_n = 0$ (or more accurately, to some small numerical cut-off). The dimension \mathcal{M}_K of the Krylov basis compared to the dimension \mathcal{D} of the Hilbert space is $\mathcal{M}_K \leq \mathcal{D}^2 - \mathcal{D} + 1$. In the Krylov basis, the superoperator takes a tridiagonal form

$$L_{nm} := (O_n|\mathcal{L}|O_m) = \begin{pmatrix} 0 & b_1 & 0 & 0 & \cdots \\ b_1 & 0 & b_2 & 0 & \cdots \\ 0 & b_2 & 0 & b_3 & \cdots \\ 0 & 0 & b_3 & 0 & \ddots \\ \vdots & \vdots & \vdots & \ddots & \ddots \end{pmatrix}. \quad (5.14)$$

With this form of the superoperator, the operator "hops" to higher basis elements in the Krylov chain over time, with higher- n elements having larger non-local support and complexity. For a chaotic 2-local superoperator - say the tilted field Ising model, the Krylov operator $|O_n)$ will typically have support over $n+1$ sites. We can represent the time-evolved operator in Krylov basis as

$$|O(t)) = \sum_{n=1}^{\mathcal{K}} \psi_n(t)|O_n). \quad (5.15)$$

Knowing that typically the higher n basis elements in the Krylov "chain" are in general more complex, a good indicator of complexity is to ask where the expected position of the operator on the chain. This is the Krylov complexity

$$K(t) = \frac{1}{\mathcal{Z}} \sum_n n |\psi_n(t)|^2, \quad (5.16)$$

where $\mathcal{Z} = \sum_n \|\psi_n(t)\|^2$. Closer study of the Krylov complexity has given additional insight into operator growth [253, 254], deriving the conditions needed for a model to saturate an upper bound on its rate of change. The Sachdev-Ye-Kitaev (SYK) model [204] is such a system, we will formally introduce it later. The OGH itself focuses on the Lanczos coefficients. the OGH states that the asymptotic growth of the Lanczos coefficients is maximal for chaotic systems. Specifically, this is characterised by a linear rate, $\alpha > 0$, such that $b_n = \alpha n + \gamma$ where γ is a constant. The growth rate, α , upper bounds the Lyapunov exponent obtained from the OTOC when the infinite temperature inner product is taken

$$2\alpha \geq \lambda_L. \quad (5.17)$$

The OGH has been successful in demonstrating the linear growth of Lanczos coefficients for chaotic

systems, both analytically and numerically, for a number of models [255–258]. However, while chaotic systems exhibit a linear growth in the Lanczos coefficients, unstable yet integrable systems may do the same [211, 259]. Quantum chaos implies a linear growth in the Lanczos coefficients, but the converse does not necessarily follow.

We can extend the framework of Krylov complexity case when the time evolution of an operator X_0 is governed by a Markovian GKSL master equation

$$\begin{aligned} \frac{dX_0}{dt} &= i\mathcal{L}X_0, \\ &= i[H, X_0] + \sum_n \mu_n [\pm L_n^\dagger X_0 L_n - \frac{1}{2}\{L_n^\dagger L_n, X_0\}], \end{aligned} \quad (5.18)$$

where “–” is taken when both the operator X_0 and the jump operators L_n are fermionic [260] and “+” otherwise. We again take the infinite-temperature inner product $(A|B) := \text{Tr}[A^\dagger B]/\text{Tr}[1]$. A variety of methods to create an orthonormal basis in this setting have been explored [250, 260–263]. We shall focus on the bi-Lanczos algorithm [250, 264], which recovers the Lanczos algorithm for zero decoherence. The bi-Lanczos algorithm evolves the left and right vectors of X_0 separately, enforcing orthonormality between elements of each set. We first fix $b_0 = c_0 = 0$, and then proceed with the bi-Lanczos algorithm

$$\begin{aligned} |A_n\rangle &:= (\mathcal{L} - a_{n-1})|O_{n-1}\rangle - c_{n-1}|O_{n-2}\rangle, \\ |B_n\rangle &:= (\mathcal{L}^\dagger - a_{n-1}^*)|O_{n-1}\rangle - b_{n-1}|O_{n-2}\rangle, \\ |O_n\rangle &:= b_n^{-1}|A_n\rangle, \quad (\tilde{O}_n| = c_n^{-1}(B_n|), \quad \text{with} \\ a_n &:= (\tilde{O}_n|\mathcal{L}|O_n), \quad b_n = \sqrt{(A_n|A_n)}, \quad c_n = \frac{\sqrt{(B_n|A_n)}}{b_n}. \end{aligned} \quad (5.19)$$

The algorithm terminates when $b_n=0$ for finite systems or when successive Krylov basis elements align. Again, both termination conditions involve a numerical tolerance. We therefore remark that the dimension of the Krylov space calculated reflects the number of numerically relevant elements, which may not be the exact dimension of Krylov space. We output two sets of vectors for which we have the orthogonality relation $(\tilde{O}_n|O_m) = \delta_{nm}$, where we remark that each set by itself is not necessarily orthogonal and in the bi-Lanczos basis the superoperator takes the tri-diagonal form

$$\mathcal{L} = \sum_{n,m} (\tilde{O}_n|\mathcal{L}|O_m)|O_n\rangle\langle O_m| = \begin{pmatrix} a_0 & b_1 & 0 & \dots \\ c_1 & a_1 & b_2 & \dots \\ 0 & c_2 & a_2 & \dots \\ \vdots & \vdots & \vdots & \ddots \end{pmatrix}. \quad (5.20)$$

The superoperator is again analogous to the tight-binding chain. We note that the a_n coefficients are purely imaginary, while the b_n and c_n are purely real. We can write the time-evolved

operator in both spaces as

$$|X_t\rangle = \sum_{n=0} i^n \phi_n(t) |O_n\rangle, \quad (X_t| = \sum_{n=0} (-i)^n \varphi_n^*(t) (\tilde{O}_n|. \quad (5.21)$$

We can again write the Krylov complexity [250]

$$K(t) = \frac{\sum_{n=0}^{M_K-1} n \varphi_n^*(t) \phi_n(t)}{\sum_{n=0}^{M_K-1} \varphi_n^*(t) \phi_n(t)}, \quad (5.22)$$

where M_K is the dimension of Krylov space. Due to the fact that the norm of the operator is not preserved in time for open dynamics, we have to renormalise the populations. The Krylov basis output by the bi-Lanczos algorithm is the minimal basis for describing the open dynamics of a particular operator, making it the natural choice of basis from which to extract universal behaviour. While the bi-Lanczos algorithm lets us probe operator complexity for dynamics generated by a Markovian master equation, it remains to be seen how one can generate the Krylov basis for general (potentially non-Markovian) open system dynamics, or even those for which the superoperator is not accessible such as a collision model [265, 266].

This provides the starting point of our work, in which we propose a tractable method for characterising chaotic dynamics and operator complexity in quantum systems. In particular, we introduce the *operator spread entropy* as a general notion for examining operator growth that provides a measure of complexity as well as allowing for insights into the operator population dynamics.

5.3 Spread Complexity

Consider a general orthonormal Hermitian operator basis $\mathcal{G} = \{|G_n\rangle\}$. The normalised overlap of an operator, $|X_t\rangle$, at a time t with the n^{th} element of this basis is

$$P_{\mathcal{G}}(n, t) = \frac{|(G_n|X_t)|^2}{\sum_m |(G_m|X_t)|^2}. \quad (5.23)$$

The population distribution of an operator can be used to study the onset of quantum chaos and has been shown to be intrinsically related to the OTOC [267, 268]. It is explicitly applied to the Krylov space for closed dynamics in Ref. [269]. To turn it into a measure of complexity we first demand that $|G_0\rangle = |X_0\rangle$.

The extent of the operator in a given basis [270] is given by the complexity (which can be recognised as both the diversity [271] and perplexity [272] of a distribution)

$$C_{\mathcal{G}}(t) = e^{F_{\mathcal{G}}(t)}, \quad (5.24)$$

where $F_{\mathcal{G}}(t) = -\sum_n P_{\mathcal{G}}(n, t) \ln P_{\mathcal{G}}(n, t)$ is the Shannon entropy for the operator distribution. For $t = 0$ we have $C_{\mathcal{G}}(0) = 1$, which increases with time due to scrambling of the operator, ultimately

saturating at long times if the operator is maximally spread over all available basis elements.

Two things must be noted about this measure: Firstly, we must choose *a-priori* a basis to measure the spread of the system over. The initial operator must be a distinct element of the basis - we assume it starts in a “low-complexity” configuration. Secondly, this measure distinguishes average operator size and complexity. For instance, consider a spin chain system described using a basis constructed from the strings of Pauli matrices. One could imagine a scenario where the time evolved operator has full *spatial* support over the chain, but is nevertheless “simply” a linear combination of a few strings of this maximal length. The spread complexity will be low in this case, therefore reflecting its low complexity in the bulk of the spin chain. This can be the case for certain Clifford circuits [273]. It is therefore relevant to consider whether other bases, aside from the minimal one, capture operator dynamics accurately.

5.4 Minimisation of the spread complexity

To show that the Krylov basis minimises the operator spread complexity we will utilise a similar approach as that given for the spread complexity of a state governed by the Schrödinger equation, derived in [237]. We modify their starting point to that of the evolution of an operator governed by a superoperator, with the only caveat being that we can obtain the Krylov space for the dynamics. Taking k derivatives of eq. (5.23) gives

$$\begin{aligned} P_{\mathcal{G}}^{(k)}(n, t) &\equiv \frac{\partial^k P_{\mathcal{G}}(n, t)}{\partial^k t} \\ &= \frac{\sum_{j=0}^k i^k (-1)^j \binom{k}{j} (X_t | \mathcal{L}^{\dagger j} | G_n) (G_n | \mathcal{L}^{k-j} | X_t)}{\|X_t\|^2} + \frac{(X_t | G_n) (G_n | X_t) \partial_t \|X_t\|^2}{\|X_t\|^4}, \end{aligned} \quad (5.25)$$

where we recognise that for a complete basis we have

$$\sum_n |(G_n | X_t)|^2 = \|X_t\|^2. \quad (5.26)$$

Let us assume for both a general basis, \mathcal{G} , and the Krylov basis $\{|O_n\rangle\} \in \mathcal{K}$ that the first element, i.e, $n = 0$, is X_0 , and that the following $m - 1$ elements are common to both. Therefore for $n < m$, we have that

$$P_{\mathcal{K}}^{(k)}(n, t) = P_{\mathcal{G}}^{(k)}(n, t). \quad (5.27)$$

We wish to isolate when the spread complexity differs between the two basis. We can take advantage of the orthogonality of the Krylov basis to show that a number of derivatives of the basis populations disappear.

Lemma 5.1 If the first m elements of \mathcal{G} are those of \mathcal{K} then $P_{\mathcal{G}}^{(k)}(n, 0) = 0$ for $n \geq m$ and $k < 2m$.

Proof. We first note that for all $n > 0$, the final term in eq. (5.25) is zero at $t = 0$ as $(G_n|X_0) = \delta_{n,0}$. From eq. (5.25) we see that $P_{\mathcal{G}}^{(k)}(n, 0)$ has at most k applications of the superoperator to $|X_0\rangle$. Taking $k < m$, it is clear that for $n \geq m$ we have $(G_n|\mathcal{L}^k|X_0) = (X_0|\mathcal{L}^{\dagger k}|G_n) = 0$ as $\mathcal{L}^k|X_0\rangle$ requires at least $k = m$ applications of \mathcal{L} to generate overlap with the first element of \mathcal{G} that is not also a Krylov element, $|G_m\rangle$. For $k < 2m$, all of the terms in the sum for $P_{\mathcal{G}}^{(k)}(n, 0)$ will be zero as either $(X_0|\mathcal{L}^{\dagger j}|G_n)$ or $(G_n|\mathcal{L}^{k-j}|X_0)$ will involve less than m applications of the superoperator to $|X_0\rangle$, making it zero by the same argument, proving the lemma. \square

The spread complexity differs between the two cases when $n \geq m$. We write the Shannon entropy of the terms that differ from the Krylov basis as

$$F_{n \geq m}(t) = - \sum_{n \geq m} P_{\mathcal{G}}(n, t) \ln P_{\mathcal{G}}(n, t). \quad (5.28)$$

We invoke the lemma to identify that the first non-zero term in the Taylor series expansion of $P_{\mathcal{G}}(n, t)$ around $t = 0$ occurs when $k = 2m$,

$$\begin{aligned} P_{\mathcal{G}}(n, t) &= \sum_k \frac{P_{\mathcal{G}}^{(k)}(n, 0)t^k}{k!} \\ &= \frac{P_{\mathcal{G}}^{(2m)}(n, 0)t^{2m}}{(2m)!} + \mathcal{O}(t^{2m+1}). \end{aligned} \quad (5.29)$$

We substitute in Eq. (5.29) into Eq. (5.4), and split the logarithm term into two separate parts

$$F_{n \geq m}(t) = -\frac{\ln(t)t^{2m}}{(2m-1)!} \sum_{n \geq m} P_{\mathcal{G}}^{(2m)}(n, 0) - \sum_{n \geq m} \frac{P_{\mathcal{G}}^{(2m)}(n, 0)t^{2m}}{(2m)!} \ln \left[\frac{P_{\mathcal{G}}^{(2m)}(n, 0)}{(2m)!} \right] \quad (5.30)$$

The non-zero part of $P_{\mathcal{G}}^{(2m)}(n, 0)$ can be written as

$$P_{\mathcal{G}}^{(2m)}(n, 0) = \binom{2m}{m} (X_0|\mathcal{L}^{\dagger m}|G_n)(G_n|\mathcal{L}^m|X_0), \quad (5.31)$$

noting that $\|X_0\| = 1$ and that the final term in Eq. (5.25) is zero for all $n > 0$. The non-zero contribution here comes from $|Y\rangle$, which is the part of $\mathcal{L}^m|X_0\rangle$ orthogonal to the first m basis elements. We then write

$$\sum_{n \geq m} P_{\mathcal{G}}^{(2m)}(n, 0) = \sum_{n \geq m} \binom{2m}{m} (Y|G_n)(G_n|Y). \quad (5.32)$$

As $|Y\rangle$ is orthogonal to the first m elements of the basis, we can extend this sum to start at zero, and invoke the completeness of \mathcal{G} to write

$$\sum_{n \geq m} P_{\mathcal{G}}^{(2m)}(n, 0) = \binom{2m}{m} (Y|Y), \quad (5.33)$$

which greatly simplifies the first part Eq. (5.30) into something that is basis independent. The second term has the form $f(x) = \frac{x}{(2m)!} \ln \frac{x}{(2m)!}$ with $x = P_{\mathcal{G}}^{(2m)}(n, 0)$. This is a convex function that is negative for the domain considered. $P_{\mathcal{G}}^{(2m)}(n, 0)$ is a positive number for which the sequence $(\alpha_i) = \left(\binom{2m}{m} (Y|Y), 0, 0, \dots\right)$ trivially majorises any other sequence (β_i) of positive numbers that add to $\binom{2m}{m} (Y|Y)$. This implies, by Karamata's inequality [274], that $\sum f(\alpha_i) \geq \sum f(\beta_i)$, i.e., that the entropy (once we take the overall minus sign) is always greater than or equal to the case where $\sum_{n \geq m} P_{\mathcal{G}}^{(2m)}(n, 0)$ has only contribution from a single basis element, meaning that the Krylov basis element $|O_m\rangle$ must be part of the basis to minimise this term, allowing us (by induction) to conclude that the Krylov basis minimises the entropy for the population distribution for both closed evolution and under dynamics generated by a Markovian master equation.

5.5 Sachdev-Ye-Kitaev Model

To demonstrate our framework, we analyse the SYK model, which consists of N interacting Majorana fermions. This system is a paradigmatic model of quantum chaos [275]. Majorana fermions, ψ_i , are defined through their anti-commutation relation $\{\psi_i, \psi_j\} = \delta_{ij}$ and the dimension of the Hilbert space of N Majorana fermions is $2^{N/2}$. The SYK model is an all-to-all coupled model with the Hamiltonian

$$H_{SYK} = (i)^{q/2} \sum_{1 \leq i_1 < i_2 < \dots < i_q \leq N} J_{i_1 i_2 \dots i_q} \psi_{i_1} \psi_{i_2} \dots \psi_{i_q}, \quad (5.34)$$

where q denotes the number of fermions that interact in a vertex, $q = 2$ being an integrable free fermion model, and $q > 2$ giving rise to chaotic behaviour. The sum is ordered in such a way as to include interactions between any q fermions once, and the interaction strength is a real number $J_{i_1 i_2 \dots i_q}$ drawn from a random Gaussian distribution with a zero mean and a variance

$$\overline{J_{i_1 i_2 \dots i_q}^2} = \frac{J^2 (q-1)!}{N^{q-1}}, \quad (5.35)$$

where the overline denotes the disorder average.

The SYK model is both a maximally chaotic model (viewed through the framework of the operator growth hypothesis [204]) and a fast scrambler [276, 277]. Other models exhibit this behaviour, such as random unitary circuits [276, 277]. Importantly, it saturates the bound on the rate of change of Krylov complexity [253, 254].

Recently the open-system dynamics of the SYK model has gained much attention [278–283].

We consider a Markovian GKSL master equation for the SYK model as given by Eq. (5.18) with the minus sign taken. The fermionic jump operators are $L_n = \sqrt{\mu}\psi_n$ where μ governs the strength of the dissipation. We write it as $\mathcal{L} = \mathcal{L}_U + \mathcal{L}_D$ where

$$\mathcal{L}_U \bullet = [H_{SYK}, \bullet], \quad (5.36)$$

$$\mathcal{L}_D \bullet = i\mu \sum_{n=1}^N \left(\psi_n \bullet \psi_n + \frac{1}{4} \{ \mathbf{1}, \bullet \} \right), \quad (5.37)$$

and we have used the anti-commutation relation of the Majorana operators and that they are Hermitian.

As we shall discuss, the action of the dissipative part of the master equation leads to a dampening of the Majorana string terms contributing to the time evolved operator at a rate proportional to their size. We define a Majorana string S_i of length s_i to be an operator formed as a product of s_i Majorana fermions ordered such that the indices are in ascending order from left to right, e.g., $\psi_1\psi_3\psi_7$ is a string of length three. We will use the set of Majorana strings as an orthonormal basis for the spread complexity of the SYK model. For the $q=4$ SYK model under dissipation, we only need half of the complete basis since only strings of Majorana fermions of odd length can be generated by the interaction vertices provided the initial operator has odd length. Unlike the Krylov basis for the SYK model, this basis is fixed and identical for each iteration for the SYK model. As a basis it is physically well-motivated as it can be directly used to track the size of operators [284].

5.6 Complexity vs decoherence

We will now analytically show the competition between decoherence and operator complexity for the SYK Lindbladian. We assume an initial operator $X_0 = \sum_i p_i S_i$.

Considering the action of the non-unitary, decohering term on one of the strings for now, we find

$$\mathcal{L}_D S_i = i\mu \sum_{n=1}^N \psi_n S_i \psi_n + i\mu \frac{N}{2} S_i. \quad (5.38)$$

Now, we anti-commute the first ψ_n through S_i which will allow us to then square it to $\mathbf{1}/2$. This typically takes s_i anti-commutations to move it through, unless ψ_n appears in the string S_i , in which case it takes $s_i - 1$, leaving

$$\mathcal{L}_D S_i = \frac{i\mu}{2} \left[(-1)^{s_i} (N - s_i) + (-1)^{s_i-1} s_i + N \right] S_i. \quad (5.39)$$

Depending on whether s_i is odd or even, the right-hand side reads $i\mu s_i S_i$ or $i\mu(N - s_i) S_i$ respectively. Once we apply the same process to each of the strings that appear in a linear

combination to make X_0 , we obtain an operator that is co-linear with X_0

$$\mathcal{L}_D X_0 = i\mu \sum_i \alpha_i p_i S_i, \quad (5.40)$$

where $\alpha_i = s_i$ or $N - s_i$ depending on whether s_i is odd or even. Note that for our purposes, only odd strings are relevant for the dynamics, meaning that the decoherence term dampens strings at a rate proportional to their length. It is clear that the unitary part is the source of the new operators appearing in the support of the time evolved operator to Majorana strings not originally present in X_0 , as described in Ref. [284]. In the limit of strong decoherence, the Lindbladian does not generate any new support from its action on the initial operator, so viewed through the lens of the Lanczos algorithm, it terminates immediately, giving $M_{\mathcal{K}} = 1$.

This has similarities to Ref. [208], where the model of decoherence acts like a measurement operator that is sensitive to the string length. The interplay between information scrambling and decoherence interpolates between the closed case, where the system generates as much support as is available to it, and the “Zeno-blocked” case where decoherence term is measuring the initial string sufficiently strongly such that it does not grow in support. In the limit of strong decoherence, the operator evolves as

$$X_t \approx \sum_i p_i e^{-\mu s_i t} S_i. \quad (5.41)$$

Therefore, in the limit of strong decoherence, we see that any operator strings are eigenoperators for the Lindbladian.

We next compare how the two bases—the Krylov basis \mathcal{K} generated from applying the bi-Lanczos algorithm and the Majorana string basis \mathcal{S} [208, 284] capture the spread complexity. Clearly the Krylov basis is the natural choice to examine universal behaviour and growth rates for systems. However, the latter is arguably a more natural basis for understanding the dynamics explicitly in terms of length of operator size. We fix $\sqrt{2}\psi_1$ as the initial operator, but note in that the choice of any Majorana operator of length one will reproduce qualitatively similar results.

Fig. 5.1(a) depicts the Krylov complexity for the open SYK model over 200 disorder realisations for a range of dissipation strengths. We also show the closed case (topmost blue line), i.e., $\mu = 0$, where the bi-Lanczos algorithm reduces to the regular Lanczos algorithm. We see that initial growth in the closed case and under weak decoherence is similar, however they saturate at different levels. This behaviour is consistent with the large-N behaviour of the SYK Lindbladian model as established in [283], where the Krylov complexity is shown to plateau at smaller levels for increasing dissipation strength. The saturation level of the Krylov complexity for a range of decoherence strengths is shown in Fig. 5.1(b). Its decreasing value as the open system effects become stronger indicates that information scrambles less throughout the system when subject to decoherence and the dynamics become less “complex”. Why the complexity of the dynamics is reduced under decoherence becomes clear when we plot the dimension of the Krylov basis for the SYK Lindbladian vs decoherence strength in Fig. 5.1(c). The dimension of the Krylov space corresponds to the number of elements needed to encode $\{\mathcal{L}^n |X_0\rangle\}$. Even in the closed

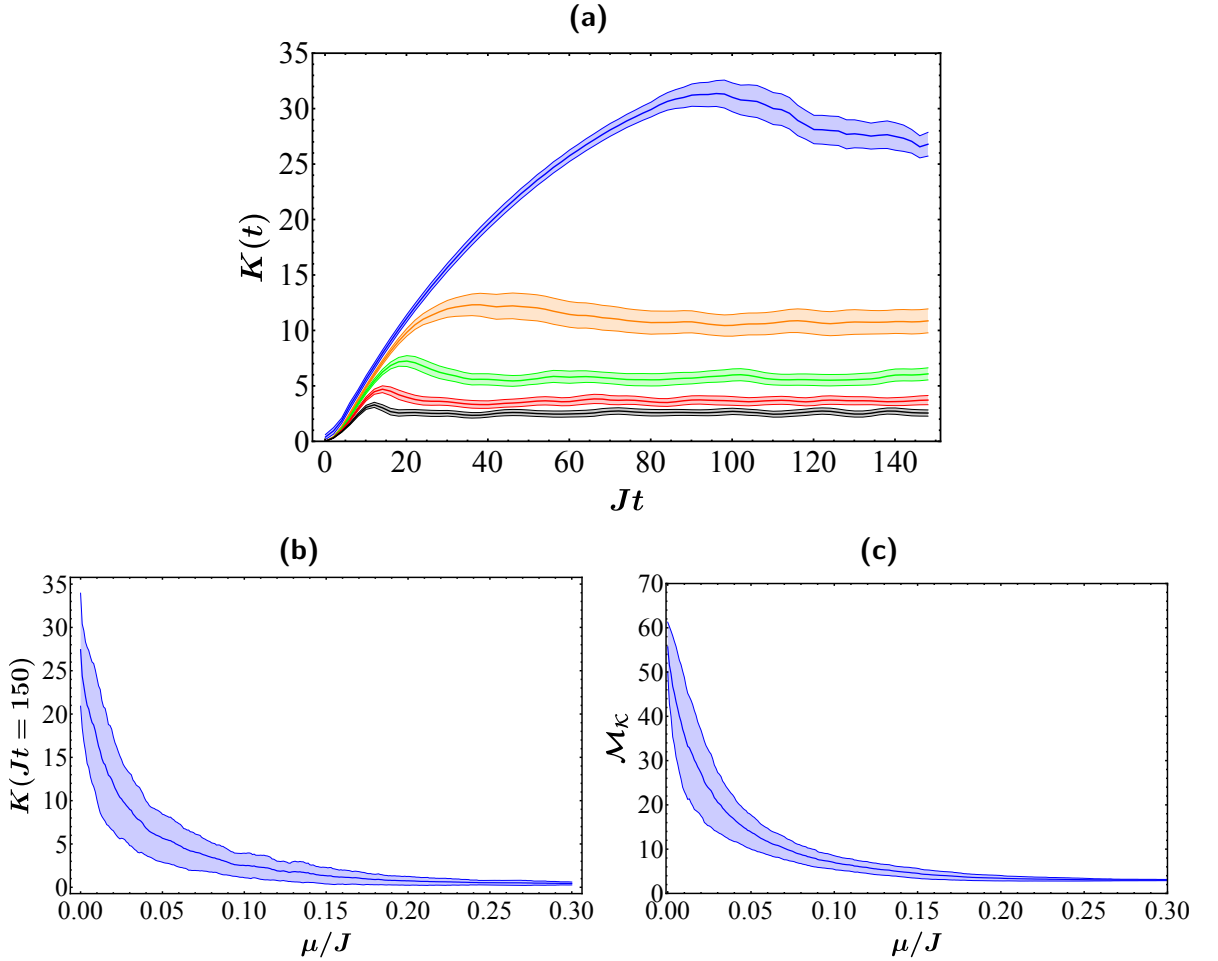


Figure 5.1: Dynamics for the open SYK model with $N = 8$ and 200 disorder realisations. Variance is shown as a shaded region (scaled to 20% of its value in panel (a) for clarity). (a) The average Krylov complexity (eq. (5.22)) with $\mu/J = 0.0, 0.025, 0.05, 0.075, 0.1$ corresponding to blue, orange, green, red, and black, respectively. (b) The average Krylov complexity at $Jt = 120$ vs decoherence strength μ/J . (c) The average dimension of the Krylov space for the dynamics vs μ/J .

case we see that the Lanczos algorithm compresses this information down into fewer basis states than needed for the entire Hilbert space. As it becomes less likely for our operator to inhabit regions of Krylov space with increasing decoherence strength, this set can be compressed down further. The scaling of the complexity naturally corresponds to the scaling of the Krylov space. This suggests a competition between information loss to the environment and the ability for a system to scramble its information internally. Somewhat naturally, the cardinality of the Krylov basis appears as *the* quantity to infer the scrambling nature of a system. For instance, we would expect that for an integrable system, the effect of weak decoherence would serve to increase the cardinality of the Krylov subspace as symmetries in the system are broken. We would still see the complexity decrease for larger values of decoherence strength for the same reasons outlined for a

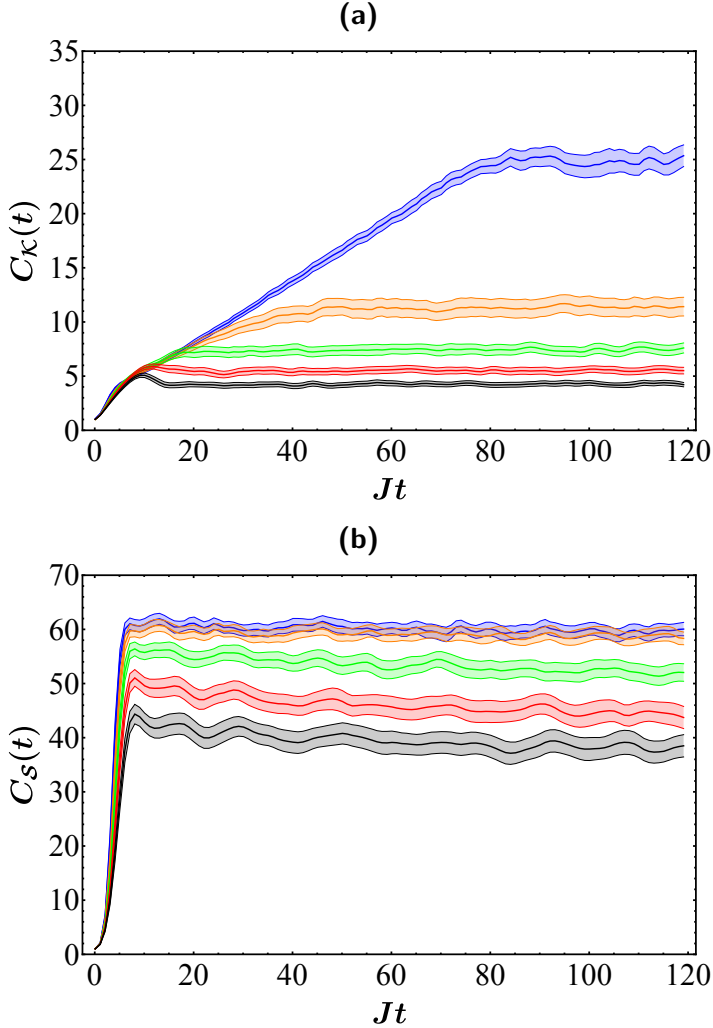


Figure 5.2: Dynamics for the open SYK model with $N = 8$ and 200 disorder realisations with $\mu/J = 0.0, 0.025, 0.05, 0.075, 0.1$ corresponding to blue, orange, green, red, and black, respectively. Variance is shown as a shaded region scaled to 20 % of its value for clarity. **(a)** Average spread complexity eq. (5.24) in the Krylov basis. **(b)** Average spread complexity in the string basis.

non-integrable system.

While the cardinality gives us an insight into the competition between scrambling and decoherence, only the complexity is a genuinely dynamical quantity from which scrambling times and growth rates can be derived. Hence, we plot the operator spread complexity Eq. (5.24) vs time in Fig. 5.2. Both the Krylov and string bases show the same hierarchy in spread complexity for different decoherence strengths. The rapid early growth of spread complexity in the string basis case comes from the inherent non-local nature of the SYK model. A few applications of the superoperator is all that is needed to have contributions from all strings in the basis. We postulate that for a local model, the qualitative growth of the spread complexity in both the Krylov and

(Majorana or Pauli) string bases should be closer. This opens the door to moving past Markovian dynamics, allowing to assess whether information back flow into the system has a potential competing effect alongside decoherence and internal scrambling. Maps that generate dynamics with information back flow, even if they can be written in a master equation form, are not amenable to the bi-Lanczos approach. A pre-chosen basis, such as the string basis, removes this roadblock. Since this basis still allows to accurately capture the correct qualitative behavior as evidenced from Fig. 5.2, it therefore allows one to study the operator complexity in more general settings.

5.7 Conclusions

We have explored competition between information scrambling within a system and information leakage to the environment as described by a Markovian master equation. We demonstrated that the Krylov basis, constructed via the bi-Lanczos algorithm, minimises the spread complexity and showed that qualitatively consistent operator dynamics can be captured by considering other suitable bases. Regardless of the specific choice of basis, we established that decoherence caps the size of operators, consistent with earlier results in the thermodynamic limit [285]. Typically decoherence is seen as a sink for quantum information from a system. While interactions with an environment does cause this to happen, it also has an effect on the information dynamics within the system itself. For the channel considered, we saw how it skews the operator population distribution to shorter lengths, preventing the proliferation of many-body entanglement within the system. A systematic review of the effect of other quantum channels on the operator population distribution would be of interest. Additionally, throughout this thesis we have typically viewed the environment as a one-way carrier for quantum information, extracting it from the system - with the one exception being the accessible environmental fragments in Chapter 4. Allowing the environment to have a memory of the earlier state of the system may reveal interesting phenomena relevant for both information scrambling and quantum Darwinism. Our results demonstrate that a basis other than the minimal one can still provide insight into the spread complexity of operator dynamics, opening the possibility to explore the effect of the backflow of information on the competition between scrambling and decoherence. A natural framework for these is using master equations with time-dependent rates [2] or collision models with non-zero Markov order. The primary limitation for the study of information scrambling and quantum chaos in general is that numerical studies in the literature are limited to few-body systems, where finite-size effects become relevant quickly. The operator growth hypothesis itself is a statement about asymptotic growth of the Lanczos coefficients. Extracting enough Lanczos coefficients to meaningfully define a growth rate relies on finding models that can be solved efficiently numerically, such as the LMG model [211], or ones that admit analytical treatment in the thermodynamic limit [286]. The latter offer an interesting framework for exploring non-Markovianity and finite temperature effects in a tractable manner, potentially by analytically deriving the autocorrelation function of the same system as was considered in [286] and probing the high-frequency response of its spectral function.

Chapter 6

Conclusions and Outlook

The central thread of this thesis is the exploration of information dynamics in quantum systems. We have examined scenarios where ideal coherent dynamics are achieved through control, as well as phenomena arising from uncontrolled dynamics where the system is allowed to decohere. By examining the interplay between coherence, control, and the influence of environmental degrees of freedom, this work provides a broad perspective for understanding and leveraging these dynamics in a variety of quantum settings. The disparate topics covered — ranging from counterdiabatic control and gate implementation to the emergence of classical objectivity and operator complexity — are unified by a central inquiry into the dynamics of quantum information.

Quantum systems naturally exhibit complex dynamics. The tensor product structure of Hilbert space creates an exponentially vast state space, making it challenging to store and simulate such systems on classical computers as the size of the system increases. This motivates the use of quantum devices that can, in principle, simulate the systems of interest. Remarkably, the complexity of quantum information dynamics not only permits simulation but also enables efficient algorithms for solving classical problems. While large-scale, fully-programmable, fault-tolerant quantum computers remain decades away, current quantum technologies developed en route to this goal have significant practical potential. However, the transformation of quantum theory into practical technology relies on quantum control. We explored quantum control for the purpose of engineering coherent dynamics in Chapter 2 and Chapter 3. In the former we proposed a novel protocol for counterdiabatic control in critical systems, while in the latter we leveraged a number of control protocols for the implementation of quantum gates. Both works emphasised the energetic cost of control, highlighting resource efficiency as a critical issue for scalable quantum information processing.

From the viewpoint of quantum control, decoherence and the environment at large are viewed as deleterious sinks for quantum information. Quantum information in general tries to maximise its support in Hilbert space, a phenomenon that underpins thermalisation in closed quantum settings. What was once local quantum information is hidden in highly complex many-body and long-range correlations. This is generic for typical interactions, and typically leaves the reduced state of a subsystem in a classical mixture resembling a Gibbs state. However, the world is not a cold,

thermalised place (yet). Careful treatment of what is typically traced out or something that places bounds on timescales for “interesting” dynamics can instead give insights into the emergence of the classical world. We discussed this treatment, Quantum Darwinism, in Chapter 4. With the right choice of interactions between the system and the environment, we see that as quantum information propagates from the system it will leave in its wake a rich correlation structure between the system and environment that allows the latter to view the former in a classically objective manner. Our work in Chapter 4 asks an uncomfortable question of Quantum Darwinism. If the system couples to multiple environmental fragments with non-commuting interaction Hamiltonians then we can no longer define a pointer basis for the system, and Darwinism is suppressed. This can be circumvented by demanding a separation of timescales, that one environmental channel is stronger than the other. This allowed us to approximately define an effective pointer basis and see the signatures of classical objectivity transitively, before the other interaction term becomes relevant and thermalises the system. Our results would imply that the strongest interactions between classical objects and the information medium should be purely dephasing in the same basis, that is that there should be a dominant interaction axis. How finely-tuned this solution is remains the subject of further work.

The environment is not the only sink for local quantum information. Closed many-body quantum systems scramble quantum information. Any information about the configuration of the system at a point in time will be lost to many-body correlations within the system. Accessible degrees of freedom as sinks for quantum information through residual interactions has already received much attention as a potential roadblock to the scalability of quantum devices [287]. The interplay between these two competing sinks for quantum information can give rise to rich phenomena. We saw in Chapter 5 that decoherence does not simply cause information to leak out of the system, but fundamentally restructures the information that remains there. Typically, decoherence lowers the complexity of the many-body correlations internal to the system, biasing information to few-body correlations. However, the system-environment relationship does not have to be a one-way sink for information, non-Markovian dynamics can allow for information backflow into the system. What this implies for the internal information structure remains a topic for further study.

Throughout this thesis we have explored both the dynamics of controlled quantum systems and the dynamics of many-body systems (the latter typically in an open system setting). While the two topics are seemingly disparate, we wish to highlight that in recent times tools from the former have started to be applied to the problem of classifying and probing many-body dynamics. We refer again to the adiabatic gauge potential (AGP), introduced in Chapter 1,

$$\langle m(\lambda) | A_\lambda | n(\lambda) \rangle = \frac{i \langle m(\lambda) | \partial_\lambda H_0(\lambda) | n(\lambda) \rangle}{E_n(\lambda) - E_m(\lambda)}, \quad \forall m \neq n. \quad (6.1)$$

The AGP is typically employed for quantum control, as demonstrated in Chapters 2 and 3. However, the AGP has been used to explore quantum speed limits [41] and recover critical scaling

exponents [288]. The AGP clearly encodes information about the spectrum of the system and the evolution of eigenstates, as well as information about non-equilibrium phenomena it is typically used to suppress. Surprising connections with other areas of quantum physics can be made. The rate of change of a state as a parameter (in this case λ) is changed for an eigenstate $|n\rangle$, known as the fidelity susceptibility, is given by

$$\chi_\lambda^{(n)} = \langle \partial_\lambda n | \partial_\lambda n \rangle - \langle \partial_\lambda n | n \rangle \langle n | \partial_\lambda n \rangle. \quad (6.2)$$

We recall that the AGP is the generator of eigenstate evolution, which allows us to neatly recast the fidelity susceptibility as the variance of the AGP,

$$\chi_\lambda^{(n)} = \langle n | A_\lambda^2 | n \rangle - \langle n | A_\lambda | n \rangle^2. \quad (6.3)$$

If we average the fidelity susceptibility evenly over all eigenstates we find that the total fidelity susceptibility is nothing but the Frobenius norm of the AGP - something we characterised as the cost of control

$$\chi_\lambda = \sum_n \chi_\lambda^{(n)} \mathbb{1} = \|A_\lambda\|^2 = \sum_n \sum_{m \neq n} \frac{|\langle m | A_\lambda | n \rangle|^2}{(E_n - E_m)^2}. \quad (6.4)$$

The scaling of the cost of control has been shown to be a sensitive probe of quantum chaos [223,224], scaling exponentially with system size for chaotic systems and scaling polynomially with system size for integrable ones. Most remarkably, exponential scaling of the AGP norm is seen for systems with very weakly broken integrability, where the corresponding level spacing statistics are closer to Poissonian than Wigner-Dyson. This approach therefore separates chaos from ergodicity, the latter characterised by level-spacing statistics, and the former by exponential sensitivity of eigenstate perturbations. Further work exploring integrability breaking and the transition to ergodic dynamics with these methods may be fruitful, perhaps by splitting contributions to the AGP norm by eigenstate and probing the statistics found. In the same spirit, we can use the tools from controlled closed quantum systems to probe open many-body quantum systems. An analogue of the AGP for open systems can be derived in a similar fashion to that for unitary dynamics [289]. While control and adiabatic dynamics in non-Hermitian settings has been explored before [289–291], insights from the AGP and its norm in this setting have the potential to define steady-state complexity (something we probed before using the cardinality of the Krylov subspace for a given dissipation strength in Chapter 5), to diagnose and characterise dissipative phase transitions (analogously to how the fidelity susceptibility is typically used for quantum phase transitions), and to characterise non-equilibrium effects in driven open systems through the cost of using the AGP to enforce transitionless dynamics. This potential outlook is quite exciting, as it uniquely blends the topics discussed in this thesis and reinforces a saying of my advisor that “*you learn a lot about a quantum system from what it takes to control it.*”

Bibliography

- [1] E. Carolan, A. Kiely, and S. Campbell. Counterdiabatic control in the impulse regime. *Phys. Rev. A*, 105:012605, 2022.
- [2] E. Ryan, E. Carolan, S. Campbell, and M. Paternostro. Commutativity and the emergence of classical objectivity. *J. Phys. Commun.*, 6(9):095005, 2022.
- [3] E. Carolan, B. Çakmak, and S. Campbell. Robustness of controlled hamiltonian approaches to unitary quantum gates. *Phys. Rev. A*, 108(2):022423, 2023.
- [4] E. Carolan, A. Kiely, S. Campbell, and S. Deffner. Operator growth and spread complexity in open quantum systems. *EPL*, 147:38002, 2024.
- [5] C. P. Koch, U. Boscain, T. Calarco, G. Dirr, S. Filipp, S. J. Glaser, R. Kosloff, S. Montangero, T. Schulte-Herbrüggen, D. Sugny, and F. K. Wilhelm. Quantum optimal control in quantum technologies. strategic report on current status, visions and goals for research in europe. *EPJ Quantum Technology*, 9(1):19, 2022.
- [6] A. Auffèves. Quantum technologies need a quantum energy initiative. *PRX Quantum*, 3:020101, 2022.
- [7] M. Planck. Ueber das gesetz der energieuerteilzung im norrnalspectrzm. *Ann. Phys.*, 309:553–563, 1901.
- [8] N. Bohr. On the constitution of atoms and molecules. *The London, Edinburgh, and Dublin Philosophical Magazine and Journal of Science*, 26(151):1–25, 1913.
- [9] Erwin Schrödinger. *Collected papers on wave mechanics*, volume 302. American Mathematical Soc., 2003.
- [10] E. Schrödinger. Quantisierung als eigenwertproblem. *Annalen der Physik*, 384(4):361–377, 1926.
- [11] E. Merzbacher. *Quantum mechanics*. John Wiley & Sons, 1998.
- [12] S.. McGlynn, L.G. Vanquickenborne, M. Kinoshita, and D.G. Carroll. *Introduction to applied quantum chemistry*. Holt, Reinhart, Winston, 1973.

- [13] Y. Cao, J. Romero, J. P. Olson, M. Degroote, P. D. Johnson, M. Kieferová, I. D. Kivlichan, T. Menke, B. Peropadre, N. Sawaya, et al. Quantum chemistry in the age of quantum computing. *Chemical reviews*, 119(19):10856–10915, 2019.
- [14] M. Reiher, N. Wiebe, K. M. Svore, D. Wecker, and M. Troyer. Elucidating reaction mechanisms on quantum computers. *Proceedings of the National Academy of Sciences*, 114(29):7555–7560, 2017.
- [15] H. Stærkind, K. Jensen, J. H. Müller, V. O. Boer, E. T. Petersen, and E. S. Polzik. Precision measurement of the excited state landé g-factor and diamagnetic shift of the cesium d 2 line. *Phys. Rev. X*, 13(2):021036, 2023.
- [16] M. Berry. Quantal phase factors accompanying adiabatic changes. *Proceedings of the Royal Society of London. A. Mathematical and Physical Sciences*, 392(1802):45–57, 1984.
- [17] M. Berry. Transitionless quantum driving. *J. Phys. A: Math. Theor.*, 42:365303, 2009.
- [18] J. von Neumann. *Mathematical foundations of quantum mechanics: New edition*, volume 53. Princeton University Press, 2018.
- [19] J. von Neumann. Wahrscheinlichkeitstheoretischer aufbau der quantenmechanik. *Nachrichten von der Gesellschaft der Wissenschaften zu Göttingen, Mathematisch-Physikalische Klasse*, 1927:245–272, 1927.
- [20] M. A Nielsen and I. Chuang. *Quantum Computation and Quantum Information*. Cambridge University Press, Cambridge, 2000.
- [21] H.P. Breuer and F. Petruccione. *The theory of open quantum systems*. Oxford University Press, USA, 2002.
- [22] I. H. Deutsch. Harnessing the power of the second quantum revolution. *PRX Quantum*, 1:020101, 2020.
- [23] J. Preskill. Quantum computing in the NISQ era and beyond. *Quantum*, 2:79, 2018.
- [24] S. J. Glaser, U. Boscain, T. Calarco, C. P. Koch, W. Köckenberger, R. Kosloff, I. Kuprov, B. Luy, S. Schirmer, T. Schulte-Herbrüggen, D. Sugny, and F. K. Wilhelm. Training Schrödinger’s cat: quantum optimal control. *Euro. Phys. J. D*, 69:1–24, 2015.
- [25] E. Torrontegui, S. Ibáñez, S. Martínez-Garaot, M. Modugno, A. del Campo, D. Guéry-Odelin, A. Ruschhaupt, X. Chen, and J. G. Muga. Shortcuts to Adiabaticity. *Adv. At. Mol. Opt. Phys.*, 62:117, 2013.
- [26] D. Guéry-Odelin, A. Ruschhaupt, A. Kiely, E. Torrontegui, S. Martínez-Garaot, and J. G. Muga. Shortcuts to adiabaticity: Concepts, methods, and applications. *Rev. Mod. Phys.*, 91:045001, 2019.

- [27] H. Saberi, T. Opatrný, K. Mølmer, and A. del Campo. Adiabatic tracking of quantum many-body dynamics. *Phys. Rev. A*, 90:060301, 2014.
- [28] S. Campbell, G. De Chiara, M. Paternostro, G. M. Palma, and R. Fazio. Shortcut to Adiabaticity in the Lipkin-Meshkov-Glick Model. *Phys. Rev. Lett.*, 114:177206, 2015.
- [29] A Kiely and S. Campbell. Fast and robust magnon transport in a spin chain. *New J. Phys.*, 23:033033, 2021.
- [30] C. Whitty, A. Kiely, and A. Ruschhaupt. Quantum control via enhanced shortcuts to adiabaticity. *Phys. Rev. Research*, 2:023360, 2020.
- [31] D. Sels and A. Polkovnikov. Minimizing irreversible losses in quantum systems by local counterdiabatic driving. *Proceedings of the National Academy of Sciences*, 114(20):E3909–E3916, 2017.
- [32] J. D. Sau and K. Sengupta. Suppressing defect production during passage through a quantum critical point. *Phys. Rev. B*, 90:104306, 2014.
- [33] M. Demirplak and S. A. Rice. Adiabatic population transfer with control fields. *J. Chem. Phys. A*, 107:9937, 2003.
- [34] Y. Zheng, S. Campbell, G. De Chiara, and D. Poletti. Cost of counterdiabatic driving and work output. *Phys. Rev. A*, 94:042132, 2016.
- [35] A. Tobalina, J. Alonso, and J. G. Muga. Energy consumption for ion transport in a segmented Paul trap. *New J. Phys.*, 20:065002, 2018.
- [36] E. Torrontegui, I. Lizuain, S. González-Resines, A. Tobalina, A. Ruschhaupt, R. Kosloff, and J. G. Muga. Energy consumption for shortcuts to adiabaticity. *Phys. Rev. A*, 96:022133, 2017.
- [37] O. Abah and E. Lutz. Energy efficient quantum machines. *EPL*, 118(4):40005, 2017.
- [38] B. Çakmak and Ö. E. Müstecaplıoğlu. Spin quantum heat engines with shortcuts to adiabaticity. *Phys. Rev. E*, 99:032108, 2019.
- [39] K. Funo, J.-N. Zhang, C. Chatou, K. Kim, M. Ueda, and A. del Campo. Universal work fluctuations during shortcuts to adiabaticity by counterdiabatic driving. *Phys. Rev. Lett.*, 118:100602, 2017.
- [40] X. Chen and J. G. Muga. Engineering of fast population transfer in three-level systems. *Phys. Rev. A*, 86:033405, 2012.
- [41] S. Campbell and S. Deffner. Trade-off between speed and cost in shortcuts to adiabaticity. *Phys. Rev. Lett.*, 118:100601, 2017.

- [42] R. Puebla, S. Deffner, and S. Campbell. Kibble–zurek scaling in quantum speed limits for shortcuts to adiabaticity. *Phys. Rev. Research*, 2:032020, 2020.
- [43] O. Abah, R. Puebla, A. Kiely, G. De Chiara, M. Paternostro, and S. Campbell. Energetic cost of quantum control protocols. *New J. Phys.*, 21:103048, 2019.
- [44] C. L. Latune. Energetic advantages of nonadiabatic drives combined with nonthermal quantum states. *Phys. Rev. A*, 103:062221, 2021.
- [45] A. C. Santos and M. S. Sarandy. Superadiabatic controlled evolutions and universal quantum computation. *Sci. Rep.*, 5:15775, 2015.
- [46] S. Deffner. Energetic cost of hamiltonian quantum gates. *EPL*, 134(4):40002, 2021.
- [47] M. M. Rams, P. Sierant, O. Dutta, P. Horodecki, and J. Zakrzewski. At the limits of criticality-based quantum metrology: Apparent super-heisenberg scaling revisited. *Phys. Rev. X*, 8:021022, 2018.
- [48] B. Gardas and S. Deffner. Quantum fluctuation theorem for error diagnostics in quantum annealers. *Sci. Rep.*, 8:17191, 2018.
- [49] A. Hartmann and W. Lechner. Rapid counter-diabatic sweeps in lattice gauge adiabatic quantum computing. *New Journal of Physics*, 21(4):043025, 2019.
- [50] N. N. Hegade, K. Paul, Y. Ding, M. Sanz, F. Albarrán-Arriagada, E. Solano, and X. Chen. Shortcuts to adiabaticity in digitized adiabatic quantum computing. *Phys. Rev. Applied*, 15:024038, 2021.
- [51] T. W. B. Kibble. Topology of cosmic domains and strings. *J. Phys. A*, 9:1387–1398, 1976.
- [52] W. H. Zurek. Cosmological experiments in superfluid helium? *Nature*, 317:505–508, 1985.
- [53] A. Del Campo, T. W.B. Kibble, and W. H. Zurek. Causality and non-equilibrium second-order phase transitions in inhomogeneous systems. *Journal of Physics Condensed Matter*, 25:24025443, 2013.
- [54] M. J. M. Power and G. De Chiara. Dynamical symmetry breaking with optimal control: Reducing the number of pieces. *Phys. Rev. B*, 88:214106, 2013.
- [55] A. Del Campo, G. De Chiara, G. Morigi, M. B. Plenio, and A. Retzker. Structural defects in ion chains by quenching the external potential: The inhomogeneous Kibble–Zurek mechanism. *Phys. Rev. Lett.*, 105:075701, 2010.
- [56] A. Del Campo, A. Retzker, and M. B. Plenio. The inhomogeneous Kibble–Zurek mechanism: vortex nucleation during Bose–Einstein condensation. *New J. Phys.*, 13:083022, 2011.

- [57] D. Sadhukhan, A. Sinha, A. Francuz, J. Stefaniak, M. M. Rams, J. Dziarmaga, and W. H. Zurek. Sonic horizons and causality in phase transition dynamics. *Phys. Rev. B*, 101:144429, 2020.
- [58] S. Deffner. Kibble-Zurek scaling of the irreversible entropy production. *Phys. Rev. E*, 96:052125, 2017.
- [59] F. J. Gómez-Ruiz and A. del Campo. Universal dynamics of inhomogeneous quantum phase transitions: Suppressing defect formation. *Phys. Rev. Lett.*, 122:080604, 2019.
- [60] A. Benseny and K. Mølmer. Adiabatic theorem revisited: The unexpectedly good performance of adiabatic passage. *Phys. Rev. A*, 103:062215, 2021.
- [61] S. Sachdev. *Quantum Phase Transitions*. Cambridge University Press, Cambridge, UK, 2nd edition, 2011.
- [62] M. E. Fisher. The renormalization group in the theory of critical behavior. *Rev. Mod. Phys.*, 46:597–616, 1974.
- [63] B. Damski. The simplest quantum model supporting the kibble-zurek mechanism of topological defect production: Landau-zener transitions from a new perspective. *Phys. Rev. Lett.*, 95:035701, 2005.
- [64] A. del Campo, M. M. Rams, and W. H. Zurek. Assisted finite-rate adiabatic passage across a quantum critical point: Exact solution for the quantum ising model. *Phys. Rev. Lett.*, 109:115703, 2012.
- [65] B. Damski. Counterdiabatic driving of the quantum Ising model. *J. Stat. Mech.*, page P12019, 2014.
- [66] M. Demirplak and S. A. Rice. On the consistency, extremal, and global properties of counterdiabatic fields. *J. Chem. Phys.*, 129:154111, 2008.
- [67] C. Zener. Non-adiabatic crossing of energy levels. *Proc. R. Soc. A*, 33:696–702, 1932.
- [68] B. Damski and W. H. Zurek. Adiabatic-impulse approximation for avoided level crossings: From phase-transition dynamics to landau-zener evolutions and back again. *Phys. Rev. A*, 73:063405, 2006.
- [69] A. Del Campo and W. H. Zurek. Universality of phase transition dynamics: Topological defects from symmetry breaking. *International Journal of Modern Physics A*, 29:1–49, 2014.
- [70] W. H. Zurek, U. Dorner, and P. Zoller. Dynamics of a quantum phase transition. *Phys. Rev. Lett.*, 95:105701, 2005.
- [71] N. V. Vitanov and B. M. Garraway. Landau-zener model: Effects of finite coupling duration. *Phys. Rev. A*, 53:4288–4304, 1996.

- [72] J. Dziarmaga. Dynamics of a quantum phase transition: Exact solution of the quantumising model. *Phys. Rev. Lett.*, 95:245701, 2005.
- [73] B. C. Sanders. *How to Build a Quantum Computer*. IOP Publishing, Bristol, United Kingdom, 2017.
- [74] M. Kjaergaard, M. E. Schwartz, J. Braumüller, P. Krantz, J. I.-Jan. Wang, S. Gustavsson, and W. D. Oliver. Superconducting qubits: Current state of play. *Annu. Rev. Condens. Matter Phys.*, 11(1):369–395, 2020.
- [75] S.E. Rasmussen, K.S. Christensen, S.P. Pedersen, L.B. Kristensen, T. Bækkegaard, N.J.S. Loft, and N.T. Zinner. Superconducting circuit companion—an introduction with worked examples. *PRX Quantum*, 2:040204, 2021.
- [76] C. D. Bruzewicz, J. Chiaverini, R. McConnell, and J M. Sage. Trapped-ion quantum computing: Progress and challenges. *App. Phys. Rev.*, 6(2):021314, 2019.
- [77] S. Slussarenko and G. J. Pryde. Photonic quantum information processing: A concise review. *App. Phys. Rev.*, 6(4):041303, 2019.
- [78] M. A. Nielsen. Cluster-state quantum computation. *Rep. Math. Phys.*, 57(1):147–161, 2006.
- [79] A. M. Childs, E. Deotto, E. Farhi, J. Goldstone, S. Gutmann, and A. J. Landahl. Quantum search by measurement. *Phys. Rev. A*, 66:032314, 2002.
- [80] A. M. Childs, D. W. Leung, and M. A. Nielsen. Unified derivations of measurement-based schemes for quantum computation. *Phys. Rev. A*, 71:032318, 2005.
- [81] Robert Raussendorf, Daniel E. Browne, and Hans J. Briegel. Measurement-based quantum computation on cluster states. *Phys. Rev. A*, 68:022312, 2003.
- [82] A. Barenco, C. H. Bennett, R. Cleve, D. P. DiVincenzo, N. Margolus, P. Shor, T. Sleator, J. A. Smolin, and H. Weinfurter. Elementary gates for quantum computation. *Phys. Rev. A*, 52:3457–3467, 1995.
- [83] E. Farhi, J. Goldstone, S. Gutmann, and M. Sipser. Quantum Computation by Adiabatic Evolution. *arXiv:0001106*, 2000.
- [84] E. Farhi, J. Goldstone, S. Gutmann, J. Lapan, A. Lundgren, and D. Preda. A quantum adiabatic evolution algorithm applied to random instances of an NP-complete problem. *Science*, 292(5516):472–475, 2001.
- [85] D. Aharonov. A simple proof that toffoli and hadamard are quantum universal. *arXiv:0301040*, 2003.

- [86] G. García-Pérez, M. A. C. Rossi, and S. Maniscalco. Ibm q experience as a versatile experimental testbed for simulating open quantum systems. *npj Quantum Inf.*, 6(1):1, 2020.
- [87] N. Keenan, N. F. Robertson, T. Murphy, S. Zhuk, and J. Goold. Evidence of Kardar-Parisi-Zhang scaling on a digital quantum simulator. *npj Quantum Information*, 9(1):72, 2023.
- [88] J. D. Guimarães, J. Lim, M. I. Vasilevskiy, S. F. Huelga, and M. B. Plenio. Noise-assisted digital quantum simulation of open systems using partial probabilistic error cancellation. *PRX Quantum*, 4(4):040329, 2023.
- [89] D. Sels and A. Polkovnikov. Minimizing irreversible losses in quantum systems by local counterdiabatic driving. *Proc. Natl. Acad. Sci. U.S.A.*, 114(20):E3909–E3916, 2017.
- [90] A. C. Santos and M. S. Sarandy. Generalized shortcuts to adiabaticity and enhanced robustness against decoherence. *J. Phys. A*, 51(2):025301, 2017.
- [91] I. Čepaitė, A. Polkovnikov, A. J. Daley, and C. W. Duncan. Counterdiabatic optimized local driving. *PRX Quantum*, 4:010312, 2023.
- [92] H. Tajima, N. Shiraishi, and K. Saito. Uncertainty relations in implementation of unitary operations. *Phys. Rev. Lett.*, 121:110403, 2018.
- [93] H. Tajima, N. Shiraishi, and K. Saito. Coherence cost for violating conservation laws. *Phys. Rev. Res.*, 2:043374, 2020.
- [94] S. Deffner. Energetic cost of hamiltonian quantum gates. *EPL*, 134(4):40002, 2021.
- [95] Y. Yang, R. Renner, and G. Chiribella. Energy requirement for implementing unitary gates on energy-unbounded systems. *J. Phys. A*, 55(49):494003, 2022.
- [96] G. Chiribella, Y. Yang, and R. Renner. Fundamental energy requirement of reversible quantum operations. *Phys. Rev. X*, 11:021014, 2021.
- [97] W. H. Zurek. Thermodynamic cost of computation, algorithmic complexity and the information metric. *Nature*, 341(6238):119–124, 1989.
- [98] O. Abah, R. Puebla, A. Kiely, G. De Chiara, M. Paternostro, and S. Campbell. Energetic cost of quantum control protocols. *New Journal of Physics*, 21(10):103048, 2019.
- [99] V. Cimini, S. Gherardini, M. Barbieri, I. Gianani, M. Sbroscia, L. Buffoni, M. Paternostro, and F. Caruso. Experimental characterization of the energetics of quantum logic gates. *npj Quantum Inf.*, 6(1):96, 2020.
- [100] Yi-Zheng Zhen, Dario Egloff, Kavan Modi, and Oscar Dahlsten. Universal bound on energy cost of bit reset in finite time. *Phys. Rev. Lett.*, 127:190602, 2021.

- [101] J. Stevens, D. Szombati, M. Maffei, C. Elouard, R. Assouly, N. Cottet, R. Dassonneville, Q. Ficheux, S. Zeppetzauer, A. Bienfait, A. N. Jordan, A. Auffèves, and B. Huard. Energetics of a single qubit gate. *Phys. Rev. Lett.*, 129:110601, 2022.
- [102] D. J. Bedingham and O. J. E. Maroney. The thermodynamic cost of quantum operations. *New J. Phys.*, 18(11):113050, 2016.
- [103] R. Takagi and H. Tajima. Universal limitations on implementing resourceful unitary evolutions. *Phys. Rev. A*, 101:022315, 2020.
- [104] M. Huber, M. Perarnau-Llobet, K. V. Hovhannisyan, P. Skrzypczyk, C. Klöckl, N. Brunner, and A. Acín. Thermodynamic cost of creating correlations. *New J. Phys.*, 17(6):065008, 2015.
- [105] D. Basilewitsch, L. Marder, and C. P. Koch. Dissipative quantum dynamics and optimal control using iterative time ordering: an application to superconducting qubits. *Eur. Phys. J. B*, 91(7):161, 2018.
- [106] M. H. Goerz, D. M. Reich, and C. P. Koch. Optimal control theory for a unitary operation under dissipative evolution. *New J. Phys.*, 16(5):055012, 2014.
- [107] A. C. Santos and M. S. Sarandy. Generalized transitionless quantum driving for open quantum systems. *Phys. Rev. A*, 104:062421, 2021.
- [108] J. Xuereb, P. Erker, F. Meier, M. T. Mitchison, and M. Huber. Impact of imperfect time-keeping on quantum control. *Physical Review Letters*, 131(16):160204, 2023.
- [109] E. Knill, R. Laflamme, and W. H. Zurek. Resilient quantum computation: error models and thresholds. *Proc. R. Soc. London Ser. A: Math., Phys. Eng. Sci.*, 454(1969):365–384, 1998.
- [110] S. Deffner and S. Campbell. *Quantum Thermodynamics*. Morgan & Claypool, San Rafael, California (USA), 2019.
- [111] J. Goold, M. Huber, A. Riera, L. del Rio, and P. Skrzypczyk. The role of quantum information in thermodynamics—a topical review. *J. Phys. A*, 49(14):143001, 2016.
- [112] I. Hen. Fourier-transforming with quantum annealers. *Frontiers Phys.*, 2, 2014.
- [113] Itay Hen. Quantum gates with controlled adiabatic evolutions. *Phys. Rev. A*, 91:022309, 2015.
- [114] Mustafa Demirplak and Stuart A. Rice. Assisted adiabatic passage revisited. *J. Phys. Chem. B*, 109(14):6838–6844, 2005.
- [115] P. W. Claeys, M. Pandey, D. Sels, and A. Polkovnikov. Floquet-engineering counterdiabatic protocols in quantum many-body systems. *Phys. Rev. Lett.*, 123:090602, 2019.

- [116] A. C. Santos. Quantum gates by inverse engineering of a hamiltonian. *J. Phys. B*, 51(1):015501, 2017.
- [117] C. Jarzynski. Generating shortcuts to adiabaticity in quantum and classical dynamics. *Phys. Rev. A*, 88(4):040101, 2013.
- [118] C. Weitenberg and J. Simonet. Tailoring quantum gases by floquet engineering. *Nat. Phys.*, 17(12):1342–1348, 2021.
- [119] F. Blanes, S. and Casas, J. Oteo, and J. Ros. The magnus expansion and some of its applications. *Physics reports*, 470(5-6):151–238, 2009.
- [120] X. Chen, A. Ruschhaupt, S. Schmidt, A. del Campo, D. Guéry-Odelin, and J. G. Muga. Fast optimal frictionless atom cooling in harmonic traps: Shortcut to adiabaticity. *Phys. Rev. Lett.*, 104:063002, 2010.
- [121] Y. H. Kang, Y. H. Chen, Q. C. Wu, B. H. Huang, Y. Xia, and J. Song. Reverse engineering of a hamiltonian by designing the evolution operators. *Sci. Rep.*, 6:30151, 2016.
- [122] X. Chen, E. Torrontegui, and J. G. Muga. Lewis-Riesenfeld invariants and transitionless quantum driving. *Phys. Rev. A*, 83:062116, 2011.
- [123] M. Bukov, D. Sels, and A. Polkovnikov. Geometric speed limit of accessible many-body state preparation. *Phys. Rev. X*, 9(1):011034, 2019.
- [124] R. C. Bialczak, M. Ansmann, M. Hofheinz, E. Lucero, M. Neeley, A. D. O’Connell, D. Sank, H. Wang, J. Wenner, and M. Steffen. Quantum process tomography of a universal entangling gate implemented with josephson phase qubits. *Nature Physics*, 6(6):409–413, 2010.
- [125] D. M. Reich, G. Gualdi, and C. P. Koch. Minimum number of input states required for quantum gate characterization. *Phys. Rev. A*, 88:042309, 2013.
- [126] A. C. Santos and M. S. Sarandy. Superadiabatic Controlled Evolutions and Universal Quantum Computation. *Sci. Rep.*, 5(1):15775, 2015.
- [127] A. Kiely, S. Campbell, and G. T. Landi. Classical dissipative cost of quantum control. *Phys. Rev. A*, 106:012202, 2022.
- [128] Y. Ding, X. Chen, R. Magdalena-Benedito, and J. D. Martín-Guerrero. Closed-loop control of a noisy qubit with reinforcement learning. *Machine Learning: Science and Technology*, 4(2):025020, 2023.
- [129] T. Huang, Y. Ban, E. Y. Sherman, and X. Chen. Machine-learning-assisted quantum control in a random environment. *Phys. Rev. Appl.*, 17:024040, 2022.

- [130] M.-Z. Ai, Y. Ding, Y. Ban, J. D. Martín-Guerrero, J. Casanova, J.-M. Cui, Y.-F. Huang, Xi Chen, C.-F. Li, and G.-C. Guo. Experimentally realizing efficient quantum control with reinforcement learning. *Science China Physics, Mechanics and Astronomy*, 65:250312, 2022.
- [131] A. N. Pearson, Y. Guryanova, P. Erker, E. A. Laird, G. A. D. Briggs, M. Huber, and N. Ares. Measuring the thermodynamic cost of timekeeping. *Phys. Rev. X*, 11:021029, 2021.
- [132] Qi Zhang, Xi Chen, and David Guéry-Odelin. Robust control of linear systems and shortcut to adiabaticity based on superoscillations. *Phys. Rev. Appl.*, 18:054055, 2022.
- [133] F. Kleißler, A. Lazariev, and S. Arroyo-Camejo. Universal, high-fidelity quantum gates based on superadiabatic, geometric phases on a solid-state spin-qubit at room temperature. *npj Quantum Inf.*, 4(1):49, 2018.
- [134] T. Wang, Z. Zhang, L. Xiang, Z. Jia, P. Duan, W. Cai, Z. Gong, Z. Zong, M. Wu, J. Wu, et al. The experimental realization of high-fidelity ‘shortcut-to-adiabaticity’ quantum gates in a superconducting xmon qubit. *New J. Phys.*, 20(6):065003, 2018.
- [135] T. Wang, Z. Zhang, L. Xiang, Z. Jia, P. Duan, Z. Zong, Z. Sun, Z. Dong, J. Wu, Yi Yin, et al. Experimental realization of a fast controlled-z gate via a shortcut-to-adiabaticity. *Phys. Rev. Applied*, 11(3):034030, 2019.
- [136] Y. Yan, C. Shi, A. Kinos, H. Syed, S. P. Horvath, A. Walther, L. Rippe, X. Chen, and S. Kröll. Experimental implementation of precisely tailored light-matter interaction via inverse engineering. *npj Quantum Information*, 7:138, 2021.
- [137] W. H. Zurek. Decoherence, einselection, and the quantum origins of the classical. *Rev. Mod. Phys.*, 75:715–775, 2003.
- [138] W. H. Zurek. Quantum Darwinism. *Nat. Phys.*, 5:181, 2009.
- [139] R. Blume-Kohout and W. H. Zurek. Quantum Darwinism: Entanglement, branches, and the emergent classicality of redundantly stored quantum information. *Phys. Rev. A*, 73:062310, 2006.
- [140] T. P. Le and A. Olaya-Castro. Strong quantum Darwinism and strong independence are equivalent to spectrum broadcast structure. *Phys. Rev. Lett.*, 122:010403, 2019.
- [141] T. P. Le and A. Olaya-Castro. Objectivity (or lack thereof): Comparison between predictions of quantum Darwinism and spectrum broadcast structure. *Phys. Rev. A*, 98:032103, 2018.
- [142] T. P. Le and A. Olaya-Castro. Witnessing non-objectivity in the framework of strong quantum Darwinism. *Quantum Sci. Technol.*, 5:045012, 2020.
- [143] R. Horodecki, J. K. Korbicz, and P. Horodecki. Quantum origins of objectivity. *Phys. Rev. A*, 91:032122, 2015.

- [144] J. K. Korbicz, P. Horodecki, and R. Horodecki. Objectivity in a noisy photonic environment through quantum state information broadcasting. *Phys. Rev. Lett.*, 112:120402, 2014.
- [145] J. K. Korbicz, E. A. Aguilar, P. Ćwikliński, and P. Horodecki. Generic appearance of objective results in quantum measurements. *Phys. Rev. A*, 96:032124, 2017.
- [146] D. Tripathy, A. Touil, B. Gardas, and S. Deffner. Quantum information scrambling in two-dimensional bose–hubbard lattices. *Chaos*, 34(4):043121, 2024.
- [147] W. H. Zurek. Decoherence, einselection, and the quantum origins of the classical. *Rev. Mod. Phys.*, 75(3):715, 2003.
- [148] J. Faye. Copenhagen interpretation of quantum mechanics. *Stanford Encyclopedia of Philosophy*, 2002.
- [149] W. H. Zurek. Pointer basis of quantum apparatus: Into what mixture does the wave packet collapse? *Phys. Rev. D*, 24(6):1516, 1981.
- [150] H. D. Zeh. On the interpretation of measurement in quantum theory. *Foundations of Physics*, 1(1):69–76, 1970.
- [151] V. B. Braginsky, Y. I. Vorontsov, and K. S. Thorne. Quantum nondemolition measurements. *Science*, 209(4456):547–557, 1980.
- [152] W. H. Zurek. Preferred states, predictability, classicality and the environment-induced decoherence. *Progress of Theoretical Physics*, 89(2):281–312, 1993.
- [153] J. K. Korbicz. Roads to objectivity: quantum darwinism, spectrum broadcast structures, and strong quantum darwinism—a review. *Quantum*, 5:571, 2021.
- [154] K. Roszak and J. K. Korbicz. Entanglement and objectivity in pure dephasing models. *Phys. Rev. A*, 100:062127, 2019.
- [155] S. Campbell, B. Çakmak, Ö. E. Müstecaplıoğlu, M. Paternostro, and B. Vacchini. Collisional unfolding of quantum Darwinism. *Phys. Rev. A*, 99:042103, 2019.
- [156] M. Zwolak and W. H. Zurek. Complementarity of quantum discord and classically accessible information. *Sci. Rep.*, 3:1729, 2013.
- [157] M. Zwolak and W. H. Zurek. Amplification, decoherence, and the acquisition of information by spin environments. *Sci. Rep.*, 6:25277, 2016.
- [158] M. Zwolak and W. H. Zurek. Redundancy of einselected information in quantum Darwinism: The irrelevance of irrelevant environment bits. *Phys. Rev. A*, 95:030101(R), 2017.
- [159] P. A. Knott, T. Tufarelli, M. Piani, and G. Adesso. Generic emergence of objectivity of observables in infinite dimensions. *Phys. Rev. Lett.*, 121:160401, 2018.

- [160] N. Balanescovica. Random unitary evolution model of quantum darwinism with pure decoherence. *Eur. Phys. J. D*, 69:232, 2015.
- [161] N. Balanescovica and M. Mendler. Dissipation, dephasing and quantum darwinism in qubit systems with random unitary interactions. *Eur. Phys. J. D*, 70:177, 2016.
- [162] S. Lorenzo, M. Paternostro, and G. M. Palma. Anti-zeno-based dynamical control of the unfolding of quantum darwinism. *Phys. Rev. Research*, 2:013164, 2020.
- [163] G. García-Pérez, D. A. Chisholm, M. A. C. Rossi, G. M. Palma, and S. Maniscalco. Decoherence without entanglement and quantum Darwinism. *Phys. Rev. Research*, 2:012061, 2020.
- [164] G. Pleasance and B. M. Garraway. Application of quantum Darwinism to a structured environment. *Phys. Rev. A*, 96:062105, 2017.
- [165] M. Zwolak, H. T. Quan, and W. H. Zurek. Redundant imprinting of information in nonideal environments: Objective reality via a noisy channel. *Phys. Rev. A*, 81:062110, 2010.
- [166] M. Zwolak, H. T. Quan, and W. H. Zurek. Quantum Darwinism in a mixed environment. *Phys. Rev. Lett.*, 103:110402, 2009.
- [167] A. Touil, B. Yan, D. Girolami, S. Deffner, and W. H. Zurek. Eavesdropping on the decohering environment: Quantum darwinism, amplification, and the origin of objective classical reality. *Phys. Rev. Lett.*, 128:010401, 2021.
- [168] N. Mirkin and D. A. Wisniacki. Many-body localization and the emergence of quantum Darwinism. *Entropy*, 23:1377, 2021.
- [169] B. Çakmak, Ö. E. Müstecaplıoğlu, M. Paternostro, B. Vacchini, and S. Campbell. Quantum darwinism in a composite system: Objectivity versus classicality. *Entropy*, 23:995, 2021.
- [170] E. Ryan, M. Paternostro, and S. Campbell. Quantum Darwinism in a structured spin environment. *Phys. Lett. A*, 416:127675, 2021.
- [171] C. J. Riedel, W. H. Zurek, and M. Zwolak. The rise and fall of redundancy in decoherence and quantum darwinism. *New J. Phys.*, 14:083010, 2012.
- [172] T. P. Le, G. Adesso, and A. Winter. Thermality versus objectivity: Can they peacefully coexist? *Entropy*, 23:1506, 2021.
- [173] J. K. Korbicz. Roads to objectivity: Quantum Darwinism, Spectrum Broadcast Structures, and Strong quantum Darwinism. *Quantum*, 5:571, 2021.
- [174] J. Tuziemski, A. Lampo, M. Lewenstein, and J. K. Korbicz. Reexamination of the decoherence of spin registers. *Phys. Rev. A*, 99:022122, 2019.

- [175] M. Kiciński and J. K. Korbicz. Decoherence and objectivity in higher spin environments. *Phys. Rev. A*, 104:042216, 2021.
- [176] M. A. Ciampini, G. Pinna, P. Mataloni, and M. Paternostro. Experimental signature of quantum Darwinism in photonic cluster states. *Phys. Rev. A*, 98:020101(R), 2018.
- [177] M.-C. Chen, H.-S. Zhong, Y. Li, D. Wu, X.-L. Wang, L. Li, N.-L. Liu, C.-Y. Lu, and J.-W. Pan. Emergence of classical objectivity on a quantum Darwinism simulator. *Science Bulletin*, 64:580, 2019.
- [178] T. K. Unden, D. Louzon, M. Zwolak, W. H. Zurek, and F. Jelezko. Revealing the emergence of classicality using nitrogen-vacancy centers. *Phys. Rev. Lett.*, 123:140402, 2019.
- [179] A. Lampo, J. Tuziemski, M. Lewenstein, and J. K. Korbicz. Objectivity in the non-Markovian spin-boson model. *Phys. Rev. A*, 96:012120, 2017.
- [180] F. Galve, R. Zambrini, and S. Maniscalco. Non-Markovianity hinders Quantum Darwinism. *Sci. Rep.*, 6:19607, 2016.
- [181] G. L. Giorgi, F. Galve, and R. Zambrini. Quantum Darwinism and non-Markovian dissipative dynamics from quantum phases of the spin-1/2 XX model. *Phys. Rev. A*, 92:022105, 2015.
- [182] N. Milazzo, S. Lorenzo, M. Paternostro, and G. M. Palma. Role of information backflow in the emergence of quantum darwinism. *Phys. Rev. A*, 100:012101, 2019.
- [183] N Megier, A Smirne, S. Campbell, and B. Vacchini. Correlations, information backflow, and objectivity in a class of pure dephasing models. *Entropy*, 24:304, 2022.
- [184] F. Ciccarello, S. Lorenzo, V. Giovannetti, and G M. Palma. Quantum collision models: open system dynamics from repeated interactions. *Phys. Rep.*, 954:1, 2022.
- [185] S. Campbell and B. Vacchini. Collision models in open system dynamics: A versatile tool for deeper insights? *EPL*, 133:60001, 2021.
- [186] G. García-Pérez, M. A. C. Rossi, and S. Maniscalco. IBM Q Experience as a versatile experimental testbed for simulating open quantum systems. *npj Quantum Inf.*, 6:1, 2020.
- [187] S. Lorenzo, F. Ciccarello, and G. M. Palma. Composite quantum collision models. *Phys. Rev. A*, 96:032107, 2017.
- [188] G. Guarnieri, D. Morrone, B. Çakmak, F. Plastina, and S. Campbell. Non-equilibrium steady-states of memoryless quantum collision models. *Phys. Lett. A*, 384:126576, 2020.
- [189] T. Baumgratz, M. Cramer, and M. B. Plenio. Quantifying coherence. *Phys. Rev. Lett.*, 113:140401, 2014.

- [190] S. Campbell, M. Paternostro, S. Bose, and M. S. Kim. Probing the environment of an inaccessible system by a qubit ancilla. *Phys. Rev. A*, 81:050301, 2010.
- [191] S. Campbell, A. Smirne, L. Mazzola, N. Lo Gullo, B. Vacchini, Th. Busch, and M. Paternostro. Critical assessment of two-qubit post-markovian master equations. *Phys. Rev. A*, 85:032120, 2012.
- [192] M. Popovic, B. Vacchini, and S. Campbell. Entropy production and correlations in a controlled non-Markovian setting. *Phys. Rev. A*, 98:012130, 2018.
- [193] S. Hamedani Raja, M. Borrelli, R. Schmidt, J. P. Pekola, and S. Maniscalco. Thermodynamic fingerprints of non-markovianity in a system of coupled superconducting qubits. *Phys. Rev. A*, 97:032133, 2018.
- [194] N. Yunger Halpern, P. Faist, J. Oppenheim, and A. Winter. Microcanonical and resource-theoretic derivations of the thermal state of a quantum system with noncommuting charges. *Nat. Commun.*, 7:12051, 2016.
- [195] N. Yunger Halpern, M. E. Beverland, and A. Kavendish. Noncommuting conserved charges in quantum many-body thermalization. *Phys. Rev. E*, 101:042117, 2020.
- [196] D. R. M. Arvidsson-Shukur, J. C. Drori, and N. Yunger Halpern. Conditions tighter than noncommutation needed for nonclassicality. *J. Phys. A*, 54:284001, 2021.
- [197] J. Kołodyński, J. B. Brask, M. Perarnau-Llobet, and B. Bylicka. Adding dynamical generators in quantum master equations. *Phys. Rev. A*, 97:062124, 2018.
- [198] C. J. Riedel, W. H. Zurek, and M. Zwolak. The rise and fall of redundancy in decoherence and quantum darwinism. *New Journal of physics*, 14(8):083010, 2012.
- [199] P. Duruisseaux, A. Touil, and S. Deffner. Pointer states and quantum darwinism with two-body interactions. *Entropy*, 25(12):1573, 2023.
- [200] E. Bernstein and U. Vazirani. Quantum complexity theory. In *Proceedings of the twenty-fifth annual ACM symposium on Theory of computing*, pages 11–20, 1993.
- [201] S. Aaronson. The complexity of quantum states and transformations: from quantum money to black holes. *arXiv:1607.05256*, 2016.
- [202] D. Poulin, A. Qarry, R. Somma, and F. Verstraete. Quantum simulation of time-dependent hamiltonians and the convenient illusion of Hilbert space. *Phys. Rev. Lett.*, 106(17):170501, 2011.
- [203] M. A. Nielsen, M. R. Dowling, M. Gu, and A. C. Doherty. Quantum computation as geometry. *Science*, 311(5764):1133–1135, 2006.

- [204] D. E. Parker, X. Cao, A. Avdoshkin, T. Scaffidi, and E. Altman. A universal operator growth hypothesis. *Phy. Rev. X*, 9(4):041017, 2019.
- [205] X. Chen, Z. C. Gu, and X. G. Wen. Local unitary transformation, long-range quantum entanglement, wave function renormalization, and topological order. *Phys. Rev. B*, 82(15):155138, 2010.
- [206] L. Susskind. Why do things fall? *arXiv:1802.01198*, 2018.
- [207] L. Li, K. Bu, D. E. Koh, A. Jaffe, and S. Lloyd. Wasserstein complexity of quantum circuits. *arXiv:2208.06306*, 2022.
- [208] T. Schuster and N. Y. Yao. Operator growth in open quantum systems. *Phys. Rev. Lett.*, 131(16):160402, 2023.
- [209] X. L. Qi, E. J. Davis, A. Periwal, and M. Schleier-Smith. Measuring operator size growth in quantum quench experiments. *arXiv:1906.00524*, 2019.
- [210] C. Lanczos. An iteration method for the solution of the eigenvalue problem of linear differential and integral operators. *Journal of Research of the National Bureau of Standards*, 1950.
- [211] B. Bhattacharjee, X. Cao, P. Nandy, and T. Pathak. Krylov complexity in saddle-dominated scrambling. *J. High Energy Phys.*, 2022(5):174, 2022.
- [212] B. L. Espa  ol and D. A. Wisniacki. Assessing the saturation of krylov complexity as a measure of chaos. *Phys. Rev. E*, 107(2):024217, 2023.
- [213] F. G. S. L. Brand  o, W. Chemissany, N. Hunter-Jones, R. Kueng, and J. Preskill. Models of quantum complexity growth. *PRX Quantum*, 2(3):030316, 2021.
- [214] O. Bohigas, M.-J. Giannoni, and C. Schmit. Characterization of chaotic quantum spectra and universality of level fluctuation laws. *Phys. Rev. Lett.*, 52(1):1, 1984.
- [215] M. Berry. Quantum chaology, not quantum chaos. *Phys. Scr.*, 40(3):335, 1989.
- [216] H. Kim and A. Polkovnikov. Integrability is attractive. *arXiv:2308.09745*, 2023.
- [217] D. A. Abanin, E. Altman, I. Bloch, and M. Serbyn. Colloquium: Many-body localization, thermalization, and entanglement. *Rev. Mod. Phys.*, 91(2):021001, 2019.
- [218] E. P. Wigner. Characteristic vectors of bordered matrices with infinite dimensions I. *The Collected Works of Eugene Paul Wigner: Part A: The Scientific Papers*, pages 524–540, 1993.
- [219] F. J. Dyson. A Brownian-motion model for the eigenvalues of a random matrix. *Journal of Mathematical Physics*, 3(6):1191–1198, 1962.

- [220] O. Bohigas, R. U. Haq, and A. Pandey. Fluctuation properties of nuclear energy levels and widths: comparison of theory with experiment. In *Nuclear Data for Science and Technology: Proceedings of the International Conference Antwerp 6–10 September 1982*, pages 809–813. Springer, 1983.
- [221] E. B. Bogomolny, B. Georgeot, M. J. Giannoni, and C. Schmit. Chaotic billiards generated by arithmetic groups. *Phys. Rev. Lett.*, 69(10):1477, 1992.
- [222] M. Srednicki. Chaos and quantum thermalization. *Phys. Rev. E.*, 50(2):888, 1994.
- [223] M. Pandey, P. W. Claeys, D. K. Campbell, A. Polkovnikov, and D. Sels. Adiabatic eigenstate deformations as a sensitive probe for quantum chaos. *Phys. Rev. X*, 10(4):041017, 2020.
- [224] C. Lim, K. Matirko, A. Polkovnikov, and M. O. Flynn. Defining classical and quantum chaos through adiabatic transformations. *arXiv:2401.01927*, 2024.
- [225] I. García-Mata, R. A. Jalabert, and D. A. Wisniacki. Out-of-time-order correlators and quantum chaos. *arXiv:2209.07965*, 2022.
- [226] I. Kukuljan, S. Grozdanov, and T. Prosen. Weak quantum chaos. *Phys. Rev. B*, 96(6):060301, 2017.
- [227] T. Xu, T. Scaffidi, and X. Cao. Does scrambling equal chaos? *Phys. Rev. Lett.*, 124(14):140602, 2020.
- [228] N. Dowling, P. Kos, and K. Modi. Scrambling is necessary but not sufficient for chaos. *Phys. Rev. Lett.*, 131(18):180403, 2023.
- [229] S. Kettemann, D. Klakow, and U. Smilansky. Characterization of quantum chaos by the autocorrelation function of spectral determinants. *Phys. A Math. Gen.*, 30(10):3643, 1997.
- [230] A. Chenu, I. L. Egusquiza, J. Molina-Vilaplana, and A. del Campo. Quantum work statistics, Loschmidt echo and information scrambling. *Sci. Rep.*, 8(1):12634, 2018.
- [231] V. Khemani, A. Vishwanath, and D. A. Huse. Operator spreading and the emergence of dissipative hydrodynamics under unitary evolution with conservation laws. *Phys. Rev. X*, 8(3):031057, 2018.
- [232] M. Blake, H. Lee, and H. Liu. A quantum hydrodynamical description for scrambling and many-body chaos. *J. High Energy Phys.*, 2018(10):127, 2018.
- [233] J. F. Wienand, S. Karch, A. Impertro, C. Schweizer, E. McCulloch, R. Vasseur, S. Gopalakrishnan, M. Aidelsburger, and I. Bloch. Emergence of fluctuating hydrodynamics in chaotic quantum systems. *Nature Physics*, 2024.
- [234] T. Rakovszky, C. W. von Keyserlingk, and F. Pollmann. Dissipation-assisted operator evolution method for capturing hydrodynamic transport. *Phys. Rev. B*, 105(7):075131, 2022.

- [235] T. Rakovszky, F. Pollmann, and C. W. Von Keyserlingk. Diffusive hydrodynamics of out-of-time-ordered correlators with charge conservation. *Phys. Rev. X*, 8(3):031058, 2018.
- [236] C. W. von Keyserlingk, T. Rakovszky, F. Pollmann, and S. L. Sondhi. Operator hydrodynamics, OTOCs, and entanglement growth in systems without conservation laws. *Phys. Rev. X*, 8(2):021013, 2018.
- [237] V. Balasubramanian, P. Caputa, J. M. Magan, and Q. Wu. Quantum chaos and the complexity of spread of states. *Phys. Rev. D*, 106(4):046007, 2022.
- [238] A. Bhattacharya, R. N. Das, B. Dey, and J. Erdmenger. Spread complexity for measurement-induced non-unitary dynamics and Zeno effect. *J. High Energy Phys.*, 2024(179):179, 2024.
- [239] P. Caputa, H.-S. Jeong, S. Liu, J. F. Pedraza, and L.-C. Qu. Krylov complexity of density matrix operators. *J. High Energy Phys.*, 2024(5):337, 2024.
- [240] A. Bhattacharya, S. S. Haque, G. Jafari, J. Murugan, and D. Rapotu. Krylov complexity and spectral form factor for noisy random matrix models. *J. High Energy Phys.*, 2023(10):157, 2023.
- [241] A. Touil and S. Deffner. Information scrambling versus decoherence—two competing sinks for entropy. *PRX Quantum*, 2(1):010306, 2021.
- [242] P. Zanardi and N. Anand. Information scrambling and chaos in open quantum systems. *Phys. Rev. A*, 103(6):062214, 2021.
- [243] A. Larzul, S. J. Thomson, and M. Schiro. Are fast scramblers good thermal baths? *arXiv:2204.06434*, 2022.
- [244] V. Mohan. Krylov complexity of open quantum systems: from hard spheres to black holes. *J. High Energy Phys.*, 2023(11):222, 2023.
- [245] Z. Xu, L. P. García-Pintos, A. Chenu, and A. Del Campo. Extreme decoherence and quantum chaos. *Phys. Rev. Lett.*, 122(1):014103, 2019.
- [246] Z. Weinstein, S. P. Kelly, J. Marino, and E. Altman. Scrambling transition in a radiative random unitary circuit. *Phys. Rev. Lett.*, 131(22):220404, 2023.
- [247] A. M. García-García, J. J. M. Verbaarschot, and J. Zheng. Lyapunov exponent as a signature of dissipative many-body quantum chaos. *Phys. Rev. D*, 110(8):086010, 2024.
- [248] L. Sá , P. Ribeiro, and T. Prosen. Complex spacing ratios: A signature of dissipative quantum chaos. *Phys. Rev. X*, 10(2):021019, 2020.
- [249] J. Li, T. Prosen, and A. Chan. Spectral statistics of non-hermitian matrices and dissipative quantum chaos. *Phys. Rev. Lett.*, 127(17):170602, 2021.

- [250] A. Bhattacharya, P. Nandy, P. P. Nath, and H. Sahu. On krylov complexity in open systems: an approach via bi-lanczos algorithm. *J. High Energy Phys.*, 2023(12):66, 2023.
- [251] J. Maldacena, S. H. Shenker, and D. Stanford. A bound on chaos. *Journal of High Energy Physics*, 2016(8):1–17, 2016.
- [252] P. Caputa, J. M. Magan, and D. Patramanis. Geometry of Krylov complexity. *Phys. Rev. Res.*, 4(1):013041, 2022.
- [253] N. Hörnedal, N. Carabba, A. S. Matsoukas-Roubeas, and A. del Campo. Ultimate speed limits to the growth of operator complexity. *Commun. Phys.*, 5(1):207, 2022.
- [254] N. Hörnedal, N. Carabba, K. Takahashi, and A. del Campo. Geometric operator quantum speed limit, wegner hamiltonian flow and operator growth. *Quantum*, 7:1055, 2023.
- [255] B. Bhattacharjee, P. Nandy, and T. Pathak. Krylov complexity in large q and double-scaled SYK model. *J. High Energy Phys.*, 2023(8):99, 2023.
- [256] B. Bhattacharjee, S. Sur, and P. Nandy. Probing quantum scars and weak ergodicity breaking through quantum complexity. *Phys. Rev. B*, 106(20):205150, 2022.
- [257] E. Rabinovici, A. Sánchez-Garrido, R. Shir, and J. Sonner. Krylov complexity from integrability to chaos. *J. High Energy Phys.*, 2022(7):151, 2022.
- [258] J. D. Noh. Operator growth in the transverse-field ising spin chain with integrability-breaking longitudinal field. *Phys. Rev. E*, 104(3):034112, 2021.
- [259] K.-B. Huh, H.-S. Jeong, and J. F. Pedraza. Spread complexity in saddle-dominated scrambling. *arXiv:2312.12593*, 2023.
- [260] C. Liu, H. Tang, and H. Zhai. Krylov complexity in open quantum systems. *Phys. Rev. Res.*, 5(3):033085, 2023.
- [261] N. S. Srivatsa and C. von Keyserlingk. Operator growth hypothesis in open quantum systems. *Phys. Rev. B*, 109(12):125149, 2024.
- [262] B. Bhattacharjee, X. Cao, P. Nandy, and T. Pathak. Operator growth in open quantum systems: lessons from the dissipative SYK. *J. High Energy Phys.*, 2023(3):54, 2023.
- [263] A. Bhattacharya, P. Nandy, P. P. Nath, and H. Sahu. Operator growth and krylov construction in dissipative open quantum systems. *J. High Energy Phys.*, 2022(12):81, 2022.
- [264] S. W. Gaaf and E. Jarlebring. The infinite bi-Lanczos method for nonlinear eigenvalue problems. *SIAM J. Sci. Comput.*, 39(5):S898–S919, 2017.

- [265] H. T. Şenyaşa, Ş. Kesgin, G. Karpat, and B. Çakmak. Entropy production in non-Markovian collision models: Information backflow vs. system-environment correlations. *Entropy*, 24(6):824, 2022.
- [266] Y. Li, X. Li, and J. Jin. Dissipation-induced information scrambling in a collision model. *Entropy*, 24(3):345, 2022.
- [267] S. Omanakuttan, K. Chinni, P. D. Blocher, and P. M. Poggi. Scrambling and quantum chaos indicators from long-time properties of operator distributions. *Phys. Rev. A*, 107(3):032418, 2023.
- [268] P. D. Blocher, K. C., S. O., and P. M. Poggi. Probing scrambling and operator size distributions using random mixed states and local measurements. *Phys. Rev. Res.*, 6(1):013309, 2024.
- [269] J. L. F. Barbón, E. Rabinovici, R. Shir, and R. Sinha. On the evolution of operator complexity beyond scrambling. *J. High Energy Phys.*, 2019(10):264, 2019.
- [270] L. L. Campbell. Exponential entropy as a measure of extent of a distribution. *Probab. Theory Relat. Fields*, 5(3):217–225, 1966.
- [271] L. Jost. Entropy and diversity. *Oikos*, 113(2):363–375, 2006.
- [272] F. Jelinek, R. L. Mercer, L. R. Bahl, and J. K. Baker. Perplexity—a measure of the difficulty of speech recognition tasks. *J. Acoust. Soc. Am.*, 62(S1):S63–S63, 1977.
- [273] M. P. A. Fisher, V. Khemani, and S. Nahum, A. and Vijay. Random quantum circuits. *Annual Review of Condensed Matter Physics*, 14:335–379, 2023.
- [274] Z. Kadelburg, D. Dukic, M. Lukic, and I. Matic. Inequalities of karamata, schur and muirhead, and some applications. *Teach. Math.*, 8(1):31–45, 2005.
- [275] Subir Sachdev and Jinwu Ye. Gapless spin-fluid ground state in a random quantum Heisenberg magnet. *Phys. Rev. Lett.*, 70(21):3339–3342, 1993.
- [276] Y. Sekino and L. Susskind. Fast scramblers. *J. High Energy Phys.*, 2008(10):065, 2008.
- [277] R. Belyansky, P. Bienias, Y. A. Kharkov, A. V. Gorshkov, and B. Swingle. Minimal model for fast scrambling. *Phys. Rev. Lett.*, 125(13):130601, 2020.
- [278] Z. Xu, A. Chenu, T. Prosen, and A. del Campo. Thermofield dynamics: Quantum chaos versus decoherence. *Phys. Rev. B*, 103(6):064309, 2021.
- [279] A. Kulkarni, T. Numasawa, and S. Ryu. Lindbladian dynamics of the Sachdev-Ye-Kitaev model. *Phys. Rev. B*, 106(7):075138, 2022.

- [280] K. Kawabata, A. Kulkarni, J. Li, T. Numasawa, and S. Ryu. Dynamical quantum phase transitions in Sachdev-Ye-Kitaev lindbladians. *Phys. Rev. B*, 108(7):075110, 2023.
- [281] K. Kawabata, A. Kulkarni, J. Li, T. Numasawa, and S. Ryu. Symmetry of open quantum systems: Classification of dissipative quantum chaos. *PRX Quantum*, 4(3):030328, 2023.
- [282] L. Sá, P. Ribeiro, and T. Prosen. Lindbladian dissipation of strongly-correlated quantum matter. *Phys. Rev. Res.*, 4(2):L022068, 2022.
- [283] B. Bhattacharjee, P. Nandy, and T. Pathak. Operator dynamics in Lindbladian SYK: a krylov complexity perspective. *J. High Energy Phys.*, 2024(1):94, 2024.
- [284] D. A. Roberts, D. Stanford, and A. Streicher. Operator growth in the SYK model. *J. High Energy Phys.*, 2018(6):122, 2018.
- [285] J. Liu, R. Meyer, and Z.-Y. Xian. Operator size growth in Lindbladian SYK. *J. High Energy Phys.*, 2024(8):92, 2024.
- [286] K. Su, P. Zhang, and H. Zhai. Page curve from non-Markovianity. *J. High Energy Phys.*, 2021(6):1–18, 2021.
- [287] A Nico-Katz, N Keenan, and J Goold. Can quantum computers do nothing? *npj Quantum Information*, 10(1):124, 2024.
- [288] S. Campbell. Quantum work statistics of controlled evolutions. *EPL*, 143(6):68001, 2023.
- [289] G. Vacanti, R. Fazio, S. Montangero, G.M. Palma, M. Paternostro, and V. Vedral. Transitionless quantum driving in open quantum systems. *New Journal of Physics*, 16(5):053017, 2014.
- [290] S. Alipour, A. Chenu, A. T. Rezakhani, and A. del Campo. Shortcuts to adiabaticity in driven open quantum systems: Balanced gain and loss and non-markovian evolution. *Quantum*, 4:336, 2020.
- [291] K. Takahashi. Counterdiabatic driving for periodically driven open quantum systems. *Philosophical Transactions of the Royal Society A*, 380(2239):20210276, 2022.